Operation of Distribution Systems with PEVs and Smart Loads

by

Isha Sharma

A thesis
presented to the University of Waterloo
in fulfillment of the
thesis requirement for the degree of
Doctor of Philosophy
in
Electrical and Computer Enginering

Waterloo, Ontario, Canada, 2014

I hereby declare that I am the sole author of this thesis. This is a true copy of the thesis, including any required final revisions, as accepted by my examiners.

I understand that my thesis may be made electronically available to the public.

Abstract

With the evolving concept of smart grids, Local Distribution Companies (LDCs) are gradually integrating advanced technologies and intelligent infrastructures to maximize distribution system capability, modernize the grid, and lay the foundation for smart loads. With the development of smart grids, utilities and customers will be able to coordinately send, retrieve, visualize, process and/or control their energy needs for the benefit of both.

This thesis first presents a novel smart distribution system operation framework for smart charging of plug-in electric vehicles (PEVs). Thus, a three-phase Distribution Optimal Power Flow (DOPF) model is proposed, which incorporates comprehensive models of underground cables, transformers, voltage dependent loads, taps and switch capacitors, and their respective limits, to determine optimal feeder voltage-control settings and PEV smart-charging schedules. Various objective functions from the perspective of the LDC and customers are considered, and controlled tap, switch capacitors, and charging schemes are determined for various scenarios to address the shortcomings of uncontrolled charging, using two realistic feeder models to test and validate the proposed approach. Probabilistic studies are carried out on these two feeders, based on Monte Carlo Simulations (MCS), to account for the uncertainty in customers' driving patterns reflected in the initial PEV state-of-charge (SOC) and charging starting time.

The thesis also presents mathematical models for price-responsive and controllable loads to study for the first time the smart operation of unbalanced distribution systems with these types of smart loads, based on the previously proposed DOPF model. The price-responsive load models are represented using linear and exponential functions of the price, while a constant energy load model, controllable by the LDC, is proposed to model critical and deferrable loads. The effect of feeder peak demand constraints on the controllable loads is also examined, based on the results obtained for two realistic feeder models. The two feeders are also used to study, using MCS, the variability of elasticity parameters and their impact on the output of the DOPF.

Finally, the thesis presents a load model of an EHMS residential micro-hub using neural networks (NN), based on measured and simulated data. The inputs of the NN are weather, Time-of-Use (TOU) tariffs, time, and a peak demand cap imposed by the LDC. Various NN structures are trained, tested, validated, and compared to obtain the best fit for the given data. The developed function can be readily applied to the proposed DOPF for real-time optimal operation and control of LDC distribution feeders in smart grids.

Acknowledgements

First, my deepest gratitude and appreciation to my supervisors, Professor Claudio Cañizares and Professor Kankar Bhattacharya, for their invaluable support, encouragement and guidance during the course of my PhD studies. It has been an honor and privilege to have completed my research under their supervision.

I would also like to acknowledge the following members of my PhD Committee for their valuable comments and inputs: Professor Anjan Bose from the Department of Electrical and Computer Engineering at the Washington State University, USA; Professor Jatin Nathwani from the Department of Management Sciences at the University of Waterloo; and Professors Mehrdad Kazerani and Siddharth Garg from the Department of Electrical and Computer Engineering at the University of Waterloo.

I gratefully acknowledge the funding support received from University of Waterloo, and the partners of Energy Hub Management Systems Project namely Ontario Centers of Excellence, Hydro One Inc., Energnet Inc., Milton Hydro Inc., and Ontario Power Authority. I also acknowledge Natural Sciences and Engineering Research Council (NSERC) Canada, Hydro One, IBM Canada, and ABB Corporate Research USA for partial funding of this research.

I thank all my current and past colleagues in the Electricity Market Simulation and Optimization Laboratory (EMSOL) for providing a pleasant and friendly working environment. I also thank the support staff of the Department of Electrical and Computer Engineering for their help in many direct and indirect ways.

Finally, I extend my gratitude to my family for their unconditional love, support, and encouragement.

I dedicate this thesis to:
my loving parents Prof. Ashwani and Saroj Sharma,
my sisters Dr. Ashu and Shagun Sharma, and
my brother-in-law Dr. Ashish Malhotra.

Table of Contents

List of Tables **xv**

List of Figures **xvii**

List of Acronyms **xxi**

1 Introduction **1**

1.1 Motivation 1

1.2 Literature Review 3

1.2.1 Distribution System Operation 4

1.2.2 Price Responsive Loads and Demand Response 6

1.2.3 Plug-in Electric Vehicles (PEVs) 7

1.2.4 Energy Hub Management System (EHMS) and Load Modeling . . . 9

1.3 Research Objectives 10

1.4 Thesis Outline 11

2 Background **13**

2.1 Introduction 13

2.2 Smart Grids 13

2.3 Power Distribution Systems 15

2.3.1 Distribution System Components 15

2.3.2 Distribution Automation (DA) . . . 18
2.3.3 Volt/Var Control . . . 19
2.3.4 Demand Side Management and Demand Response . . . 20
2.4 Plug-in Electric Vehicles (PEVs) . . . 22
2.4.1 Types of PEVs . . . 22
2.4.2 Levels of Charging . . . 23
2.4.3 PEV Charging Schemes . . . 24
2.4.4 Battery Charging Terminology . . . 26
2.5 Mathematical Programming . . . 28
2.5.1 Linear Programming (LP) . . . 28
2.5.2 Non-linear Programming (NLP) . . . 29
2.5.3 Mathematical Modeling Tools . . . 31
2.6 Neural Network (NN) Models . . . 31
2.7 The Energy Hub Management System [51] . . . 34
2.8 Summary . . . 35

3 Smart Charging of PEVs in Residential Distribution Systems 37
3.1 Introduction . . . 37
3.2 Nomenclature . . . 38
3.3 Smart Distribution System Model . . . 39
3.3.1 Three-phase Distribution System . . . 40
3.3.2 Smart Distribution System Operation . . . 43
3.4 Assumptions and Scenarios . . . 45
3.4.1 Assumptions . . . 45
3.4.2 Scenarios . . . 47
3.5 IEEE 13-node Test Feeder Results . . . 49
3.5.1 Case 1 . . . 50
3.5.2 Case 2 . . . 51

3.5.3 Comparison of Smart Charging Scenarios . . . 57
3.5.4 Effect of ZIP Load Models on PEV Smart Charging . . . 59
3.5.5 Probabilistic Analysis . . . 64
3.6 Real Distribution Feeder Results . . . 68
3.7 Computational Details . . . 69
3.8 Summary . . . 70

4 Smart Distribution System Operations with Price-Responsive and Controllable Loads 73
4.1 Introduction . . . 73
4.2 Nomenclature . . . 74
4.3 Mathematical Modeling Framework . . . 75
4.3.1 Uncontrolled Price-Responsive Loads . . . 75
4.3.2 LDC Controlled Loads . . . 80
4.4 Smart Distribution System Operations . . . 82
4.4.1 Scenario 1: Uncontrolled Price-Responsive Loads . . . 84
4.4.2 Scenario 2: LDC Controlled Loads . . . 85
4.5 Results and Analysis . . . 85
4.5.1 IEEE 13-node Feeder . . . 86
4.5.2 Realistic LDC Feeder . . . 95
4.5.3 Modeling, Algorithm, and Computational Challenges . . . 98
4.6 Summary . . . 100

5 Residential Micro-hub Load Model using Neural Networks 101
5.1 Introduction . . . 101
5.2 Nomenclature . . . 102
5.3 EHMS Residential Micro-hub Model [50] . . . 102
5.4 Residential NN Load Model . . . 103

5.4.1 Inputs . . . 103
5.4.2 NN Structure . . . 104
5.5 Results and Analysis . . . 105
5.5.1 Choice of Data Division Function . . . 105
5.5.2 Effect of Varying N_H . . . 106
5.5.3 Mathematical Functions of NN Model . . . 110
5.6 Summary . . . 111

6 Conclusions **113**
6.1 Summary . . . 113
6.2 Contributions . . . 114
6.3 Future Work . . . 115

References **117**

List of Tables

2.1 Energy requirements for different types of PHEV20. 27
2.2 Charging schedule for compact sedan PHEV20 and Level 1 charging. . . . 27

3.1 Scenarios of uncontrolled charging. 48
3.2 Scenarios of smart charging. 49
3.3 Number of PEVs at each node and phase in the IEEE 13-node test feeder. 50
3.4 Summary results of uncontrolled PEV charging scenarios for the 13-node feeder. 53
3.5 Summary results of smart PEV charging scenarios for the 13-node feeder. . 59
3.6 Summary results of smart charging scenarios with ZIP loads. 62
3.7 VDI for smart charging scenarios with ZIP and constant impedance loads. 63
3.8 Probabilistic studies for uncontrolled charging scenario S_1. 64
3.9 Probabilistic studies for smart charging scenarios. 68
3.10 Number of PEVs at each node and phase for the real distribution feeder. . 68
3.11 Summary results of uncontrolled PEV charging scenarios for the real feeder. 70
3.12 Summary results of smart PEV charging scenarios for the real feeder. . . . 70
3.13 Model and computational statistics. 70

4.1 Results for Scenario 1. 88
4.2 Model parameter hourly uncertainties in Scenario 1. 92
4.3 Possible discrete combinations of tap and capacitor values. 96

4.4 Continuous and discrete DOPF solution for linear price-responsive model. . 96
4.5 Results for Scenario 1 for a realistic LDC feeder. 98
4.6 Results for controlled loads for Scenario 2 for a realistic LDC feeder. 98
4.7 Computational statistics. 99

5.1 Comparison of data division functions and NN performance. 109
5.2 Effect of varying N_H on NN performance. 109

List of Figures

2.1 A typical distribution system and its components [58]. 16
2.2 Demand Side Management Techniques [64]. 21
2.3 Coordinated PEV charging. 25
2.4 Feed forward NN topology. 32
2.5 Supervised training as function approximation [83]. 33
2.6 Configuration of a residential micro-hub [11]. (Used with permission of the EHMS project.) 35
2.7 Overall picture of the EHMS [11]. (Used with permission of the EHMS project.) 36

3.1 The proposed smart distribution system operations framework. 41
3.2 Ontario HOEP for a weekday on 30 June, 2011. 47
3.3 IEEE 13-node test feeder [95]. 50
3.4 Total demand for S_1 and S_2. 51
3.5 Phase-wise Feeder 650-632 current for uncontrolled charging S_1 and S_2. . . 52
3.6 Phase voltage magnitude at 8 PM for uncontrolled charging S_1. 52
3.7 Total demand with and without peak-demand constraint for S_3. 53
3.8 Phase-wise total demand with and without PEV loads for S_3. 54
3.9 Total demand for scenario S_4. 55
3.10 Phase-wise total demand with and without PEV loads for S_4. 55
3.11 Total demand with and without peak-demand constraint for S_5. 56

3.12 Phase-wise total demand with and without PEV loads for S_5. 56
3.13 Total demand with and without peak-demand constraint for S_6. 57
3.14 Phase-wise total demand with and without PEV loads for S_6. 58
3.15 Phase voltages at Node 675 for S_3-S_6. 60
3.16 Phase-wise Feeder 692-675 current for S_3-S_6. 61
3.17 Phase voltages at Node 675 for ZIP loads for S_3-S_6. 63
3.18 Lognormally distributed customers' travel patterns for Node 634. 65
3.19 Decision variable values for probabilistic uncontrolled charging. 66
3.20 Decision variable values for probabilistic smart charging scenarios. 67
3.21 Real distribution feeder. 69

4.1 Smart distribution system with uncontrollable price-responsive loads. . . . 76
4.2 Linear relation between demand and electricity price. 77
4.3 Exponential relation between demand and electricity price. 79
4.4 Smart distribution system with controllable loads. 81
4.5 Linear and Exponential relationship between demand and price, $\alpha = 0.2$. . 87
4.6 Voltage magnitude at Node 675 in phase c for Scenario 1. 88
4.7 System load profile for IEEE 13-node Test feeder for J_2. 89
4.8 Effect of peak demand constraint on feeder losses for J_1. 90
4.9 System load profile for $\varphi = 0.83$, J_2. 91
4.10 System load profile for $\varphi = 0.83$, J_2. 92
4.11 Monte Carlo simulation of linear model. 93
4.12 Probability distribution of solution outputs for linear price-responsive loads. 94
4.13 Probability distribution of solution outputs for exponential price-responsive loads. 94
4.14 Continuous optimal tap_{650} and its corresponding RUp and RDn values. . . 95
4.15 System load profile for uncontrolled price-responsive loads for a realistic LDC feeder, $\alpha = 0.2$. 97

4.16 System load profile for a realistic LDC feeder for J_1. 99

5.1 NN EHMS residential micro-hub model structure. 104
5.2 Estimated output using the *dividerand* function. 107
5.3 Estimated output using the *divideblock* function. 107
5.4 Estimated output using the *divideint* function. 108
5.5 Estimated output using the *divideind* function. 108
5.6 Estimated output using the *divideind* function with N_H=7. 109

List of Acronyms

AER	All Electric Range
AMI	Advanced Metering Infrastructure
B&B	Branch and Bound
BEV	Battery Electric Vehicle
CDM	Conservation and Demand Management
DA	Distribution Automation
DAC	Distribution Automation and Control
DER	Distributed Energy Resources
DLC	Direct Load Control
DLF	Distribution Load Flow
DOPF	Distribution Optimal Power Flow
DR	Demand Response
DSM	Demand Side Management
EHMS	Energy Hub Management System
EMS	Energy Management System
EREV	Extended Range Electric Vehicles
FERC	Federal Energy Regulatory Commission
GA	Genetic Algorithm
GAMS	Generic Algebraic Modeling System
HEMS	Home Energy Management System
HEV	Hybrid Electric Vehicle
HOEP	Hourly Ontario Electricity Price
IPM	Interior-Point Method
ISO	Independent System Operator
LDC	Local Distribution Company
LP	Linear Programming
LTC	Load Tap Changers
MCS	Monte Carlo Simulation

MPC	Model Predictive Control
MINLP	Mixed Integer Non Linear Programming
MILP	Mixed-Integer Linear Programming
NLP	Non-Linear Programming
NN	Neural Network
OPF	Optimal Power Flow
p.d.f.	probability density function
PCLP	PHEV Charging Load Profile
PEN	Percentage of Energy Needed
PEV	Plug-in Electric Vehicle
PHEV	Plug-in Hybrid Electric Vehicle
PSO	Particle Swarm Method
QP	Quadratic Programming
RDn	Round-Down
RTP	Real-Time Pricing
RUp	Round-Up
SC	Switched Capacitor
SCADA	Supervisory Control and Data Acquisition System
SLE	Smart Load Estimator
SNOPT	Sparse Nonlinear OPTimizer
SOC	State-of-charge
SQP	Sequential Quadratic Programming
TOU	Time-of-Use
UC	Unit Commitment
VDI	Voltage Deviation Index
VVC	Volt/Var Control
ZIP	Constant impedance (Z), constant power (P), and constant current (I)

Chapter 1

Introduction

1.1 Motivation

Electrical energy availability and energy security are very important factors that affect the economic growth of a country. As per the World Energy Outlook [1], global energy demand is expected to increase by 33% from its 2011 levels by the year 2035; concurrently, the world electricity demand is expected to increase by 66% over the period 2011-2035. Furthermore, as per the 2013 Long Term Energy Plan of Ontario [2], the peak load and energy demand of the province are expected to increase by 25% and 26%, respectively, by 2033 from their 2014 levels. All this will require adequate expansion of transmission lines and generation capacity to meet the growing demand. However, building new generation and transmission lines is capital intensive, and environmental issues also need to be considered (e.g., increasing CO_2 emissions). In view of this, there is a need to find intelligent and cost effective means to manage and reduce demand and peak loads.

Smart grid developments can help achieve the aforementioned demand/load goals, through Demand Side Management (DSM), Distribution Automation (DA), distributed generation, and Advanced Metering Infrastructure (AMI). A smart grid is an intelligent power network that incorporates technologies and communication infrastructure to maximize existing capability, modernizing the grid particularly at the distribution system and load levels [2]. In this context, intelligent control algorithms with information technologies are being implemented into the grid to manage energy consumption and thereby regulating loads. Conservation and Demand Management (CDM) and Demand Response (DR) programs are being implemented to alter the load shape in response to price signals or operator requests during critical conditions, particularly at peak demand periods.

With the evolving concept of smart grids, Local Distribution Companies (LDCs) are gradually integrating advanced technologies and intelligent infrastructure to maximize distribution system capability, modernize the grid, and lay the foundation for smart loads. For the latter, smart meters form the basic foundation, providing customers with timely and accurate information on their electricity usage via two-way communication with the LDC [2]. This could help customers manage their electricity consumption patterns and at the same time improve efficiency for the LDCs. With the development of smart grids, utilities and customers will be able to send, retrieve, visualize, process and/or control their energy needs.

Ontario has set a goal to reduce the system peak demand by 6,300 MW by 2025 through DSM, DR, and demand control programs [3]. DR programs such as DR1 and DR3 have been enacted, with a target of 214 MW reduction in peak demand and 640 GWh per year reduction in energy demand by 2014 from the industrial and commercial sectors [4]. The RETROFIT Program encourages installation of new energy efficient equipment and control systems to improve overall efficiency by providing substantial incentives [5]. The Peaksaver PLUS® is another program enacted by the Ontario Power Authority for residential customers that is expected to ease the strain on Ontario's electricity grid, by controlling central air conditioners or electric water heaters through installation of a direct load management device [6].

Ontario has also deployed smart meters throughout the province, as part of various smart grid initiatives. Time-of-Use (TOU) tariffs have been introduced with the aim of benefiting both customers and LDCs by reducing the electricity use at peak times [2]. Furthermore, other initiatives such as micro-grids and convenient charging of plug-in electric vehicles (PEVs) are being developed and should be readily available by 2020. These smart grid technologies will encourage more customers to participate in DSM, DR, and demand control programs, which are being designed and implemented by regulators, governments and LDCs to encourage customers' involvement in the supply of energy services.

The number of PEVs in the US and Canada would increase significantly by 2018, motivated by programs such as the Electric Vehicle Incentive Program in Ontario, which provides incentives to customers that range from $5,000-$8,500 (depending on battery capacity) toward the purchase or lease of a new PEV or battery electric vehicle [7]. This would result in considerable increase in charging demand [8], [9], which would need to be managed, since, although PEV loads will be distributed randomly in the distribution system, these will likely be clustered in specific areas of the network and could overload the distribution feeders. In the absence of a two-way communication between the LDCs and PEVs to facilitate "smart" charging, it would be difficult to shift the potentially high PEV charging load to off-peak hours, considering that a large number of PEVs charging

simultaneously would be a concern in residential neighborhoods if the power delivered to these loads is not controlled, particularly during peak periods. Thus, it is important to ensure that the charging of PEV loads do not create a higher or a new peak in the system. This can be accomplished by smart charging of the PEVs as discussed in [10] for the case of Ontario, which would in principle schedule PEV charging at non-peak periods of the day, such as late night to early morning hours. The elastic nature of PEV loads provides this much needed flexibility, which will facilitate the centralized control of their charging profiles.

Besides the expected growth in smart PEV loads, there are also other categories of loads which can also respond to LDC's control signals or other external signals such as prices or incentives, and hence alter the overall load profile. For example, Home Energy Management Systems (HEMS) are being implemented, allowing smart and intelligent control of customers' appliances, which can bring about significant benefits to the customer [11], and can also help LDCs reduce their overall peak demand, reshape the load profile, and consequently increase grid sustainability, since smart loads can potentially alleviate system expansion costs in the long run by deferring capacity investments in generation and distribution. In this context, Real-Time Pricing (RTP) or TOU pricing mechanisms, as part of DSM programs, are expected to alter the typical demand profile of a customer, and thus it is important for the LDC to study these changes and their impacts, so that operating decisions regarding switches, taps positions of transformers, switched capacitors, etc., can be made optimally.

From the above discussions, it is necessary to understand the behavior of smart customers and loads within the LDC system, considering that these respond to price signals and other externalities. Such knowledge could be very valuable to LDCs operating in the smart grid environment, and hence there is a need to develop smart load models through state-of-the-art estimation techniques, and integrate them within the smart distribution system operational models. These particular issues have motivated the present research with the main aim of examining the impacts of demand management in the context of smart grids, considering the LDC's and customers' perspectives, to propose models and techniques to optimally operate the distribution system to benefit both parties.

1.2 Literature Review

This section presents a critical review of the relevant research literature and developments pertaining to the topics of DA and distribution system operation; demand control, DSM and DR; PEVs; and energy hub management systems. The main objective here is to

identify the main gaps in the current technical literature pertaining to these topics, which the present thesis tries to address.

1.2.1 Distribution System Operation

Several diverse concepts for the next generation of power distribution systems and the impact of electronic control on distribution systems are summarized in [12], where it is mentioned that future distribution systems will be networked or looped, rather than radial, thus rendering them more reliable, but requiring more elaborate protection and switching provisions. It is also observed that some of the main features of a smart distribution system would include reconfiguration capability, integration of renewable resources, management of reactive power, improved reliability, and accommodating PEV loads. Furthermore, it is argued that use of electronic switching capacitors for reactive power dispatch, conversion of overhead systems to underground, networking distribution primaries and secondaries, and adding generation to the distribution system will also be part of smart distribution systems. In this context, this thesis proposes techniques through which the LDC can make optimal decisions for the smart operation of distribution feeders, optimally controlling load tap changers (LTCs), switched capacitors (SCs), PEV charging, and smart loads.

Volt/Var control (VVC) is an important aspect of distribution system operation as it regulates voltage and reactive power. Distribution transformers are equipped with LTCs for voltage control purposes, while SCs and fixed capacitors help in voltage and reactive power control. Although, the primary purpose of VVC is to regulate voltages and reactive power in distribution feeders, it can help operators achieve certain optimization objectives with the availability of additional control and communication devices. In the context of smart grids, VVC would allow LDCs to realize savings in operational costs through energy consumption reduction by determining and setting optimal load voltage profiles. In this research, such a smart VVC problem is addressed considering the presence of PEVs and smart loads in distribution feeders.

Feeder loss minimization has been the most commonly used VVC objective function reported in the literature [13, 14, 15, 16, 17, 18, 19, 20, 21], typically involving a Distribution Load Flow (DLF) solution and an iterative optimization procedure. With limited number of LTCs and SCs, enumerative techniques can be used to solve the VVC optimization problem; however, for a larger system the combinatorial solution approaches are computationally costly, and thus heuristic methods have been proposed [13, 14, 17, 18, 19]. For example, a relaxed integer programming technique, and a VVC algorithm based on combinatorial integer programming and fast power flow technique are proposed in [13] and

[17], respectively, to significantly reduce computational times. In [14], a neural network based fuzzy dynamic programming approach is presented to obtain a preliminary dispatch schedule for the LTCs and SCs; the proposed method also reduces the computational time significantly. A heuristic method based on a simplified network approach is presented in [18] to solve the reactive power control problem; the proposed method is simple, fast, and suitable for real-time application. In [19], a coordinated and centralized voltage control scheme is discussed to regulate the voltage of multiple feeders in real-time; the suggested technique relies on measurement and communication infrastructure available in smart grids.

Integrated optimization models and solution approaches have also been proposed in the literature for the VVC problem [20, 21], where the DLF model is treated as a constraint in the optimization model. An algorithm based on nonlinear interior point method and discretization penalty is presented in [22] to dispatch reactive power and control the voltage in distribution systems, with the objective of minimizing daily energy losses. In all of the aforementioned papers, the authors have mostly considered either a DLF based approach or a loss minimizing optimization problem to arrive at the optimal decisions for LTCs and SCs, while considering a balanced representation of the distribution system and only constant power loads. However, it is important to model the distribution system accurately because of the presence of untransposed three-phase feeders, single-phase laterals, and single-phase loads. To address this deficiency, in this thesis, an unbalanced three-phase distribution system has been modeled in detail considering different types of load models, PEVs, and smart loads. Furthermore, various objective functions have been considered for analysis, from the perspectives of the LDC and customers.

Distribution optimal power flows (DOPFs) with three-phase unbalanced models of the distribution feeder have been proposed in the literature. Thus, a quasi-Newton based methodology for solving an unbalanced three-phase optimal power flow (OPF) for distribution systems is presented in [20]. The proposed model seeks to optimize the distribution control resources such as loads and reactive power support; however, the work considers only SCs and interruptible loads as decision variables, while LTC taps are fixed. A generic three-phase DOPF model is proposed in [21], which incorporates detailed modeling of distribution system components; the objective is to minimize the energy drawn from the substation while also limiting the switching operations of LTCs and SCs. These detailed DOPF models are further extended and modified in this thesis by including PEVs and smart loads, to examine their operational impact on distribution feeders.

Smart grid applications have required LDCs to upgrade their system analysis tools to accurately model and analyze distribution systems. In [12, 23, 24, 25, 26], perspectives are presented on the type of distribution system analysis framework needed to support the smart grid. In these papers, the need to introduce flexibility in distribution feeder

operation with the help of centralized control of components such as LTCs, SCs, and smart loads is identified. Hence a model predictive control (MPC) approach [27] is used in this work, wherein the modified-DOPF is repeatedly executed in real-time while considering continuous feeder and load changes, to optimally control LTCs, SCs and smart loads to minimize losses, energy consumption and costs.

1.2.2 Price Responsive Loads and Demand Response

Some work has been reported in the literature to model the customers' behavior in response to prices and hence examine the DR impacts on the system. For example, customer response to spot price difference is modeled in [28], using linear and exponential functions for different categories of customers, to determine real-time interruptible tariffs and optimal interruptible loads in an OPF framework. In [29], customers' behavior is modeled using a matrix of self- and cross-elasticity; an exponential price-demand curve is considered to represent various types of customer reactions. This paper states that the price-demand relationship can be linearized for the sake of simplification in computation without any significant loss of generality. In [30], the impact of demand side price-responsiveness on the oligopoly market performance is examined considering exogenous changes in self elasticity; a linear relationship between customer demand and market price is formulated for different degrees of price-responsiveness. Incentive-based DR programs such as interruptible/curtailable loads are modeled in [31], based on price elasticity of demand and quadratic customer benefit function.

In the literature, controllable and price responsive loads have also been considered within a Unit Commitment (UC) framework. For example, in [32], a security constrained UC problem is proposed where interruptible loads are optimally curtailed or shifted in time. In [33], an economic model of responsive loads is proposed based on price elasticity of demand and customers' benefit function, and is implemented in a cost-emission based UC problem. In another UC model considering wind resources in [34], demand shifting and peak shaving decisions are determined considering customers' elasticity. In a similar UC model in [35], a critical peak pricing with a load control model is proposed. In [36], DR is integrated into an UC model, considering its short-term responsiveness, and loads are shifted across hours using self- and cross-elasticity matrices. In [37], a multi-objective optimization model is solved using compromise programming to select load control strategies. Different objectives of minimizing the peak demand, maximizing revenue generated from energy sale and minimizing the discomfort level of customers are considered. It is to be noted that in the above papers [32]-[37] the loads essentially are modeled as negative sources and are included within the traditional UC models as a load scheduling and

dispatch problem, at the aggregate system level. In all the aforementioned papers, studies have been considered to be aggregated at the transmission level, i.e., examining DR impact from the Independent System Operator's (ISO's) perspective or at the wholesale market level. However, in the context of smart grids, it is important to model customers' behavior at the retail level and study their impact on distribution feeder operations, which is one of the research objectives of this thesis, modeling price-responsive loads as linear and exponential functions, as proposed in [28].

As noted from the discussions so far, very little work has been reported on DR at the distribution level. In [38], the distribution system is included into the DR loop for effective scheduling and real-time monitoring of loads, which allows the LDC to monitor the transformers for any violations, overloads, or unbalanced conditions. DR strategies, targeted at the household level, are proposed in [39] and [40] to alleviate the need for upgrades of the distribution transformer and also prevent overload conditions. Although these papers touch upon the retail customer and the distribution system, the feeder operational impacts on nodal voltages and feeder currents from DR or PEV loads are not examined, neither is the distribution system model considered in appropriate detail. The models take into account real power demand only and hence they are constrained to examine the aggregate load profiles only.

Based on the aforementioned literature review, it can be noted that there is a need to model smart loads in an unbalanced distribution system framework, examine the impact of price-responsive loads on the distribution feeder, and develop optimal feeder and DR strategies for controllable loads, from the perspective of the LDC while considering the customer interests.

1.2.3 Plug-in Electric Vehicles (PEVs)

Much work has been reported in the literature examining the impact of PEV charging on power networks; the models used for such studies have varied from fairly simplistic dc power flow to more elaborate ac power flow models. These papers discuss aspects such as differing operating objectives, uncontrolled versus controlled charging, etc. For example, in [41], the coordinated charging of PEVs in residential distribution networks is studied considering peak shaving, loss minimization, and improving voltage regulation, using a simplified distribution system model that ignores reactive power demand, LTCs and SCs. In [42], the impact of PEV charging on a real distribution feeder is examined considering demographic and travel survey data; three charging strategies: uncontrolled, minimizing loss and price optimal are studied to evaluate the advantages of controlled charging, using

a balanced distribution feeder and OPF for the analyses. The effect of fast-charging PEVs on a distribution system is examined in [43] using power-flow, short-circuit, and protection studies. It is noted that fast charging of PEVs affect the distribution system depending on the location of the charging station, i.e., PEV load, which may limit the maximum number of vehicles that can be simultaneously charged without violating any operating limits; however, the case studies are rather simplistic (2-bus system) and only eight PEVs are considered, using a trial-and-error method to find the maximum number of PEVs that can be simultaneous charged. Similarly, real-time (every 5 min) coordinated charging of PEVs is examined in [44] considering cost of charging and energy loss minimization. In [45], the impact of coordinated and uncoordinated charging of PEVs on a distribution system is studied using both deterministic and stochastic optimization models, to minimize the power losses and maximize the grid load factor. Further, in [46], loss minimization, load factor maximization, and load variance minimization is carried out for coordinated PEV charging in a balanced distribution system. These studies discuss the overall impact of smart PEV charging, but also highlight the need for more comprehensive modeling of the distribution system and loads, including the PEV loads, to arrive at more realistic conclusions, which is one of the research objectives of this thesis.

Not much work has been reported on PEV impact studies considering low voltage distribution systems, and their detailed unbalanced system representation. For example, in [47], a locally controlled charging strategy is proposed maximizing the energy delivered to each PEV; comparisons are made with a method where charging of PEVs is centrally controlled to examine the advantages and disadvantages of both techniques, in terms of network capacity utilization and total energy delivered to the PEVs. In [48], it is shown that by controlling the charging rate of individual PEVs the existing networks can be better utilized. Although the analyses reported in these works consider a real unbalanced distribution feeders, the controlled charging objective of maximization of total charging power drawn by PEVs is rather unrealistic, both from the LDC operators' and customers' perspective.

From the aforementioned literature review, it can be noted that there is a need to develop comprehensive models of distribution feeders and PEV loads, and examine in detail their impact in distribution operation, to develop smart charging strategies from the perspectives of the LDC and customers. These are some of the main objectives of this thesis.

1.2.4 Energy Hub Management System (EHMS) and Load Modeling

The energy hub represents a network node in an electric power system that can exchange energy and information with the surrounding systems, sources, loads, and other components via multi-energy inputs and outputs [49]. It is not limited in size, and thus can vary from a single household energy system to aggregated loads and energy sources.

Mathematical optimization models of energy hubs for residential, commercial and agricultural sectors are proposed in [50], where the energy activities of the EHMS at a "micro-hub" level are optimized from the customers' point of view, such as minimizing the cost of energy consumption. A mathematical optimization model for major household devices in a typical house is formulated, which can be solved in real-time to optimally control all major residential energy loads, storage, and production components, while considering the customer preferences and comfort level. The model yields optimal operation decisions on scheduling the major loads to achieve desired objectives such as cost minimization, maximizing comfort, or minimizing CO_2 emissions, yielding modified load profiles. External inputs such as price signals, weather, system emission profiles, customers' comfort, and peak-power signals from utilities are also considered, influencing the load profile. These specific types of loads, with their variability and elasticity, are considered for analysis in the context of smart distribution system operations in the present thesis.

In [50, 51], a "macro-hub" is defined, comprising several micro-hubs that communicate with the macro-hub reporting their energy and demand usage. At the macro-hub level, the optimization model is geared towards the LDC operator, incorporating the changing load dynamics of customers that will benefit both customers and the LDCs. At this level, typical objectives may include load shape modification, peak load reduction, etc. In the present thesis, the focus is on examining the operational issues of a macro-hub, at the LDC level, in the context of smart distribution system operation.

Graphical representation of electric load data, regression-based electricity load models, and definition of various load parameters are presented in [52], to analyze commercial and industrial load data in 15-min intervals and to implement DR strategies; loads are modeled as a function of temperature and time-of-week. In [53], data-driven models are proposed to describe the dynamics of price-elasticity of customers, showing that significant amounts of load are shifted and peaks are flattened, considering a constant energy load model. Such load models, when incorporated within the distribution feeder operational models, can help the LDCs to obtain knowledge of smart loads and their response to externalities, which is one of the objectives of this thesis. Hence, some of the research presented in this thesis proposes the modeling of a load profile of a residential EHMS micro-hub, obtained

by varying weather, price signals, and peak power, which can be subsequently adopted by an LDC operator in a smart distribution system operational framework.

1.3 Research Objectives

The research presented in this thesis draws upon various features of the smart grid and associated technologies, such as the AMI, which may provide information on changing load patterns, using communication and measurement equipment to provide an updated status of the distribution system, so as to enable real-time control of controllable loads and distribution system components. Hence, based on the literature review and discussions presented in the previous section, the following are the main objectives of the research presented in this thesis:

- Develop a mathematical framework for the optimal operation of distribution systems considering comprehensive models of unbalanced distribution system components, voltage dependent loads, and PEV loads. The novel modeling framework, referred to as DOPF, will allow considering various objective functions from the LDC's and customers' perspectives.
- Examine the operational impact of smart charging of PEVs on residential distributions systems using the developed DOPF model, and considering various operational scenarios, compared with respect to uncontrolled PEV charging. Furthermore, the impact on system operation considering uncertainty in the PEV models, to take into account customers' driving patterns, will also be studied.
- Introduce price-responsive and controllable loads in the proposed DOPF model to study their impact on a distribution system operation. Various objective functions from the LDC's and customers' perspective will be formulated, such as minimization of cost of energy drawn from the grid, minimizing feeder losses, and minimizing the total cost to customers, for the operational impact studies. Analysis considering uncertainty of the elasticity parameters of load models will also be carried out to represent more realistically the behavior of customers.
- Develop a neural network (NN) based model of a residential EHMS micro-hub using real measurement data and simulated load data obtained using [50]. The inputs, measured every 5 minutes, are the outside temperature, price signals (TOU), time of day, and a peak demand cap assumed to be imposed by the LDC.

1.4 Thesis Outline

The remainder of this thesis is structured as follows:

- Chapter 2 briefly discusses the background topics and tools pertaining to the research carried out in this thesis. A review of smart grids is presented first, followed by distribution systems and some operational aspects. Thereafter, a brief outline of mathematical programming models and their solution methods is introduced, followed by overviews of PEVs, NNs, and relevant EHMS concepts.

- Chapter 3 presents a novel modeling framework for inclusion of the charging operations of PEVs within a three-phase, residential distribution system, including constant impedance (Z), constant current (I), and constant power (P), i.e., ZIP load models. Some results of applying the proposed model to two realistic test feeders are presented and discussed.

- Chapter 4 proposes a DOPF model with different objective functions for smart distribution operation with price-responsive and controllable loads. Linear and exponential functions are considered to represent uncontrolled price-responsive loads. A novel constant energy load model, controllable by the LDC through peak demand constraint, is also proposed. Finally, results of applying the proposed load models to two realistic test feeders are presented and discussed.

- Chapter 5 presents the modeling of residential EHMS micro-hub using NN to estimate their load profiles. Real and simulated data with variable weather, price signal, and peak power inputs are used to train the NN-based load profiles.

- Chapter 6 summarizes the main conclusions and contributions of the research presented in this thesis, and identifies some directions for future research.

Chapter 2

Background

2.1 Introduction

This chapter presents a background review of the main concepts and tools pertaining to the research presented in this thesis. First, a background on smart girds in presented in Section 2.2, followed by some aspects of distribution system components, infrastructure, and operations in Section 2.3. Section 2.4 presents some basic concepts related to PEV charging, levels of charging, and its charging principles. This is followed, in Section 2.5, by an overview of mathematical programming and solution methods relevant to the present research. Section 2.6 discusses the basics of NN modeling, and finally Section 2.7 briefly summarizes the main concepts of the EHMS.

2.2 Smart Grids

The US Department of Energy states: "Think of the smart grid as the internet brought to our electric system. Devices such as wind turbines, plug-in hybrid electric vehicles (PHEVs) and solar arrays are not part of the smart grid. Rather, the smart grid encompasses the technology that enables to integrate, interface with and intelligently control these innovations and others" [54]. The operation of a smart grid involves many aspects such as generation of power using alternate sources (e.g., solar, wind, geothermal); intelligent distribution of power by monitoring the demand in different regions; monitoring the power usage by customers using smart meters and intelligently deliver power when needed; integrating loads like PEVs and communication devices into the grid.

The essence of smart grids consists of the implementation of the following seven principles [12]:

1. Self-healing from power disturbance events.
2. Enabling active participation by customers in DR.
3. Operating resiliently against physical and cyber attacks.
4. Providing power quality for twenty-first century needs.
5. Accommodating all generation and storage options.
6. Enabling new products, services, and markets.
7. Optimizing assets and operating efficiently.

A smart grid comprises controls, computers, automation, and new technologies working together with the grid to respond to instantaneous/abrupt changes in demand and generation. The benefits of a smart grid include efficient power supply and delivery, fast system restoration after a disturbance, reduced peak demand, increased integration of distributed energy resources (DERs), and improved security. It also encourages customer-owned generation when power is not available from utilities [55]. The smart gird encompasses various innovations, some of which are still in the development phase, while some technologies are already in use. For example, communication and control infrastructure is prominently existent in generation and transmission systems; however, the development of similar infrastructure and technologies is required at the distribution level to realize the concept of smart grids.

Smart meters, replacing old electro-mechanical meters, provide the interface between a customer and the utility and give information on the electricity usage which can help customers cut down their energy cost. The real-time information exchange can be realized through an HEMS, that helps track energy consumption in detail, i.e., the customer can monitor the impact of various appliances on its energy consumption. The HEMS informs the customer about the TOU and RTP tariffs and creates settings to automatically turn on appropriate appliances when electricity prices are low. The utility may provide financial incentives to customers for turning off appliances automatically during peak demand hours or during an outage [11], [55].

The province of Ontario has initiated the integration of smart grid technologies in distribution feeders. For example, Hydro One has completed the installation of smart

meters in every home and small business in Ontario, and a central "Meter Data Management and Repository" system has been created to process, store and manage all smart meter data in the province [56]. In Ontario, LDCs are also engaged in various projects related to storage integration, DR, integration of PEVs into the grid, and HEMS. It is envisaged that by 2015, there would be large-scale integration of smart home technology embedded in most household appliances and devices, allowing customers to collect real-time information on their energy use and automatically respond to price signals [57]. By 2030, it is anticipated that the level of sophistication will increase significantly as smart homes, appliances, PEVs, and distributed generation will be capable of secure interaction, realizing the two-way flow and management of electricity envisioned in smart grids [57].

This thesis assumes that smart grid infrastructure is in place in distribution systems, including two-way communication, so that the LDC can send control signals to the customers to implement smart decision strategies in constant interactions with them.

2.3 Power Distribution Systems

The electric power distribution system is a part of the electric utility system that connects the transmission system to the customers. The distribution system is an expensive element of the power system, and is characterized by higher power losses, compared to other components. Distribution systems in North America generally operate at voltage levels of 34.5 kV, 23.9 kV, 14.4 kV, 13.2 kV, 12.47 kV, 4.16 kV, and others [58].

2.3.1 Distribution System Components

A typical power distribution system along with its most important components is shown in Figure 2.1 [58]. In this figure, the following components are illustrated:

- Sub-Transmission System: It links the bulk power sources to the distribution substations and delivers power from the transmission system to distribution substations.
- Distribution Substation: It represents a connection between the sub-transmission and primary distribution circuits and steps down the sub-transmission voltage for the primary distribution system. It houses power transformers, voltage regulators and switchgear.

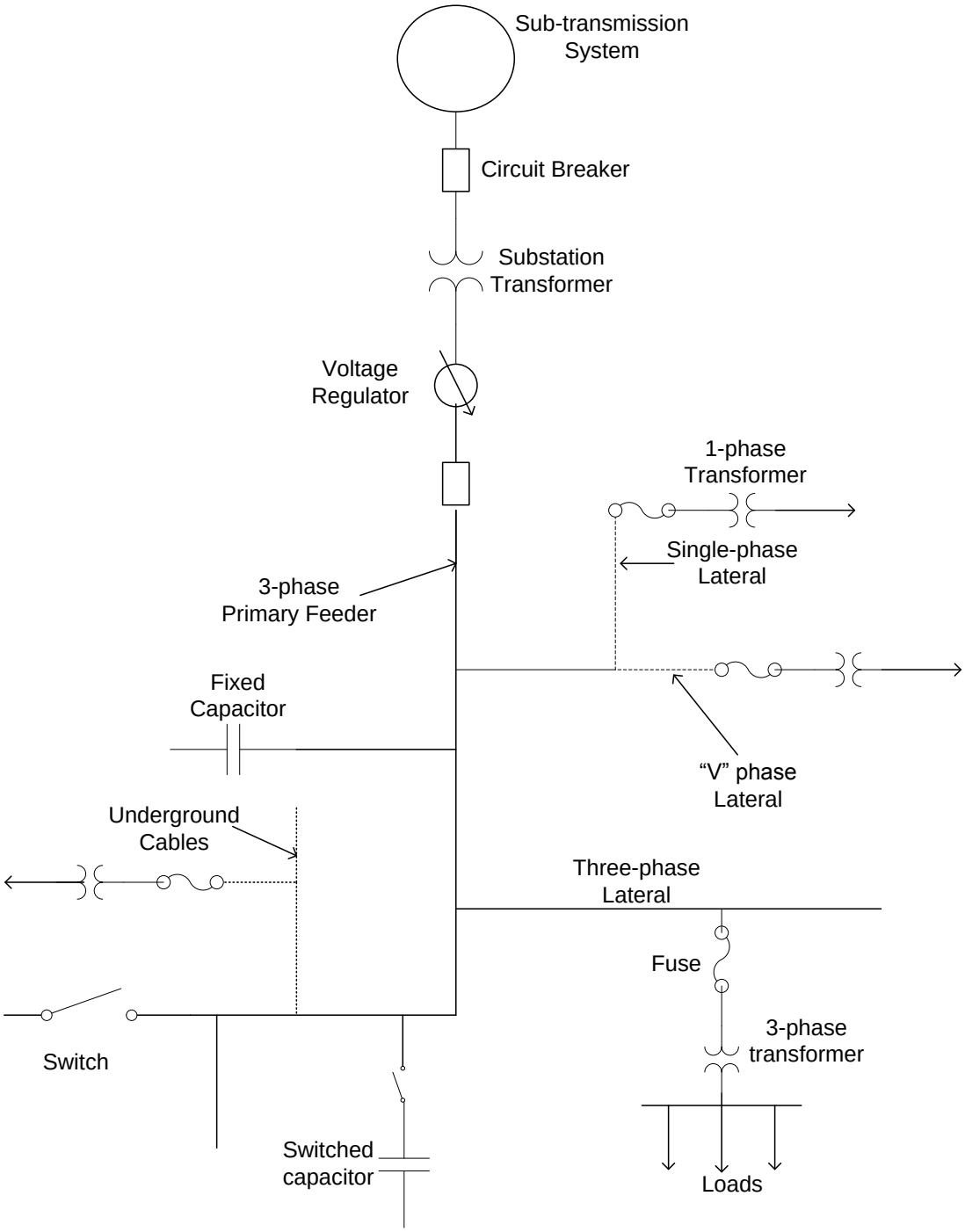

Figure 2.1: A typical distribution system and its components [58].

- Feeders: These supply electric power from the distribution substation to the customer loads. These can be three-phase feeders, two-phase or single-phase laterals, overhead lines or underground cables.

- Distribution Transformers: These transformers further step down the voltage of the primary feeder. The voltage rating of these transformers depends on the voltage levels of the primary (input voltage) and the secondary (output voltage) circuits. In distribution systems, both three-phase as well as single-phase transformers are present. Three-phase transformers could be wye grounded-wye grounded, delta-wye grounded, etc.

- Control and Protection Devices: Distribution systems are equipped with control devices such as voltage regulators and SCs, to maintain voltages within an acceptable ranges. Devices such as switches, circuit breakers, and fuses are used for system and equipment protection. Tie switches and line sectionalizers are used to reconfigure the distribution system structure. Voltage regulators can be used in substations to regulate the voltage on the primary feeders, and are transformers equipped with LTCs with many steps in the series winding. Most regulators have a $\pm 10\%$ range, usually in 32 steps, which amounts to a $5/8\%$ change per step [58]. For example, as load increases, the voltage drop increases and the transformer turns will increase to compensate for the voltage drop.

- Loads: Customer loads are typically voltage dependent and may typically behave as constant impedance, constant current, constant power, or a combination of all the three types.

- Fixed Capacitors: These are installed at various locations on the feeders to improve the load power factor and voltage profiles.

The distribution feeder is fundamentally an unbalanced system because of the presence of unequal single-phase loads, and non-equilateral conductor spacing on three-phase overhead and underground cables. Thus, conventional power flow and short-circuit analysis used for transmission systems cannot be used for distribution systems, as these methods assume a balanced system [58]. To analyze the distribution system it is important to model three-phase distribution system components in detail.

2.3.2 Distribution Automation (DA)

The main purpose of DA is to maintain reliability and efficiency of the distribution system. This requires implementation of appropriate and efficient control algorithms, which is achieved by upgrading the system to meet new design requirements, for example, by adding LTCs, SCs, fault detectors, etc. DA can be used to control the energy consumed by the load, minimize system losses, and maintain voltage limits while minimizing the switching operations of taps and capacitors. Thus, to implement DA, load characteristics, voltage profiles, reconfiguration and proper control algorithms need to be studied. The main attributes of DA are the following [59]:

1. Load Management: It allows utilities to reduce their load demand during peak hours, which can, in turn, reduce costs by eliminating the need for peaking power plants, reshape the demand profile, and increase the grid sustainability.

2. Load Control: Customer loads can be controlled by adopting an active or a passive approach. In the active approach, the LDC de-energizes some of the loads of the customer during peak hours, while in the passive approach it encourages customers to control their loads as per its requirements and, in return, the customers may receive some incentives.

3. Energy Management System (EMS): It is a system to centrally coordinate the available distribution system controls. It can serve as an important tool toward active DSM, one of the fundamental features of the smart grid by influencing the customers' energy usage and reshaping the load profile. EMS have embedded intelligence that can automate decision making and control of household appliances.

4. Voltage Control: It can be used to reduce the load and energy losses. For example, by operating the distribution system at minimum acceptable voltages, and since loads are voltage dependent, the energy drawn from the substation can be minimized. Load tap changers and SCs are used to control voltages [13, 14, 17].

5. Supervisory Control and Data Acquisition System (SCADA): It can remotely control and monitor distribution networks. For decades, SCADA systems have provided information to the utilities to control or manage the grid, yielding many advantages including: reliability through automation; elimination of the need for manual data collection; enabling operators through alarms and system-wide monitoring to quickly spot and address problems; costs reduction, worker safety improvements by allowing to detect and address automatically problem areas; improved utilization; etc.

6. Distribution Automation and Control (DAC): It can remotely control distribution equipment such as voltage and reactive power control equipment. It can also automate feeder restoration and reduce outage times by analyzing and detecting fault conditions, isolating the affected feeder sections, and restoring power to unaffected sections.

7. System Reconfiguration: Loads can be transferred from a heavily loaded feeder section to light loaded feeders using switches. This technique is referred to as reconfiguration, and can be used to reduce system losses and improve system performance during faults. This can also help with maintenance of feeders without interrupting the power from the system.

2.3.3 Volt/Var Control

Voltage regulation and reactive power control are the primary operational objectives in distribution systems. Voltage regulation means to regulate the distribution system voltage so that every customers' voltage remains within acceptable limits. Unregulated voltages can have adverse impacts on the system, since performance and life of electrical equipment can be affected because of large voltage fluctuations; for example, low voltages cause low illumination, slow heating, etc., and high voltages may cause premature device failure and reduced device life [60]. Similarly, reactive power flows in distribution systems are undesirable and results in voltage drops, increased losses and reduced power delivery capability.

LTC transformers, LTC line regulators, and capacitor banks can affect voltage and reactive power, and thus these play an important role in the control of a distribution system through VVC. Conventionally, these two devices are controlled separately. However, due to recent developments, DA tends toward centralized controls of both LTCs and capacitor banks in a coordinated manner [60]. Using controls with adaptive algorithms can result in a decrease in system losses and reduced the number of tap change operations. Benefits of substation level VVC are the following [60]:

- Voltage Regulation: Voltage regulators try to keep voltages close to nominal values and minimize voltage variations at all times under all load conditions; thus maintaining voltage quality on feeders. Since electrical loads are dependent on voltage and current, voltage can be an important means for load control.

- Power Factor: Capacitor banks are used to supply reactive power during peak demand. During off-peak demand, capacitor banks are not required and hence need to be switched off.

The present work proposes a DOPF model which determines optimal decisions on switching of LTCs and SCs, among others, to achieve similar goals as the VVC approach, with appropriate choices of LDC's objective functions. Furthermore, the loads in DOPF will be modeled as voltage dependent and in addition assumed to be elastic; therefore, the minimization of energy drawn will result in improved optimal decisions with respect to the "classical" VVC techniques.

2.3.4 Demand Side Management and Demand Response

DSM programs have been in existence and practice for several decades now [61, 62]. They encompass various options to manage the demand such as energy conservation, load management, technology change, TOU tariffs and DR, among others. One of the early works [63] presents the basic philosophy on which the generation and demand may respond to each other in a cooperative fashion and are in a state of continuous equilibrium. The authors propose that one way to reduce costs is to use direct utility-customer communications to implement a "load follow supply" concept.

Load management falls within the purview of DSM and involves altering the daily or seasonal electricity demand of residential, industrial or commercial customers between peak and off-peak hours, in six broad ways: peak clipping, valley filling, load shifting, strategic load growth, and flexible load shape. In general, the following are the possible DSM techniques that can be implemented in smart grids, as illustrated in Figure 2.2 [64]: peak clipping and valley filling are used to reduce the difference between the peak and valley level loads, thus making the load profile fairly uniform, thus reducing the burden of peak demand and increasing the security of the power grid. Load shifting is widely used as the most effective load management technique in distribution feeders, and is carried out when loads are not dependent on time and can be shifted from peak to off-peak hours. Flexible load shape is based on loads than can be controlled during critical periods in exchange for various incentives. Valley filling encourages customers to use their appliances during off-peak hours, and thus can help to improve the overall load factor of the system.

The main feature of load management is its capability to control the load at a specific time. Thus, by incorporating the right policies for load management, utilities may be able to avoid unwanted peaks and valleys. Different techniques can be used for different category

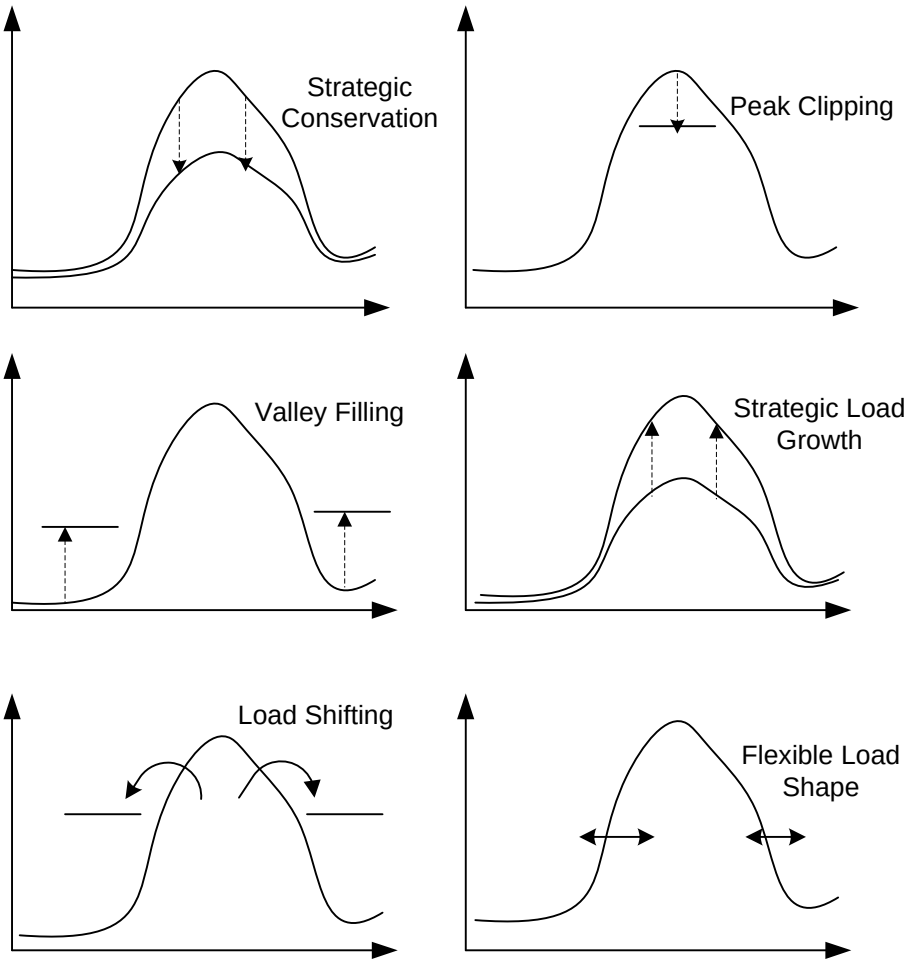

Figure 2.2: Demand Side Management Techniques [64].

of customers to encourage them to change their electricity consumption patterns by, for example, directly controlling the load, electricity tariffs, off-peak industrial operation, and others. A comprehensive review of DSM and load control programs practiced by utilities in North America is presented in [65] in the context of their contribution to system operation impacts.

DR is defined by Federal Energy Regulatory Commission (FERC) in [66] as: "Changes in electricity use by demand-side resources from their normal consumption patterns in response to changes in the price of electricity, or to incentive payments designed to induce lower electricity use at time of high wholesale market price or when system reliability is

jeopardized." There are two different categories of DR programs, identified in [66]: time-based, which includes TOU pricing, RTP, critical peak pricing with/without control, etc.; and incentive-based such as direct load control (DLC), demand side bidding and buyback, emergency demand response, non-spinning reserves, and interruptible load. DR programs encourage customers to alter their energy usage pattern by reducing energy consumption during peak hours, usually in response to price signals or operator requests, which results in load shape modifications. DR offers multiple benefits to the customer and the LDC. Benefits to the LDC include reduction in the energy supply cost, more efficient use of the electricity system, deferral of capacity expansion, etc. [61], [67], [68]. On the other hand, customers benefit by way of relaxed energy payments and from various incentives from participation in such programs [66]. Various incentive rate designs have been implemented in the past by US utilities, of which the most common have been interruptible tariffs and TOU pricing [69].

DSM and DR essentially lay the foundation of the concept of smart grids where customers can interact with the LDC and respond to their control signals. This thesis proposes the modeling and impact studies of such loads on a distribution feeder.

2.4 Plug-in Electric Vehicles (PEVs)

PEVs represent a promising future direction for the transportation sector by virtue of their potential to decrease the dependence of the sector on fossil fuels and thereby reduce emissions. PEVs are gaining popularity because of their energy efficiency, low cost recharging capability, and overall reduced cost of operation. With the development of smart grids, PEVs will be able to communicate with the grid and decide upon the best way to schedule and operate their charging activities at strategic times.

A PEV draws some, or all, of its electrical energy needs from the power grid. Recharging the PEV battery is typically carried out in residential garages equipped with standard outlets, and takes several hours. However, a specialized high voltage/high current electrical outlet can also be used for fast charging; using a higher level charging brings about significant reduction in charging time [70].

2.4.1 Types of PEVs

PEVs are a family of electric-drive vehicles with the capability to recharge using grid electricity. PEVs generally include Plug-in Hybrid Electric Vehicles (PHEV), Extended

Range Electric Vehicles (EREV), and Battery Electric Vehicles (BEV).

A typical BEV has a battery connected to an electric motor that drives the vehicle power train. The batteries are energized from the grid using a battery charger. During regenerative braking, the motor supplies power back to the battery, thus acting as a generator. The design of BEVs is simple and has a low part count, but their driving range is limited to the size of the battery and may take a few hours for recharging, depending on the state-of-charge (SOC) of the battery at the time of charging, battery type, and type of charging used [70].

The EREV is a type of vehicle where the electric motor runs on a battery for a short trip and for longer trips, gasoline powered generators supply electricity to charge the battery. Hybrid Electric Vehicles (HEV) help to reduce gasoline consumption, with the ability to recover a substantial amount of vehicle's kinetic energy in the battery storage system through regenerative braking. PHEVs are similar to HEVs but include a battery and plug-in charger for driving power from the grid. This allows PHEVs to attain a large All-Electric-Range (AER) capability for the portion of a driving trip. The main advantage of PHEV technology is that the vehicle has two fuel sources that allows it to operate even when the battery is fully depleted; the best design allows the vehicle to operate on electric power and reduce fuel consumption as mush as possible. PHEVs are characterized by their AER; for example, a PHEV which can drive x miles solely on electricity is referred to as PHEV-x. Thus, PHEV20, PHEV30 and PHEV60 denotes electric vehicles which can drive 20, 30, and 60 miles, respectively, on battery, and the rest is driven on gasoline [10].

2.4.2 Levels of Charging

The charging level has a direct effect on the charging time, using a higher level decreases the time of charging. Three levels of PEV charging are available [10]:

- Level 1 Charging: This level requires a single-phase and grounded ac line at 120 V, and 12-16 A of current. It uses a standard 3-prong plug with a ground-fault circuit interrupter, and no significant installation is required for residential charging; therefore, there is no significant operation or cost challenge for Level 1 customers and the LDC. However, Level 1 is not considered a preferred means of charging because it takes 8-30 hours to charge a battery depending on its size, which results in reduced battery life and performance.

- Level 2 Charging: This level requires grounding, ground fault protection for users, a no-load make/break interlock which prevents vehicle start-up while charging, and a

safety breakaway for the cable and connector. It uses a single phase ac supply at 240 V, and 32-70 A of current. Depending on the size and capacity of the battery, the charging level takes 2-6 hours to recharge a PEV and requires requires an upgrade of a household electric outlet. These chargers may also be found in public charging stations.

- Level 3 Charging: This level is still under development but several companies are designing these facilities and offering them to customers. These are expected to recharge 50% of a PEV battery capacity in a few minutes, by feeding direct current into the battery sets at variable voltage levels. Level 3 (480-V, three-phase supply) is beyond the capacity of most LDC transformers that serve residential and some commercial areas, and hence the distribution system will need to be redesigned in most cases to accommodate this type of charging. It may be available at specialized fuel stops for PEVs, i.e., charging stations.

2.4.3 PEV Charging Schemes

The time of the day during which PEVs are charged can either have a positive or negative impact on the grid. PEVs should preferably be charged at such hours when there is under-utilized generation capacity, low electricity prices, and the system demand is low. Charging PEVs during peak load hours can result in further increase in the demand peak and thus create a need for additional generators, transmission lines and distribution feeders. Furthermore, with an increase in the penetration level of PEVs, charging during off-peak periods may shift the demand peak to late night hours. Thus, it would be important to convey electricity prices and system conditions to PEV customers and/or smart chargers in real-time, so that optimal decisions for both LDCs and customers on charging schedules can be made.

PEV charging can be categorized as follows:

- Uncoordinated Charging: Customers do not have any communication with the LDC nor a schedule for their PEV charging. This scheme does not consider PEV charging scheduling, and it is thus assumed that the vehicles start charging immediately after they are plugged in. Therefore, customers would typically charge their vehicles as they arrive home in the evening, which could be correlated with peak load, or whenever it is convenient for them, irrespective of the price of electricity. Understandably, such uncoordinated charging would likely result in an increase in system peak demand, which would threaten grid security.

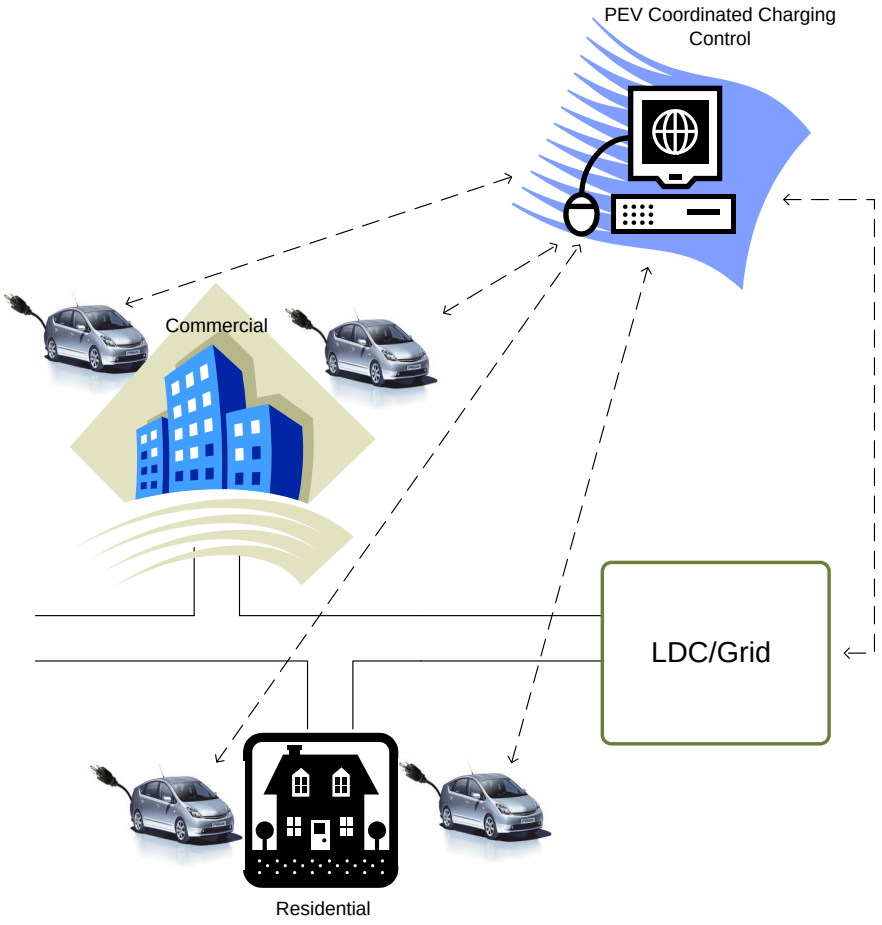

Figure 2.3: Coordinated PEV charging.

- Coordinated Charging: This is based on the idea that consumers smartly distribute their charging periods during off-peak hours, thus maximizing PEV penetration and optimizing the utilization of the grid. This is also referred to as smart charging, where information would be exchanged between cars and charging points; hence, two-way communication would be essential for smart charging technologies to take effect. Figure 2.3 shows a possible architecture for smart charging. Therefore, smart grids need to be planned and developed considering PEV charging as an integral part of the load and the associated energy management systems in households, buildings and feeders [10]. Smart charging can help customers minimize their PEV charging cost, while at the same time significant improve grid operations.

2.4.4 Battery Charging Terminology

Battery charge/discharge rate is the power-demand/delivery capability of a battery, usually stated in watts or kilowatts (W or kW). The battery charging time is determined by the rate at which a battery charges. The rate at which a battery supplies energy to the vehicle electric motor(s), determines the vehicle's acceleration and grade climbing ability in "all-electric" mode [10].

Battery SOC refers to the percentage of charge remaining in the battery. For example, an SOC of 100% means the battery is fully charged, 50% implies half-charged, and 0% SOC means a fully depleted battery [10]. A simple way to represent the SOC of a fully charged PHEV-x in terms of distance driven, is given by [71]:

$$SOC = \begin{cases} 100\left(\frac{x-d}{x}\right) & d \leq x \\ 0 & d > x \end{cases} \tag{2.1}$$

where x is the AER of the PHEV and d is the total distance driven by the vehicle.

The Percentage of Energy Needed (PEN) is the proportion of total energy required to fully charge the battery; thus [71]:

$$PEN = 100 - SOC \tag{2.2}$$

PEN and vehicle type are important factors to determine the energy required to charge a PHEV. The power capacity of an individual PEV depends on: the energy capacity of the battery, whether or not it is plugged in; the capacity of the plug circuit; the SOC of the battery at the initiation of discharge; and the time taken by the vehicle to discharge. The size of the vehicle's usable battery capacity depends on its AER and the electric drive efficiency.

Typical efficiency figures for various categories of vehicles range from 0.25 kWh/mile for compact vehicles to 0.42 kWh/mile for large SUVs. Thus, usable battery capacity is 5 kWh for a compact PHEV20, and 16.8 kWh for a large SUV PHEV40 [72]. Table 2.1 shows the battery capacity for four different types of PHEV20 [71]; by dividing the total kWh by 20 (PHEV20), the required electrical energy per mile (kWh/mile) for each type of vehicle is obtained.

Aggregated electricity demand by PHEVs in a specific region at any given time is referred to as the PHEV charging load profile (PCLP), which can be used to evaluate the distribution system operational performance due to the presence of PEV loads. The PCLP can be determined using information on when each vehicle begins to charge, how much energy is required to charge, and the level of charging available.

Table 2.1: Energy requirements for different types of PHEV20.

Type	Battery Capacity (kWh)	Energy Discharge Rate (kWh/mile)
Compact Sedan	5.65	0.2825
Mid-size Sedan	6.71	0.3355
Mid-size SUV	8.47	0.4235
Full-size SUV	10.24	0.512

Table 2.2: Charging schedule for compact sedan PHEV20 and Level 1 charging.

Hour		1	2	3	4	5	Total kWh
PEN = 100%		1.4	1.4	1.4	1.4	0.91	6.51
PEN=70%	Power Scaling	0.98	0.98	0.98	0.98	0.637	4.557
	Time Scaling	1.4	1.4	1.4	0.357	0	4.557

There are two ways to determine the charging schedule of each vehicle, given its PEN, namely, power scaling and time scaling [71]. The power scaling (constant time) approach scales the electric power delivered to each vehicle, at each hour, based on its PEN, which is multiplied by the appropriate socket capacity to obtain the power at which the PEV would be charged. On the other hand, the time scaling (constant power) approach considers the maximum power that can be delivered based on the charging level at each hour and scales the total energy required. In this approach, vehicles are charged based on the maximum power available from the electric outlet and not on PEN. For example, if the battery capacity of a particular PEV is 6.51 kWh with a 70% PEN, this means that energy required by the battery is 0.7*6.51 kWh = 4.557 kWh; assuming Level 1 charging, where the available power is 1.4 kW, the PHEV battery draws 1.4 kW in the first three hours and in the fourth hour would draw the remaining power. Table 2.2 presents a simple example to demonstrate the difference between the two charging schedules. The time scaling approach is more accurate than the power scaling approach [71].

In this work, PEV models are integrated within a DOPF to study the operational impact of uncontrolled and controlled charging schemes on distribution feeders. Various objective functions from the perspectives of LDC and the customer are considered.

2.5 Mathematical Programming

Mathematical programming is a modeling paradigm that is used in decision making problems. It encompasses optimization models, which are used to solve a problem in an optimal way while meeting all its conditions. An optimal solution of an optimization problem is any point in the feasible region that optimizes (maximizes or minimizes) the objective function.

2.5.1 Linear Programming (LP)

LP problems refer to the optimization of a linear objective function subject to linear equality and/or inequality constraints, and can be mathematically stated in the following general form [73]:

$$\begin{aligned} \min \quad & c^T x \\ \text{s.t.} \quad & A x \leq b \\ & l \leq x \leq u \end{aligned} \tag{2.3}$$

where x is an n-dimensional decision vector, A is an mxn matrix, c and b are n and m-dimensional known parameter column vectors, and l and u are the lower and upper bounds of x, respectively. The LP constraints define the polyhedron of a feasible region, with the optimal solution lying at a corner of the feasible region.

The simplex method is the most widely used method to solve an LP problem, and has been improved with methods such as revised simplex and primal-dual methods. To obtain an optimal solution, the simplex method begins with an extreme point in the feasible region and then moves along a direction that improves the objective function value to a neighboring extreme point [73]. The interior-point method (IPM) can also be used to solve an LP problem and usually requires less iterations; therefore, for large problems, the IPM is preferred over the simplex method. The IPM reaches an optimal solution by traversing the interior of the feasible region, and solves LP problems by generating a sequence of interior points from an initial interior point [73].

Mixed-integer linear programming (MILP) is an LP problem in which some variables are integers. These problems are more difficult to solve and there is no single method that performs consistently well for all problems. MILP problems can be solved using the Branch and Bound (B&B) method and the Cutting plane method [74]. The B&B algorithm separates the problem into sub-problems, each with a smaller feasible region, and calculates

the bounds on the best solution that can be obtained from these smaller problems. In the cutting-plane method, cuts/inequalities are added to the relaxed LP problem which does not remove any integer feasible solution, and cuts are added until extreme points of the feasible region are integers; cuts can be generated by inspection, as they are problem specific, or using gomory cuts. Branch-and-cut consists of a cutting-plane method that improves the relaxed LP of the integer programming problem, and then an B&B algorithm is used to solve the problem by branching; this method first solves the relaxed LP problem, and the solution is then improved by adding a cutting-plane algorithm to obtain integer solutions [74]. The cutting-plane algorithm further adds linear constraints to the relaxed LP problem, which are satisfied by all feasible integer points but violated by the current LP relaxation solution; this process is repeated until either an optimal integer solution is obtained or no more cutting planes are found.

2.5.2 Non-linear Programming (NLP)

If the objective function or at least one of the constraints in the optimization problem is a non-linear function of its decision variables, then such a problem is referred to as an NLP problem. A general NLP problem can be expressed as follows [73]:

$$\min \quad z = f(x) \tag{2.4}$$

$$\text{s.t.} \quad h(x) = 0 \tag{2.5}$$

$$g(x) \leq 0 \tag{2.6}$$

The feasible solution for NLP problems is the set of all points $(x_1, x_2, \cdots, x_n)$ that satisfy all constraints in (2.5) and (2.6) and locally minimize the objective function. Note that any maximization problem can be converted to a minimization problem by multiplying the objective function with -1. NLPs are more difficult to solve as compared to LP problems.

First-order methods evaluate the function values and its first-order derivatives (gradient). The gradient provides a direction to the search, unless it is zero. In order to choose the correct direction, the length of the direction under consideration (step size) should be restricted. A gradient descent finds a local minimum; in this case, the step is taken proportional to the negative of the gradient of the function at the current point. In practice, this method results in a zig-zag descent before reaching the optimal solution and is thus computationally expensive. Conjugate-gradient methods are used to correct the zig-zag of the steepest-descent method, and takes into account previous directions to solve larger problems [73].

Second order methods compute function values, its first derivatives (the gradient) and Hessians (second-order gradient). The Newton's method is a second-order method and is expressed by the second-order Taylor series; in this case, the solution is moved toward a new point which yields zero gradients using a correction factor (the inverse of the Hessian). The Newton's method is usually favored, as it converges very quickly when in the neighborhood of a minimum. However, the search direction of Newton's method becomes undefined when the Hessian matrix is singular. Also, the computational effort required to obtain the inverse of Hessian matrices may be large even for small problems. The Quasi-Newton method is used to overcome the computational issues of Newton's method by approximating the Hessian matrix by a positive definite matrix, which is updated so that it converges to the exact Hessian matrix [74].

Mixed Integer Non Linear Programming (MINLP) are NLP problems with integer variables. These problems are generally solved using decomposition techniques, which breaks the problem into a continuous problem and an integer problem. Different methods such as extended cutting planes and LP/NLP-based B&B can be used to solve each subproblem; the Benders' decomposition method is one of the methods used to solve large-scale MINLP problems [75]. Decomposition methods reduce the number of iterations, computational time, and required memory space. Heuristic methods are also popular methods to solve MINLP problems, with commonly used algorithms such as neural networks, and evolutionary algorithms such as Particle Swarm Optimization (PSO), Genetic Algorithms (GA), evolutionary programming, evolutionary strategy, and Tabu search. In general, all the available algorithms can be categorized into two groups: direct algorithms with finite number of operations, and iterative algorithms with sequence of iterations converging to a solution close to the optimal and satisfying the stopping criterion [76], [77].

Computational robustness and burden are the main challenges for solving the MINLP DOPF problem for real-time control purpose. The complexity of the DOPF is substantial for a 24-hour horizon, because of the large number of variables and the presence of inter-temporal constraints. Commercially available softwares, particularly BARON [78] and DICOPT [79], are not viable options, as these solvers are computationally inefficient in terms of robustness and CPU time [22]. In [21], a quadratic penalty approach is used to reduce the computational burden of the DOPF; the continuous variables are rounded up or down to their closest integer values and a heuristic approach is used to search for an optimal solution within a feasible region. However, the heuristic search method is carried out for each hour independently, and therefore the solution obtained is sub-optimal over a 24-hour horizon.

The 24-hour DOPF model with inter-temporal constraints proposed in this thesis considers LTCs and SCs as continuous variables. This renders the model an NLP problem that

can be solved easily using commercially available solvers. Since the main purpose of this work is to study the impact of PEVs and smart loads on distribution feeders, and not their optimal voltage control, and since the numerical differences in the solutions considering discrete versus continuous variables is minimal, as demonstrated in an example discussed in this thesis, the NLP problem can be considered sufficient for the studies presented in this thesis.

2.5.3 Mathematical Modeling Tools

Many commercial tools and solvers are available for solving LP and NLP problems. The General Algebraic Modeling System (GAMS) is a popular, commercially available, mathematical modeling platform used in this research [80]. Different solvers are available in GAMS to solve the optimization problems. In this work, the SNOPT (Sparse Nonlinear OPTimizer) solver is used, as it is capable of solving NLP problems even with discontinuous derivative, efficiently. This solver uses a sequential quadratic programming (SQP) method to determine the search direction from quadratic programming (QP) sub-problems, and it is designed for problems where the gradient of the objective function and constraints is known, using the quasi-Newton approximation method, which requires less memory and avoids computing second derivatives [81].

2.6 Neural Network (NN) Models

The NN can be defined as [82]: "An interconnected assembly of simple processing elements, *units* or *nodes*, whose functionality is loosely based on the animal neuron. The processing ability of the network is stored in the interunit connection strengths, or *weights*, obtained by a process of adaption to, or *learning* from, a set of training patterns." Thus, the NN comprises a set of simple processing elements called neurons, which operate on the input using activation functions. The topology of interconnection and rules employed by any NN are called the paradigm of the network. The NN can be designed to have many different paradigms depending on the intent of the network [82].

The universal approximation theorem states that any arbitrary continuous function can be approximated closely by a multi-layer NN [82]. This is valid only for a NN that uses a restricted class of activation functions such as sigmoidal functions; an example of such an activation function is the following tansigmoid activation function:

$$tanh(n) = \frac{e^n + e^{-n}}{e^n - e^{-n}} \tag{2.7}$$

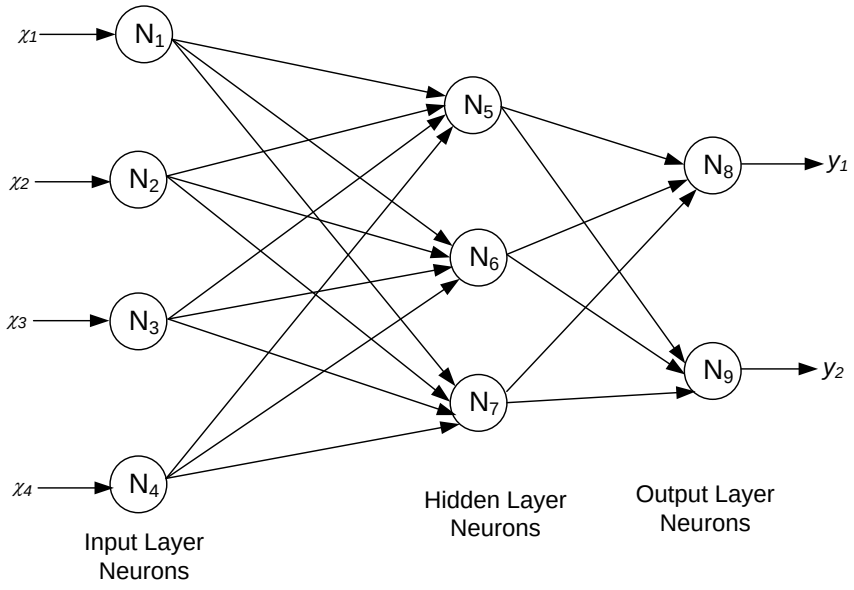

Figure 2.4: Feed forward NN topology.

There are two topologies for NNs based on the interconnectivity of the network:

- Feedforward: In this topology, each input to the network is fed into a different neuron, i.e., the neurons are laid out in layers, and each subsequent layer has an interconnection with the proceeding layer. The input layer neurons are connected to the hidden layer neurons which perform transformations on the input. The output of these neurons are defined as the output of the entire network. Such a feedforward network can transform one pattern into another, and can consequently be used for pattern detection or for associative memory. A typical topology of the feedforward network is shown in Fig 2.4.

- Feedback: This topology is also known as a recurrent NN. The output of any layer may be fed back to its proceeding layers. This network acts as a content addressable memory [83].

NNs have been widely used in engineering applications such as for signal enhancement, noise cancellation, and system identification. The literature in power system has also seen many applications of NNs, for example, in load forecasting [84], operational planning studies [85], and others. One standard application of neural networks is its use as a function approximation tool.

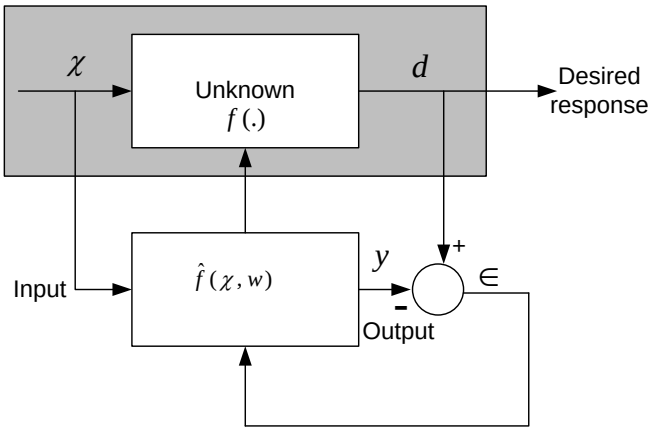

Figure 2.5: Supervised training as function approximation [83].

The NN uses external data to automatically set its parameters, i.e., it is made aware of the output through a performance feedback loop. This feedback is utilized to change the parameters through systematic procedures called learning or training rules, so that the system output improves with respect to the desired goal, i.e., the error decreases through training. Therefore, the NN can be used to model loads that are usually represented by polynomial models. Generally, the NN can achieve better approximation than mere polynomials because of its well known universal function approximation capability [86]. In order to describe the dynamic behavior of loads, NN based load models have been proposed in the literature; for example, a NN methodology applied to load modeling is presented in [86].

Given a set of input vectors χ and a set of desired responses d, the NN finds the parameters that meet these specifications. This problem is referred to as function approximation when the desired response d is an unknown fixed function of the input, i.e., $d = f(\chi)$, as shown in Figure 2.5 [83]. The goal of the function approximation problem is to "discover" the function $f(.)$ given a finite number of input-output pairs (χ, d). The output function $y = \hat{f}(\chi, w)$ depends on a set of parameters w, which can be modified to minimize the discrepancy between system output y and the desired response d. The Levenberg-Marquardt algorithm is a very common method used to minimize the performance function in NNs based on its gradient; it has an adequate performance and is not affected by the accuracy required on the function approximation.

NN-based estimation models for power system loads allow inclusion of various inputs and at the same time allows multiple outputs. By increasing the number of hidden layers,

a higher-order function can be obtained. It should be noted that determining accurate load characteristics is very important in feeder operation problems, particularly in the smart grid environment. In this thesis, a residential micro-hub load is modeled using NNs from real measurement and simulated load data.

2.7 The Energy Hub Management System [51]

The energy hub is a novel concept in smart grids, developed in the context of integrated energy systems with multiple energy carriers for real-time management of energy production, consumption, storage, and conservation at the customer level for the benefit of both customers and LDCs [87]. EHMS controls are divided into two levels: micro- and macro-hubs, the micro-hub represents a customer at the lower level while the macro-hub level corresponds to the LDC at the upper level [50].

Figure 2.6 presents an overview of the residential micro-hub that includes various appliances, energy storage systems (e.g., batteries, PEVs), energy production systems (e.g., solar photovoltaic, wind power), a smart meter and two-way communication links between these components; the optimization solver as well as the mathematical model are located within the central hub controller [50]. This controller uses the mathematical model of each appliance in the hub, their parameter settings, and external inputs such as weather forecast, energy price, and peak demand to generate the optimal operating decisions for all appliances over the scheduling horizon. The scheduling horizon can vary from a few hours to days, depending on the type of energy hub and activities taking place in the hub. For example, in a residential energy hub the scheduling horizon is typically set to 24 hours, with time intervals ranging from few minutes to 1 hour.

A typical macro-hub comprises several micro-hubs that communicate with the macro-hub, as shown in Figure 2.7. The demand patterns from individual micro-hubs can be aggregated to form the system load profile for the LDC. The DOPF model proposed here has been developed to be the intelligence of the macro-hub, so that it is used in conjunction with the load profiles, to determine optimal controls and schedules for various distribution system components, and also return a control signal to the individual micro-hubs if any changes in their demand patterns is required.

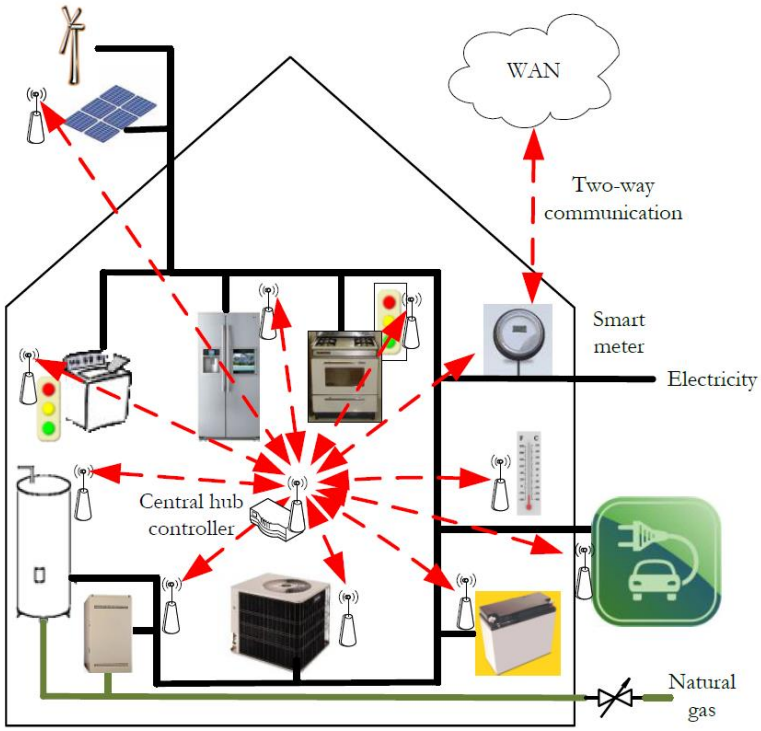

Figure 2.6: Configuration of a residential micro-hub [11]. (Used with permission of the EHMS project.)

2.8 Summary

In this chapter, first a relevant overview of smart grids has been presented, followed by power distribution systems and its components, and an introduction to DA. The VVC problem was also discussed, since it is one of the essential features of distribution system operation, pertinent to smart grids and this thesis. A background review of PEVs, its charging principles and level of charging are also presented in detail given their relevance to the present work. Furthermore, a brief review of mathematical programming problems and commonly used solution methods applicable to the DOPF problem was presented. A summary of NNs, different NN topologies, and their function approximation capability used in this thesis was presented. Finally, a summary on the EHMS concept, micro- and macro-hubs was presented.

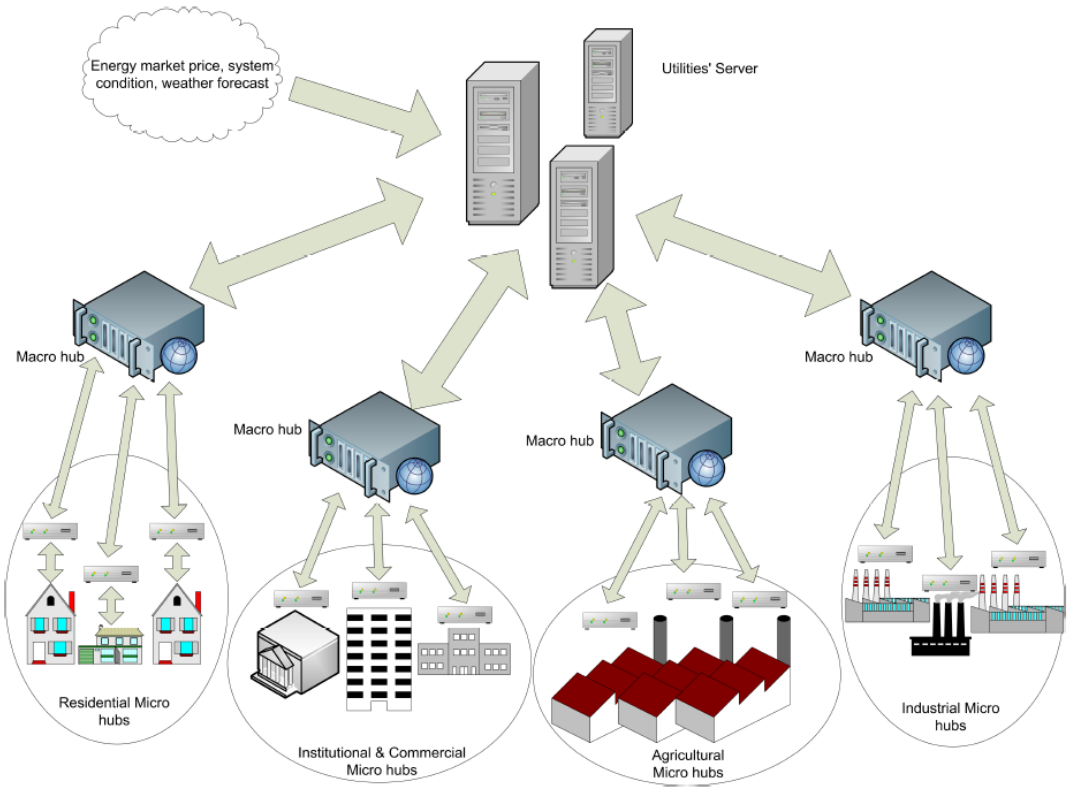

Figure 2.7: Overall picture of the EHMS [11]. (Used with permission of the EHMS project.)

Chapter 3

Smart Charging of PEVs in Residential Distribution Systems

3.1 Introduction

This chapter presents a novel modeling framework for the analysis of PEV charging in unbalanced, residential distribution systems. A DOPF framework is proposed to determine the controlled or smart charging schedules, and hence address the short-comings of uncontrolled charging. Various objective functions, namely, energy drawn by the LDC, total feeder losses, total cost of energy drawn by LDC and total cost of PEV charging, are considered. The effect of peak-demand constraints imposed by the LDC is also studied within the DOPF framework for various smart charging scenarios, and uncontrolled versus smart charging schemes are compared, from both the customer's and the LDC's perspective. Analyses are also presented considering a probabilistic representation of the initial SOC and start time of charging for various scenarios to take into account variable in customers' driving patterns.

The reminder of the chapter is structured as follows: Section 3.2 presents the nomenclature of all indices, parameters, and variables used in the modeling of the three-phase DOPF. The overall framework of the DOPF is discussed in Section 3.3. Modeling details of distribution system components including PEV loads, network equations, operating conditions, and objective functions considered, are discussed in Section 3.4. Section 3.5 presents the assumptions made to evaluate the operational impact of charging PEVs, and also discusses various scenarios considered in this work. Detailed analyses of uncontrolled and controlled charging scenarios are carried out considering constant impedance and ZIP loads for two

standard test feeders, i.e., the IEEE 13-node test feeder and an actual distribution feeder, in Section 3.6; furthermore, probabilistic studies are carried out considering uncertainties in the initial SOC and starting time of PEV charging. Finally, Section 3.7 summarizes the chapter.

3.2 Nomenclature

Indices

C	Controllable capacitor banks, $C \in n$.
C_n	Controllable capacitor banks at node n.
EV	PEV loads, $EV \in L$.
EV_n	PEV load at node n.
k	Hours, k = 1,2,...,24.
l	Series elements.
L	Loads, $L \in n$.
L_n	Loads at node n.
n	Nodes.
N_o	Set of nodes, $n \in N_o$.
p	Phases, $p = a, b, c$.
r	Receiving-end.
r_n	Receiving-ends connected at node n.
s	Sending-end.
s_n	Sending-ends connected at node n.
SS	Substation node, $SS \in n$.
t	Controllable tap changer, $t \in l$.

Parameters

ΔQ	Size of each capacitor block in capacitor banks [Var].
ΔS	Percentage voltage change for each LTC tap.
η	PEV charging efficiency.
γ	Average hourly load of a residence [W].
ρ	Hourly forecast market price [$/MWh].
τ	Time interval in hours [h].
θ	Load power factor angle [rad].
$ABCD$	Three-phase ABCD matrices; A unitless, B in Ω, C in Siemens, D unitless.
C^{max}	PEV battery capacity [Wh].

Ic^o	Load current at specified power and nominal voltage [A].
I^{max}	Maximum feeder current limits [A].
N	Number of PEVs owned by a residence.
$N^{'}$	Number of PEVs connected in each phase and node.
$\overline{N}$	Maximum number of capacitor blocks available in capacitor bank.
$\overline{P}$	Maximum power drawn by PEV battery [W].
PD	Load at n node [W].
Pc	Active power of load [W].
$\overline{PD}$	Maximum allowable peak demand [W].
Qc	Reactive power of load [Var].
SOC^f	Final state of charge of the PEV battery.
SOC^i	Initial state of charge of the PEV battery.
$\overline{tap}, \underline{tap}$	Maximum and minimum tap changer position.
V^o	Specified nominal voltage [V].
V^{max}	Maximum voltage limit [V].
V^{min}	Minimum voltage limit [V].
X	Reactance of capacitor [Ω].
Z	Load impedance at specified power and nominal voltage [Ω].

Variables

cap	Number of blocks of switched capacitor banks.
I	Current phasor [A].
$\overline{I}$	Vector of three-phase line current phasors [A].
I^o	Load current at nominal voltage [A].
$J_1 - J_4$	Objective functions.
P	Power drawn by PEV [W].
Q	Reactive power of capacitor banks [Var].
tap	Tap position.
V	Voltage phasor [V].
$\overline{V}$	Vector of three-phase line voltages [V].

3.3 Smart Distribution System Model

The proposed smart distribution system operation framework including PEV smart charging is depicted in Figure 3.1, where forecasted inputs of the LDC's load profile for the next

day, RTP, number of PEVs to be charged at a node and phase, and their initial SOCs are available. Executing the proposed DOPF, the PEV smart charging schedules and operating decisions for taps, capacitors and switches for the next day can be determined. The DOPF model can be used within a MPC framework to revise the LDC's operating decisions when there is a discrepancy between the actual inputs from their forecast values; the MPC approach incorporates forecast and newly updated information to arrive at an improved set of optimal decisions [27]. Thus, at a given time k, the forecast inputs available over a given time horizon (e.g. 24 h) can be used to solve the DOPF to obtain decisions over this time horizon; if there is a change in any of the inputs, the DOPF model could be rerun to obtain improved revised decisions.

The proposed framework cannot be implemented within the existing communication infrastructure now available in distribution feeders. More sophisticated two-way communication devices would be necessary for both LDCs and customers to realize this approach, such as those that have been implemented and deployed in the EHMS project [51].

3.3.1 Three-phase Distribution System

A generic distribution system comprises series and shunt components. The series components include conductors/cables, transformers, transformer LTCs and switches which are modeled using ABCD parameters, computed from relationships between sending- and receiving-end voltages and currents [58]:

$$\begin{bmatrix} \overline{V}_{s,p,k} \\ \overline{I}_{s,p,k} \end{bmatrix} = \begin{bmatrix} A_{(l\times p)} & B_{(l\times p)} \\ C_{(l\times p)} & D_{(l\times p)} \end{bmatrix} \begin{bmatrix} \overline{V}_{r,p,k} \\ \overline{I}_{r,p,k} \end{bmatrix} \quad \forall l, \forall p, \forall k \tag{3.1}$$

The ABCD parameters for conductors, cables, transformers and switches are constants and switches are represented as zero impedances, conductors and cables as π-equivalent circuits, and three-phase transformers are modeled based on the type of connection (wye or delta).

Voltage regulating transformers in a distribution system are equipped with LTCs, whose ABCD parameters cannot be considered constant, since they depend on the tap position at a given time k. Thus, B and C are null matrices while the A and D matrices of the LTCs are modeled using the following equations:

$$A_{t,k} = \begin{bmatrix} 1+\Delta Stap_{t,a,k} & 0 & 0 \\ 0 & 1+\Delta Stap_{t,b,k} & 0 \\ 0 & 0 & 1+\Delta Stap_{t,c,k} \end{bmatrix} \tag{3.2}$$

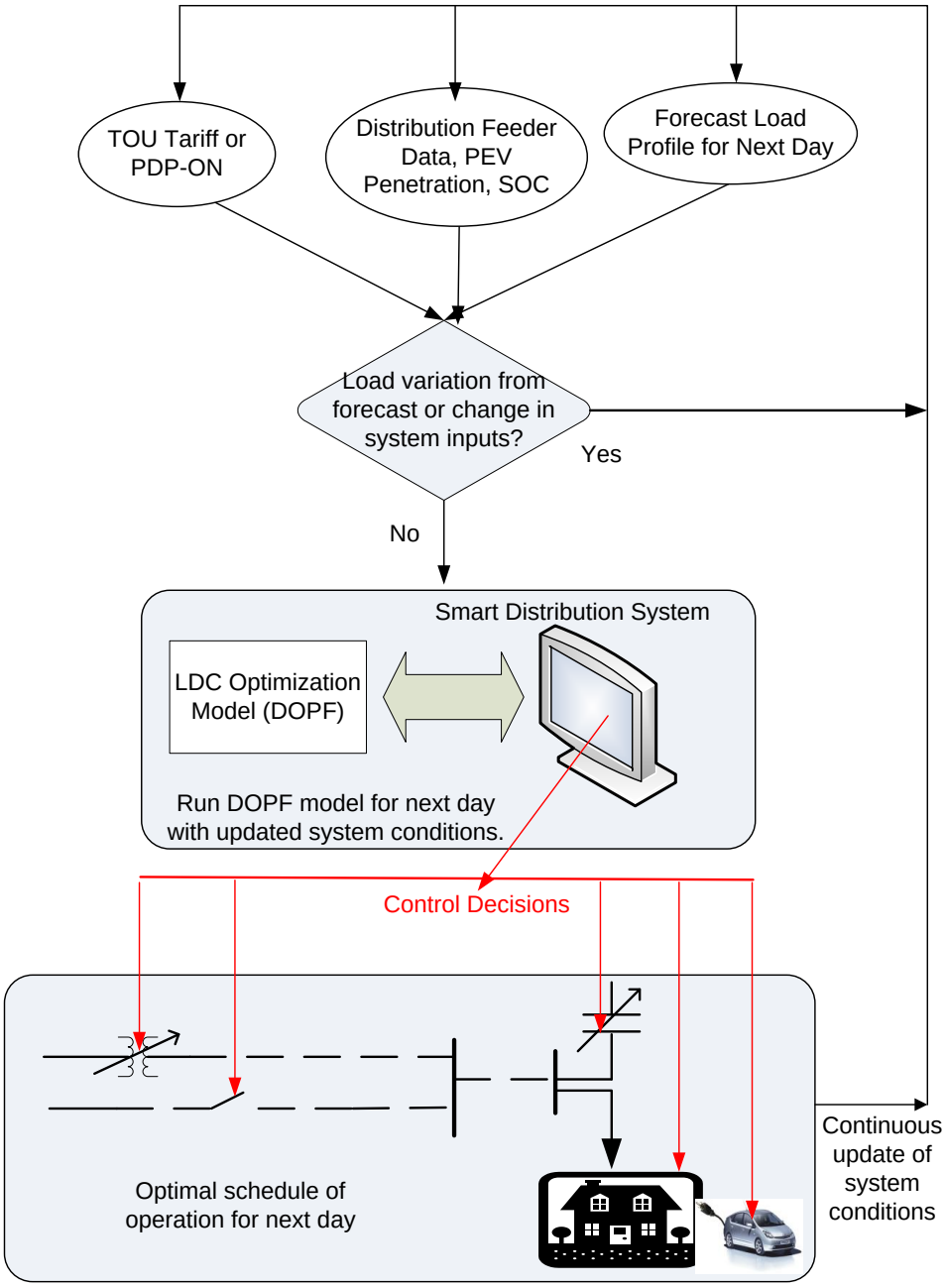

Figure 3.1: The proposed smart distribution system operations framework.

$$D_{(t\times k)} = A^{-1}_{(t\times k)} \qquad \forall t, \forall p, \forall k \tag{3.3}$$

where $tap_{t,a,k}$, $tap_{t,b,k}$ and $tap_{t,c,k}$ are tap controls in the respective phases for the LTC, and are considered continuous variables, which can take any value between -16 and +16, for a 32-step LTC. For a three-phase tap changer, the tap operations are considered identical in the three phases:

$$tap_{t,a,k} = tap_{t,b,k} = tap_{t,c,k} \qquad \forall t, \forall k \tag{3.4}$$

Shunt components comprise loads and capacitor banks and are modeled separately to represent unbalanced three-phase loads. In distribution systems, the electrical loads are typically modeled as voltage dependent to better represent the types of loads encountered in distribution feeders [88]. In this work, the loads are either modeled as constant impedance, with the following equations representing wye-connected impedance loads on a per-phase basis:

$$V_{L,p,k} = Z_{L,p,k} I_{L,p,k} \qquad \forall L, \forall p, \forall k \tag{3.5}$$

or as a mix of constant impedance (Z), constant current (I), and constant power (P), i.e, ZIP, loads. Capacitor banks are modeled as multiple capacitor blocks with switching options, on a per-phase basis, as follows:

$$V_{C,p,k} = X_{C,p,k} I_{C,p,k} \qquad \forall C, \forall p, \forall k \tag{3.6}$$

$$jX_{C,p,k} = j\frac{V^{o2}_{C,p,k}}{Q_{C,p,k}} \qquad \forall C, \forall p, \forall k \tag{3.7}$$

$$Q_{C,p,k} = cap_{C,p,k}\, \Delta Q_{C,p,k} \qquad \forall C, \forall p, \forall k \tag{3.8}$$

where $cap_{C,p,k}$ is a continuous variable, and can take any positive value from 0 to $\overline{N}_{C,p}$.

The PEV is modeled as a controlled current load, on a per-phase basis, as follows:

$$|I_{EV,p,k}|\angle I_{EV,p,k} = |I^{o}{}_{EV,p,k}|\angle V_{EV,p,k} \qquad \forall EV, \forall p, \forall k \tag{3.9}$$

$$Re(V_{EV,p,k} I^{*}_{EV,p,k}) = P_{EV,p,k} \qquad \forall k, \forall p, \forall EV \tag{3.10}$$

It is assumed that no significant reactive power is drawn by the PEV loads, thus treating them as unity power factor loads. Furthermore, the total energy drawn by the PEV battery over the charging period, taking into account its efficiency η_{EV}, is equal to the battery charging capacity; thus:

$$\tau \sum_{k} \eta_{EV} P_{EV,p,k} = (SOC^{f}_{EV,p} - SOC^{i}_{EV,p}) C^{max}_{EV,p} N'_{EV,p} \qquad \forall EV, \forall p \tag{3.11}$$

The maximum power that can be drawn by the battery is constrained by $\overline{P}_{EV}$, the socket capacity of a standard electrical outlet, which depends on the level of charging, and is given as follows:

$$P_{EV,p,k} \leq \overline{P}_{EV} N'_{EV,p} \qquad \forall EV, \forall p, \forall k \tag{3.12}$$

Equations (3.1)-(3.12) represent the various components of the three-phase distribution system including PEV loads. To model the distribution system in its totality, these elements are required to satisfy the current balance at each node and phase (Kirchhoff's Current Law):

$$\sum_{l} I_{l,p,k}(\forall r_n) = \sum_{l} I_{l,p,k}(\forall s_n) + \sum_{L} I_{L_n,p,k} + \sum_{C} I_{C_n,p,k} + \sum_{EV} I_{EV_n,p,k} \quad \forall n, \forall p, \forall k \tag{3.13}$$

And the voltage at the node and phase, at which a given set of components are connected, are the same as the corresponding nodal voltages (Kirchhoff's Voltage Law):

$$V_{l,p,k}(\forall s_n) = V_{l,p,k}(\forall r_n) = V_{L_n,p,k} = V_{C_n,p,k} = V_{EV_n,p,k} \qquad \forall p, \forall n, \forall k \tag{3.14}$$

3.3.2 Smart Distribution System Operation

The proposed three-phase DOPF model determines the PEV charging schedules for various objective functions, considering the specified range of charging periods and grid operational constraints. The decision variables in the DOPF model in this Chapter are the power drawn by the aggregate PEV loads at each node and phase, and the taps and capacitor switching decisions while the nodal voltages and feeder currents are the state variables. The different objective functions considered in this work represent the perspectives of the LDC and the customers as follows:

- Minimize the total energy drawn by the LDC over a day from the external grid:

$$J_1 = \sum_{k} \sum_{p} Re\left(V_{SS,p,k} I^*_{SS,p,k}\right) \tag{3.15}$$

  This objective represents a situation where the LDCs are stipulated by regulatory agencies, as in Ontario, Canada, to bring about a reduction in their energy consumption levels.

- Minimize total feeder losses over a day:

$$J_2 = \sum_{k} \sum_{p} \sum_{n} Re\left(V_{s_n,p,k} I^*_{s_n,p,k} - V_{r_n,p,k} I^*_{r_n,p,k}\right) \tag{3.16}$$

In the analysis of distribution systems, where loads are modeled to be voltage dependent, this objective seeks to improve the voltage profile across distribution nodes.

- Minimize the total cost of energy drawn by the LDC from the external grid over a day:

$$J_3 = \sum_k \left(\sum_p Re(V_{SS,p,k} I^*_{SS,p,k}) \right) \rho(k) \tag{3.17}$$

where $\rho(k)$ is the hourly price at which the LDC procures its energy from the external system. This price is generic and need not depend on the market structure. Thus, it can be the day-ahead price if there exits a day-ahead market settlement process, or the day-ahead forecast of the real-time price, or even a fixed price or tariff.

- Minimize the total cost of PEV charging:

$$J_4 = \sum_k \left(\sum_p \sum_{EV} P_{EV,p,k} \right) \rho_1(k) \tag{3.18}$$

This objective can be used by the LDC to study the system impact of PEV charging, expecting rational behavior of customers, i.e., customers seeking to minimize their charging costs. It is assumed that all customer homes are equipped with smart meters and are subject to RTP or TOU tariff $\rho_1(k)$, about which the customers are assumed to have sufficient information, so that they schedule their PEV charging accordingly. In real life, the two prices $\rho(k)$ and $\rho_1(k)$, are different from each other, because of the LDC's network costs, global adjustments, etc., included in the latter. However, in this work, it is assumed that $\rho(k)$ is equal to $\rho_1(k)$ without loss of generality.

The 3-phase distribution feeder and its components, modeled by (3.1)-(3.12), and the network equations (3.13)-(3.14), are the constraints of the DOPF model. Other constraints of the DOPF model comprise the feeder operating limits that include the limits on node voltages, feeder currents, taps, and capacitors, as follows:

$$V^{min} \leq |V_{n,p,k}| \leq V^{max} \qquad \forall n, \forall p, \forall k \tag{3.19}$$

$$|I_{i,j,p,k}| \leq I^{max}_{i,j} \quad \forall i \in s_n, \forall j \in r_n, \forall p, \forall k \tag{3.20}$$

$$\underline{tap}_{t,p} \leq tap_{t,p,k} \leq \overline{tap}_{t,p} \qquad \forall t, \forall p, \forall k \tag{3.21}$$

$$0 \leq cap_{C,p,k} \leq \overline{N}_{C,p} \qquad \forall C, \forall p, \forall k \tag{3.22}$$

The LDC may also impose a peak demand constraint, based on its substation capacity, as follows:

$$\sum_{L_n} \sum_{p} \left\{ Re \left(V_{L_n,p,k} I^*_{L_n,p,k} \right) + P_{EV,p,k} \right\} \leq \overline{PD}_k \tag{3.23}$$

The proposed DOPF model given by (3.1)-(3.23) is an NLP problem, which is modeled in GAMS and solved using the SNOPT solver [81]. In this work, the taps and capacitors are modeled as continuous variables, as mentioned earlier, to alleviate the introduction of integer variables and hence retain the model as an NLP problem, thereby keeping the computational burden reasonable. This is a reasonable assumption, since the main purpose of this work is to study the impact of PEV charging on feeders, and not the optimal voltage control of these feeders.

The output of the DOPF pertaining to the PEVs is the aggregated power drawn by PEV loads, at an hour, node and phase $P_{EV,p,k}$. The PEV charging current $I^o_{EV,p,k}$ can then be obtained from the model. In order to determine the number of PEVs to be charged, $P_{EV,p,k}$ can be used, after the optimization solution is obtained, as follows:

$$N^{chg}_{EV,p,k} = \frac{P_{EV,p,k}}{\overline{P}_{EV}} \tag{3.24}$$

For example, from the above equation, if a $P_{EV,p,k} = 17$ kW is obtained, and knowing that $\overline{P}_{EV} = 4.8$ kW, using (3.24), $N^{chg}_{EV,p,k}$ is calculated to be 3.54. From this, the LDC can infer that there should be three PEVs allowed to charge at this node, phase and hour, drawing 4.8 kW each, while a fourth PEV should be allowed to draw only 2.6 kW. Note that the determination of individual PEV charging levels is not considered here, since the objective is to study the charging problem from the perspective of the LDC; in this context, the simple method outlined above is a reasonable way to determine the number of PEVs charging at a node and phase.

3.4 Assumptions and Scenarios

3.4.1 Assumptions

In order to evaluate the system impact of smart charging of PEVs vis-à-vis their uncontrolled charging, the following assumptions are made:

- A 24-hour time horizon is assumed, with time interval of τ=1 h. However, the proposed DOPF can accommodate smaller time steps if required, but at increased computational costs.
- The entire load at a node on the feeder section, denoted by $PD_{p,L}$, are residential loads. Furthermore, it is assumed that if a house owns a PEV, it owns exactly $N_{p,L} = 1$ number of vehicles.
- The average monthly electricity consumption of a residence is 1500 kWh [89]. Hence, the average hourly load of the residence (γ) is calculated to be 2.08 kW.
- Mid-size sedans PHEV30 with 9.76 kWh battery capacities are considered [71]. This implies that 60% of the vehicle kilometers are driven on battery and the rest on gasoline [90].
- PEVs are the only dispatchable loads at a node and are not capable of delivering power back to the grid. Furthermore, all the PEVs at a node and phase are aggregated, which is a reasonable assumption in the context of the studies presented here, which concentrate on the feeder.
- Since all PEVs are assumed to be residential loads, these are not available for charging between 7 AM to 5 PM when people are at work.
- The charging efficiency η_{EV} is assumed to be 85%, and only Level 2 charging (208-240V/40-100A) is considered.
- For the deterministic studies, the SOC of the PEV battery at the start of charging is 20% and it is charged to 90% of its full capacity at every node. In probabilistic studies, a lognormal distribution of the initial SOC is considered for each node.
- In deterministic studies, all the PEVs are assumed to have a minimum charging time of 2 hours [91], since the value of $\overline{P}_{EV}$ considered is 4.8 kW [10]. For probabilistic studies, the minimum charging time of PEVs depends on the initial SOC.
- The charging current of the PEV is assumed to remain constant and not vary with the SOC of the battery.
- As mentioned in Section 3.4.2, $\rho(k)$ is assumed equal to $\rho_1(k)$. In this work, these prices are assumed to be the Hourly Ontario Electricity Price (HOEP) which applies uniformly and hourly to all participants in the wholesale electricity market of Ontario [92], [93], and is used for all the analysis reported here. The HOEP profile used in

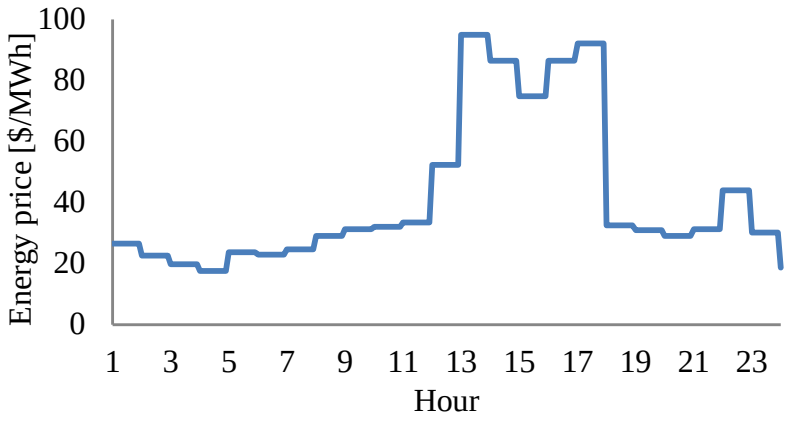

Figure 3.2: Ontario HOEP for a weekday on 30 June, 2011.

this work is depicted in Figure 3.2; and note that peak prices occur between hours 13-18.

Using the aforementioned assumptions, the number of PEVs connected in each phase and node $N'_{n,p}$ can be realistically estimated for an x p.u. penetration of PEV by:

$$N'_{n,p} = floor\left(x\ floor\left(\frac{PD_{n,p}}{\gamma}\right)N_{p,L}\right)\quad \forall n, \forall p \tag{3.25}$$

A penetration of $x = 1.0$ means that every residence has one PEV, while $x = 0$ is the base case with no PEVs in the system. All analyses presented in this chapter are carried out for $x = 0.5$, i.e., every second house has a PEV, and the PEV load being added to the existing distribution system spreads over the 13-hour charging period.

3.4.2 Scenarios

Uncontrolled Charging or Business as Usual (Case 1)

This case assumes that customers charge their PEVs as and when they want to, without any regard for system constraints, and the LDC has no control on the PEV charging schedules and hence uncontrolled charging takes place. The following two scenarios are considered in this case, as presented in Table 3.1:

Table 3.1: Scenarios of uncontrolled charging.

	S_1	S_2
Objective Function	None	J_4
Nodal voltage limits	No	No
Feeder current limits	No	No
System peak demand constraint	No	No
Charging period	20, 21 h	1-6, 18-24 h

- S_1: This scenario assumes that the customers charge their PEVs in the shortest possible time (two hours), after plugging in. Although, customers are not interested in minimizing the charging cost, they are aware of the prevailing electricity rates, such as, for example, that the off-peak TOU price begins at 7 PM, as in Ontario [94], or that the off-peak RTP commences from 7 PM as shown in Figure 3.2; accordingly, in this scenario, PEV charging is carried out between 8 to 10 PM. Also since node voltages or feeder current limits are not a concern, this scenario is simulated using a distribution load flow program without considering any limits on node voltages or feeder currents. This scenario effectively represents the worst case, as it results in concentrated buildup of charging loads, which coincides with the period of peak demand on the distribution feeder.

- S_2: This scenario assumes that customers receive fairly precise forecast of $\rho_1(k)$. And they are equipped with smart HEMS (e.g. [11]) that determines optimal operational schedules for various home appliances such as air conditioner/heating, washer, dryer, and other appliances, as well as PEV charging, so as to reduce their overall electricity cost. In this scenario, the LDC has no control on the PEV charging schedules, and hence limits on node voltages or feeder currents are not considered.

Smart Charging (Case 2)

In smart charging, the LDC is envisaged to send control signals to PEVs for charging purpose, considering grid constraints such as node voltage limits and feeder current limits. The LDC may also impose the system peak-demand constraint (3.23) while determining the PEV charging schedules. The following four different smart charging scenarios are considered, as summarized in Table 3.2:

Table 3.2: Scenarios of smart charging.

	S_3	S_4	S_5	S_6
Objective Function	J_1	J_2	J_3	J_4
Nodal voltage limits	Yes			
Feeder current limits	Yes			
System peak demand constraint	Yes			
Charging period	1-6, 18-24 h			

- S_3: In this scenario, the LDC minimizes the total energy drawn from the substation over a day, as per (3.15).
- S_4: In this case, the LDC seeks to minimize the total feeder losses in the system over a day, as per (3.16).
- S_5: In this scenario, the LDC minimizes the total cost of energy drawn from the external grid over a day, as per (3.17).
- S_6: In this case, the LDC determines the charging schedules assuming rational behavior of customers, while at the same time respecting system constraints to prevent feeder problems. Node voltage limits and feeder current limits are considered while the LDC seeks to minimize the total cost of PEV charging over a day, as per (3.18). It should be noted that this scenario is the "controlled" or "smart" version of S_2.

3.5 IEEE 13-node Test Feeder Results

The IEEE 13-node test feeder (Figure 3.3 [95]) is used in this work to examine the proposed DOPF model and smart charging aspects of PEVs in distribution systems. As mentioned earlier, the capacitors are modeled as multiple capacitor banks with switching options, i.e., the capacitor at Bus 675 is assumed to comprise five capacitor blocks of 100 kVar in each phase, and at Bus 611 comprise 5 capacitor blocks of 50 kVar in phase c. The 24-hour load profile in [96] is used in this work for the analytical studies. The number of PEVs at each node and phase for a 50% penetration is given in Table 3.3.

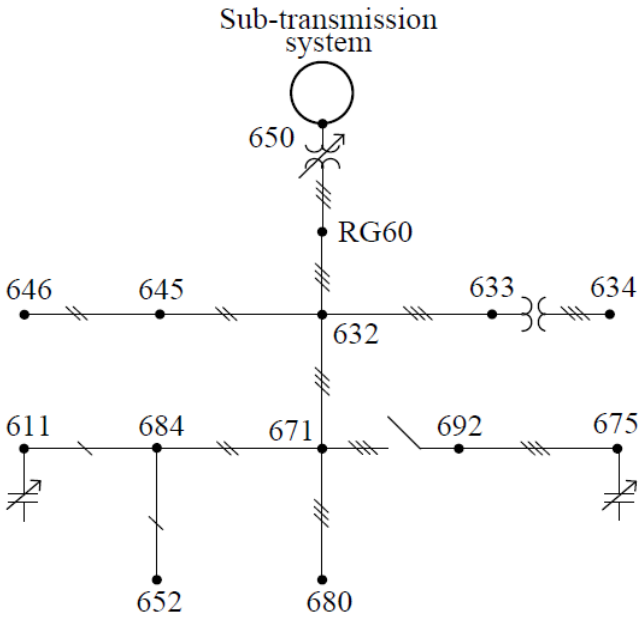

Figure 3.3: IEEE 13-node test feeder [95].

Table 3.3: Number of PEVs at each node and phase in the IEEE 13-node test feeder.

Node	a	b	c
671	92	92	92
632-671	4	15	28
692	-	-	40
611	-	-	40
634	38	28	28
675	116	16	69
652	30	-	-
646	-	55	-
645	-	40	-

3.5.1 Case 1

Figure 3.4 shows a comparison of the total system demand over a 24-hour period for the uncontrolled charging scenarios S_1 and S_2. Note that for S_1, a new peak is created at 9

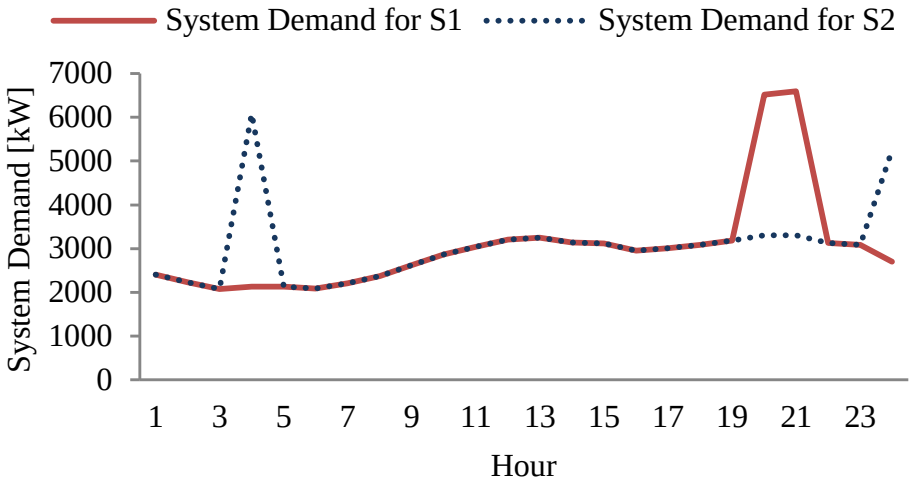

Figure 3.4: Total demand for S_1 and S_2.

PM and the system demand increases by 100% and 103% at 8 PM and 9 PM, respectively. On the other hand, in S_2 the charging occurs at 4 AM and at midnight, when the energy price is low, also creating new peaks in the system. Figure 3.5 shows how the main feeder (650-632) current is impacted in scenarios S_1 and S_2; observe that the main feeder current exceeds the maximum limit in all three phases, thereby leading to possible feeder problems. Figure 3.6 shows that the node voltages drop significantly at 8 PM, especially in phases a and c, because of uncontrolled charging in S_1.

A summary comparison of the two scenarios of uncontrolled charging S_1 and S_2 is presented in Table 3.4. Note that for uncontrolled PEV charging, without regard for charging costs or system conditions (S_1), the system impact is much more severe than when the PEV owners seek to minimize their charging costs (S_2). For instance, the energy drawn is reduced by 6.8% and the PEV charging cost is reduced by 40.3% in S_2 as compared to S_1. However, as noted in Figures 3.5 and 3.6, both S_1 and S_2 are detrimental to the system, because feeder current limits are exceeded and several bus voltages are below acceptable limits.

3.5.2 Case 2

Minimize Total Energy Drawn by LDC (S_3)
Since the loads are modeled as voltage dependent, by operating the system close to the lower

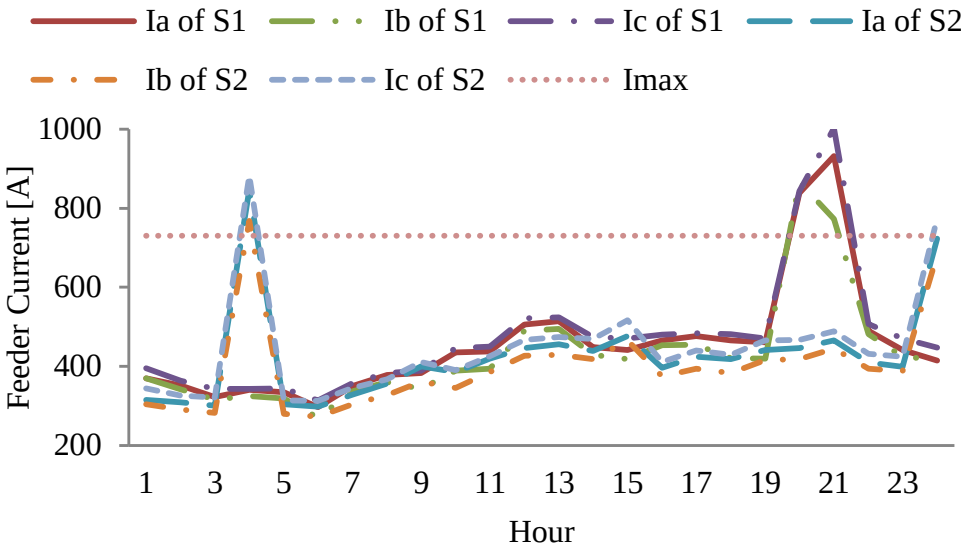

Figure 3.5: Phase-wise Feeder 650-632 current for uncontrolled charging S_1 and S_2.

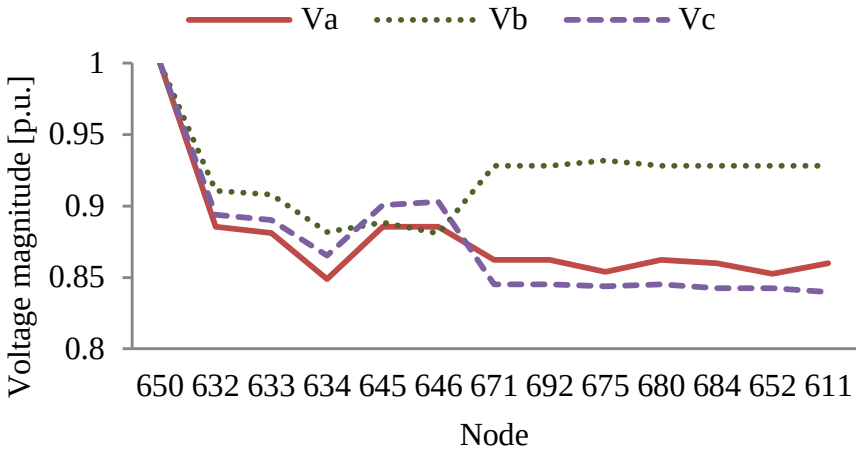

Figure 3.6: Phase voltage magnitude at 8 PM for uncontrolled charging S_1.

acceptable voltage limit of 0.95 p.u., the total energy drawn is minimized. Figure 3.7 shows the system base demand (without PEV loads) and the system demand profile including PEV charging loads, with and without the peak-demand constraint (3.23). Observe that the system demand exceeds $\overline{PD}$ at hour 21 because the PEV charging load coincides with

Table 3.4: Summary results of uncontrolled PEV charging scenarios for the 13-node feeder.

	S_1	S_2	S_2 vs S_1 change [%]
Energy drawn by LDC [kWh]	73,727	68,669	-6.8
Feeder losses [kWh]	2,232	1,950	-12.6
PEV charging cost of customers [$/day]	196	117	-40.3
Cost of energy drawn by LDC [$/day]	3,119	2,806	-10

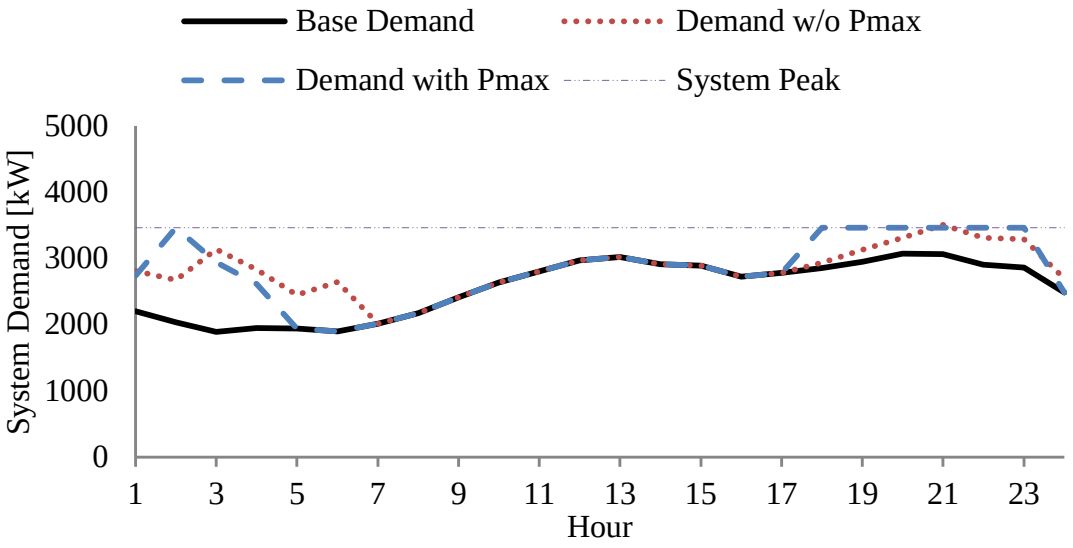

Figure 3.7: Total demand with and without peak-demand constraint for S_3.

the system peak at this hour. Note that when peak demand is limited, the PEV charging schedule is adjusted appropriately within the allowable charging hours, as the system demand is restricted. The base demands corresponding to scenarios S_3-S_5 are obtained by minimizing the respective objective functions without considering PEVs, and the base demand in S_6 is obtained by subtracting the PEV charging load from the corresponding total demand.

Figure 3.8 presents the phase-wise demand with and without PEVs. Observe that the PEV charging mainly occurs during late evening and early morning hours. It should be mentioned that the feeder current magnitudes in this scenario are within limits, and the node voltages are close to 0.95 p.u.

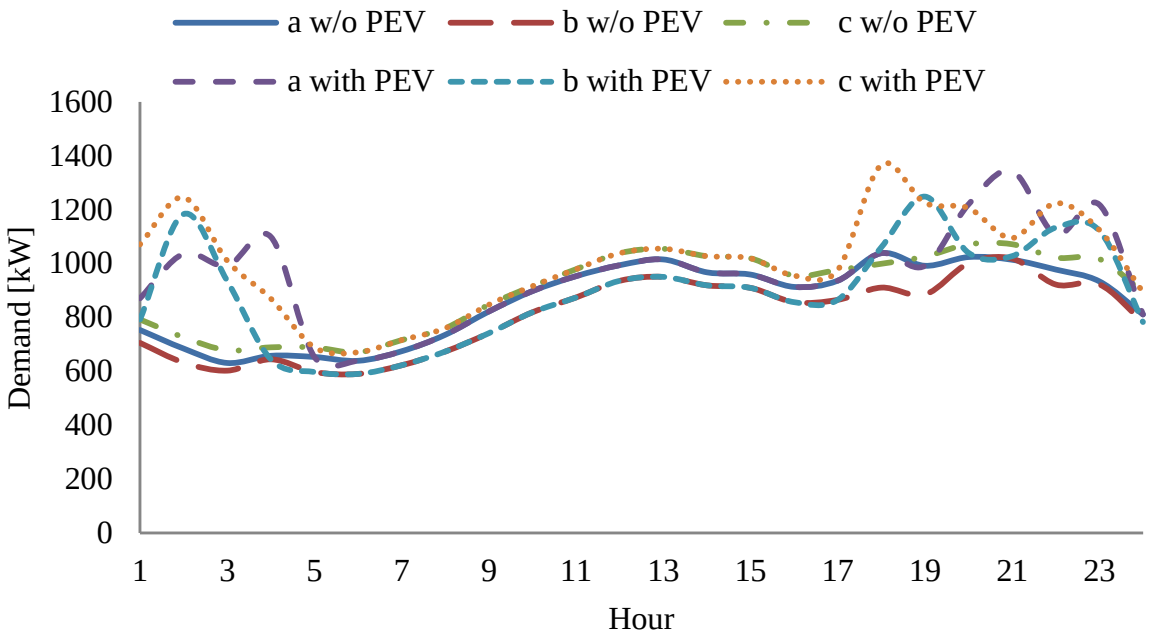

Figure 3.8: Phase-wise total demand with and without PEV loads for S_3.

Minimize Total Feeder Losses (S_4)
Figure 3.9 shows that the resulting system demand including PEV charging load is below $\overline{PD}$, in spite of constraint (3.23) being not imposed in this scenario. The nodal voltages improve and feeder current magnitudes are below their respective maximum limits. Furthermore, most of the PEV charging occurs in all phases during early morning hours, from midnight to 6 AM, when the base load is low, as shown in Figure 3.10. This scenario results in a fairly flat load profile, without any steep peaks at any hour, as compared to other scenarios, and the node voltages are significantly improved as compared to S_3.

Minimize Total Cost of Energy Drawn by LDC (S_5)
Figure 3.11 shows the total system demand with and without peak-demand constraint (3.23), considering the PEV charging load. In this scenario, the LDC schedules the charging of PEV loads when electricity prices are low, i.e., at 4 AM, midnight and 3 AM. At midnight, the PEV charging load added to the system base load results in a system peak.

Because of the increase in demand when electricity prices are low, some feeder current magnitudes reach their maximum limit at midnight and 4 AM. Including constraint (3.23) in DOPF reduces the feeder current magnitudes below their maximum limit. Consequently,

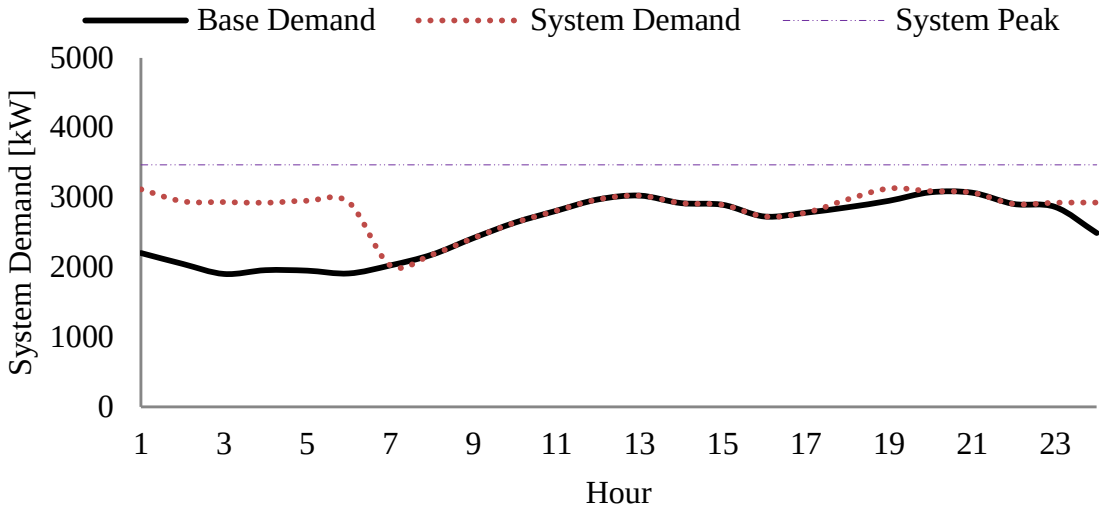

Figure 3.9: Total demand for scenario S_4.

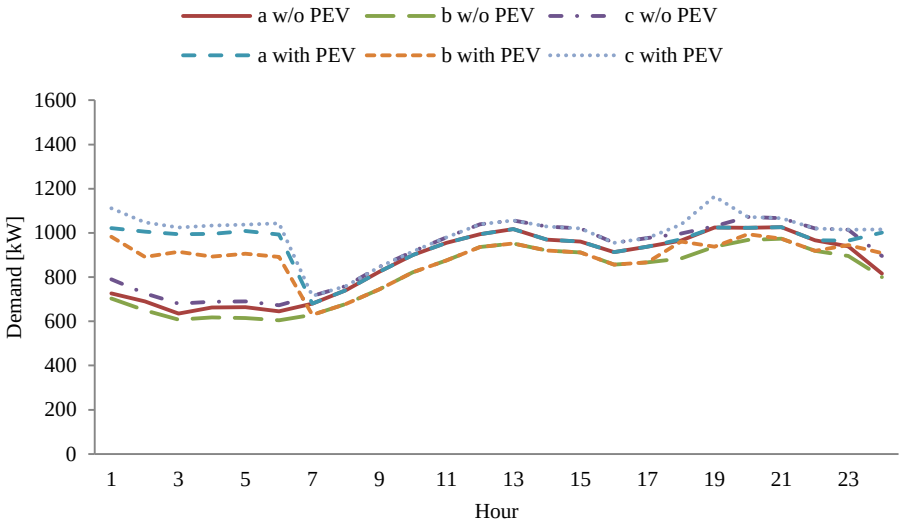

Figure 3.10: Phase-wise total demand with and without PEV loads for S_4.

the PEV charging load is now distributed across more hours, as shown in Figure 3.12. Voltages obtained in this scenario are close to their lower limit of 0.95 p.u., resulting in less energy drawn from the external grid.

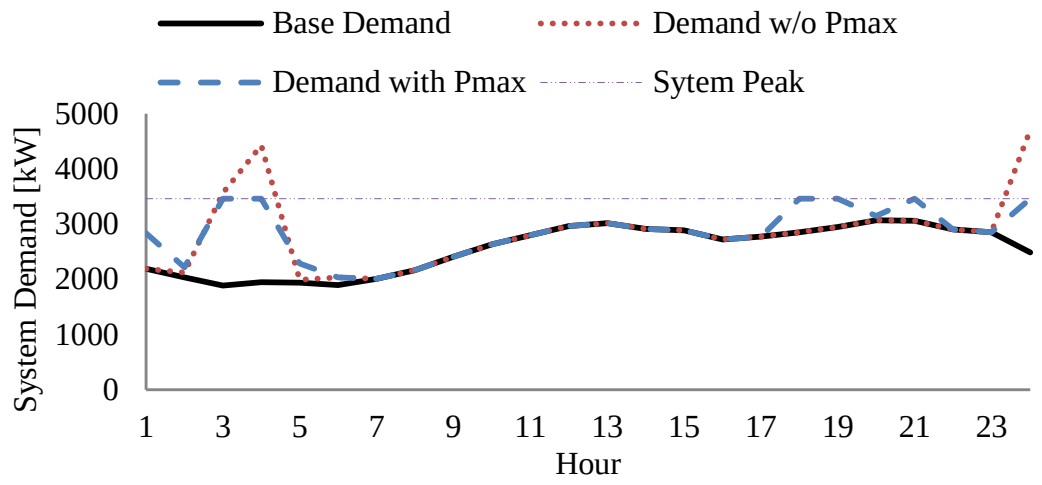

Figure 3.11: Total demand with and without peak-demand constraint for S_5.

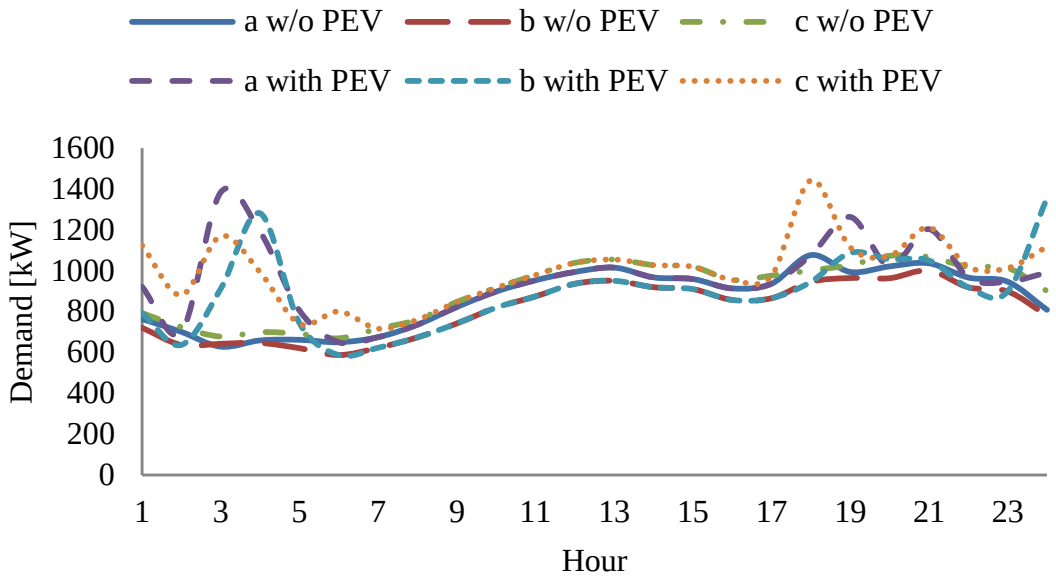

Figure 3.12: Phase-wise total demand with and without PEV loads for S_5.

Minimize Total Cost of PEV Charging (S_6)

In this scenario, the LDC schedules the charging of PEV loads considering the system limits, and at the same time assumes that customers behave rationally and seek to minimize their charging cost. From Figure 3.13, it is seen that when the peak-demand constraint (3.23)

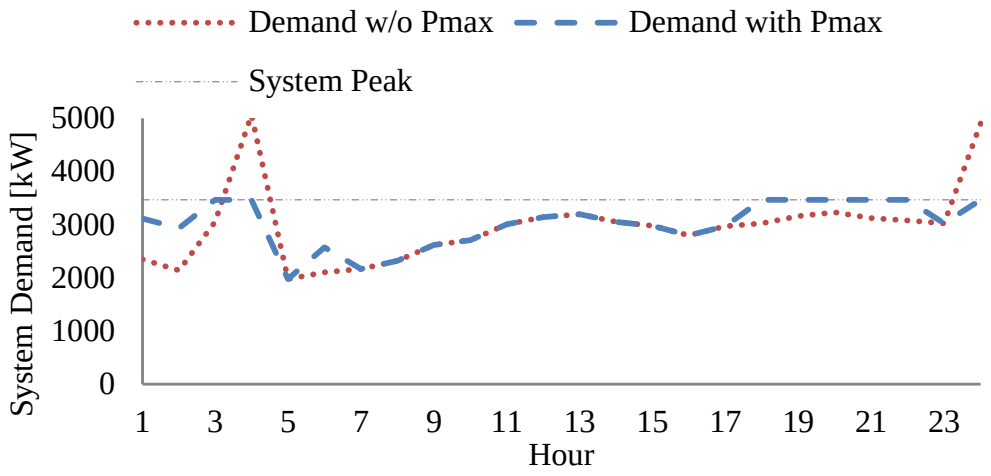

Figure 3.13: Total demand with and without peak-demand constraint for S_6.

is not imposed, the PEV charging is concentrated at 4 AM and midnight when electricity prices are low; this results in a significant increase in system demand at these hours. On the other hand, by imposing constraint (3.23), the PEV charging load is distributed over the next available cheap price hours. The phase-wise PEV charging schedules are shown in Figure 3.14.

Since the PEV charging load is concentrated at 4 AM and at midnight, some feeder current magnitudes reach their maximum limits at these hours. Imposing constraint (3.23) does not reduce these feeder currents below their limits, since the system is operating at the limits. Since minimization of energy drawn is not an objective in this scenario, the voltages are above their lower limits.

3.5.3 Comparison of Smart Charging Scenarios

A comparison of the total energy drawn by the LDC, total feeder losses, total cost of energy drawn by the LDC and the total PEV charging cost for scenarios S_3, S_4, S_5, and S_6 are presented in Table 3.5. As expected, the minimum energy drawn by the LDC from the external grid is in S_3, although the PEV charging cost for customers is maximum, because of the way their charging is scheduled by the LDC. On the other hand, S_6 results in the lowest PEV charging cost for the customers, but requires the LDC to draw a significantly larger amount of energy from the grid, thereby increasing its cost and losses.

An interesting observation can be made for scenario S_5, which seems to be the optimal

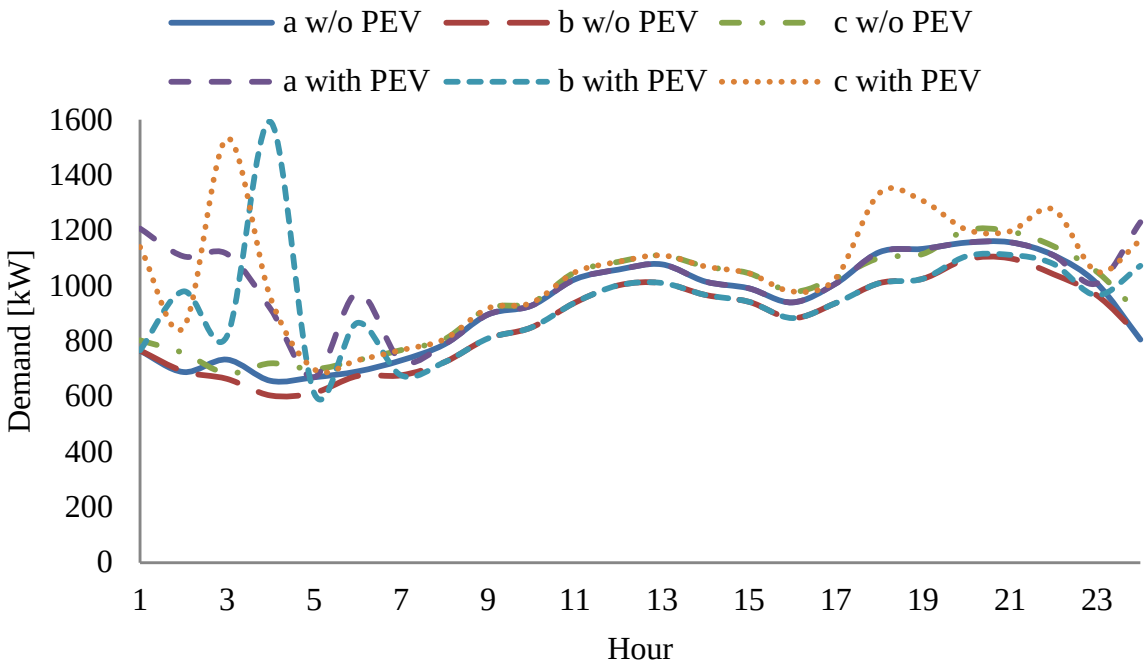

Figure 3.14: Phase-wise total demand with and without PEV loads for S_6.

choice for both the LDC and the customer from their respective perspectives. This scenario results in almost close to minimum PEV charging cost for the customers, while at the same time ensures that the LDC's energy drawn, feeder losses, and cost of energy drawn are within acceptable values. Observe that scenario S_4 also yields reasonably balanced results for both the customers and the LDC.

Figure 3.15 shows the phase-wise voltage magnitudes for the various smart charging scenarios. Scenario S_3 shows voltages close to 0.95 p.u., which results in reduction of energy drawn by the LDC. Since phase c is the most heavily loaded as compared to other phases, voltages in this phase are close to 0.95 p.u. for S_3-S_5. On the other hand, scenario S_6 results in somewhat higher voltages, closer to 1 p.u., in all phases, as compared to the other scenarios, since neither the energy drawn nor feeder losses are minimized in this case.

Figure 3.16 presents phase-wise currents of Feeder 692-675 for all smart charging scenarios. Observe that the feeder current in phase a for S_3, S_5 and S_6 are at its maximum limit for some hours, while phases b and c (mostly) are below the maximum limit.

Table 3.5: Summary results of smart PEV charging scenarios for the 13-node feeder.

	S_3	S_4	S_5	S_6
Energy drawn by LDC [kWh]	69,593	69,715	69,738	73,127
Feeder losses [kWh]	1,829	1,790	1,870	2,035
PEV charging cost of customers [$/day]	162	146	122	119
Cost of energy drawn by LDC [$/day]	2,897	2,886	2,860	3,005

3.5.4 Effect of ZIP Load Models on PEV Smart Charging

The analysis presented in this chapter thus far considers only constant impedance loads. Hence, in order to examine the charging impact for a broader representation of loads, a mix of ZIP loads are also considered here. While constant impedance loads are modeled using (3.5), constant power loads are modeled as follows:

$$Pc_{L,p,k} + jQc_{L,p,k} = V_{L,p,k} I^*_{L,p,k} \qquad \forall L, \forall p, \forall k \tag{3.26}$$

and constant current loads are modeled as:

$$|I_{L,p,k}|(\angle V_{L,p,k} - \angle I_{L,p,k}) = |Ic^o{}_{L,p,k}|\angle\theta_{L,p,k} \qquad \forall L, \forall p, \forall k \tag{3.27}$$

Thus, in the proposed DOPF model, (3.26) and (3.27) are included along with the other equations.

To model voltage independent loads, and thus analyze different cases than the previous studies, the ZIP load mix is assumed to be dominated by constant power loads. Hence, loads at nodes 634, 645, 671, 675, and 632-671 are modeled as constant power loads; loads at nodes 646 and 652 are modeled as constant impedance loads; and loads at nodes 692 and 611 are modeled as constant current loads.

Table 3.6 presents the summary results of the smart charging scenarios considering ZIP loads. All the scenarios depict an increase in energy drawn from the substation, feeder losses, and cost of energy drawn from the substation as compared to scenarios with constant impedance loads (Table 3.5), as expected, since the ZIP loads are dominated by constant power, and thus their energy consumption does not depend on the node voltages.

Figure 3.17 presents the phase voltage magnitudes at Node 675 for the smart charging scenarios with ZIP loads. Comparing these with those obtained with constant impedance loads (Figure 3.15), it can be observed that the voltage profiles are very similar for scenarios

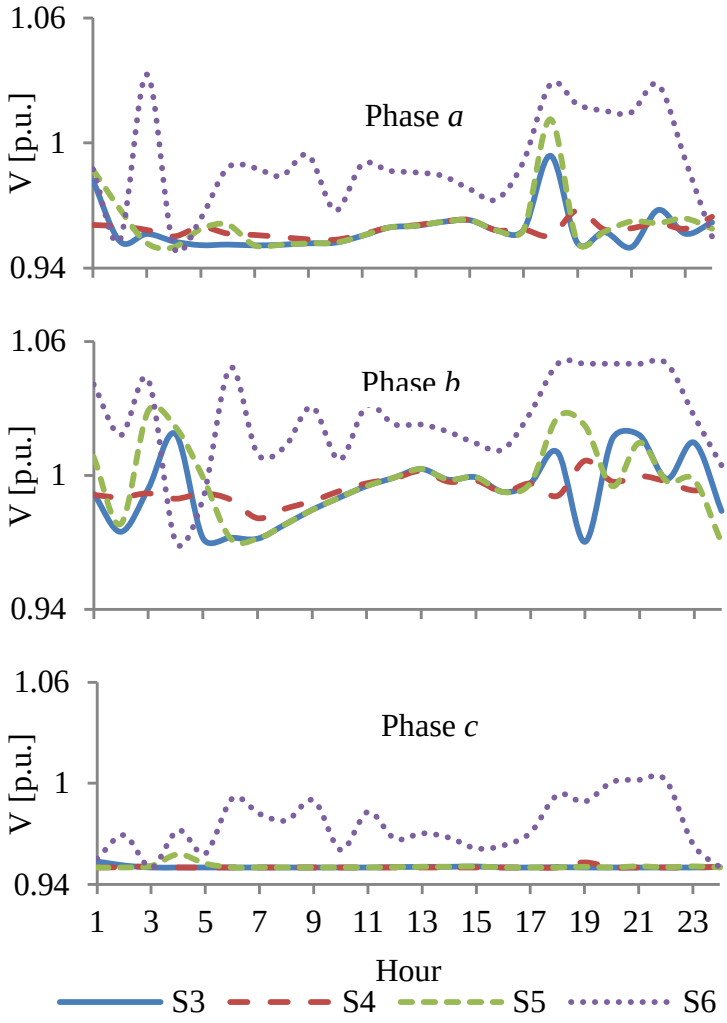

Figure 3.15: Phase voltages at Node 675 for S_3-S_6.

S_3, S_5 and S_6. In scenario S_4, the voltage profiles at Node 675 is significantly improved with ZIP loads. However, it is very difficult to draw general conclusions on the impact of load models on node voltages by analyzing individual nodes. Therefore, an aggregated, phase-wise, voltage deviation index (VDI) is defined, as follows:

$$VDI_p = \sum_k \sum_n \left[V_{n,p,k} - V^{min} \right] \tag{3.28}$$

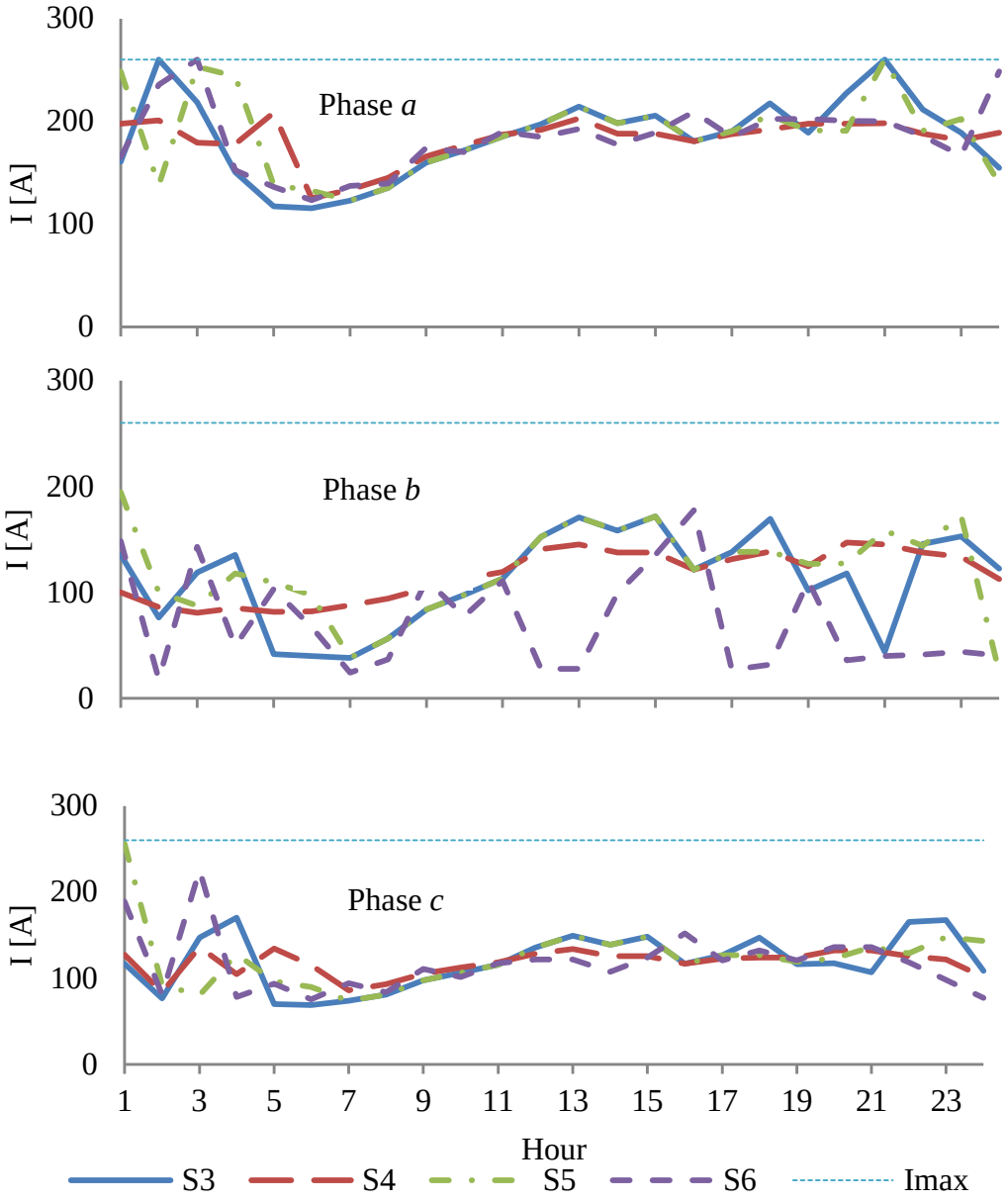

Figure 3.16: Phase-wise Feeder 692-675 current for S_3-S_6.

Table 3.6: Summary results of smart charging scenarios with ZIP loads.

	S_3	S_4	S_5	S_6
Energy drawn by LDC [kWh]	74,132	75,299	74,302	74,945
Feeder losses [kWh]	2,071	1,905	2,106	2,091
PEV charging cost of customers [$/day]	146	146	120	119
Cost of energy drawn by LDC [$/day]	3,077	3,118	3,054	3,076

Thus, in the 13-node test feeder considered, when all the node voltages are at V^{min} in a given phase p, the value of VDI will be zero, while when all node voltages are equal to 1 p.u., the VDI will take a value of 14.4. Therefore, a low value of VDI indicates node voltages close to V^{min}, while VDIs close to or higher than 14.4 indicate a node voltage profile close to or above 1.0 p.u. Table 3.7 presents phase-wise VDIs for constant impedance and ZIP load models, from which the following observations can be made:

- Constant impedance loads have low VDIs, in general, as compared to ZIP loads, implying that ZIP loads result in better voltage profiles.
- In all the scenarios, with both load models, the values of VDI_c are the lowest, since phase c is the most heavily loaded amongst the three phases.
- S_6 presents good voltage profiles, as evident from the high values of VDIs with both load models.
- S_4 with ZIP load models shows improved voltage profiles as compared to constant impedance loads.

Even though constant power loads are pre-dominant in the ZIP load models used, about 11% of the loads in phase a, 22% in phase b, and 27% in phase c are either constant impedance or constant current loads. This makes the behavior of the feeder different from a feeder with constant power loads only. Therefore, in S_3, voltages are close to their minimum allowable limits to draw minimum energy, while in S_4, voltages tend to improve so as to minimize the feeder losses, as shown in Table 3.7.

From the smart charging scenario studies discussed here, it can be observed in general that there is no significant change in the PEV charging schedules when compared to those with constant impedance loads. Hence, one can conclude that there is very little effect of the load models on PEV charging costs.

Table 3.7: VDI for smart charging scenarios with ZIP and constant impedance loads.

	Constant Z Loads			ZIP Loads		
	a	b	c	a	b	c
S_3	5.52	9.60	3.97	7.02	12.42	4.01
S_4	5.50	9.61	3.90	19.54	24.17	17.04
S_5	6.09	10.41	4.10	7.23	12.58	4.19
S_6	14.59	18.93	11.73	15.57	20.40	11.83

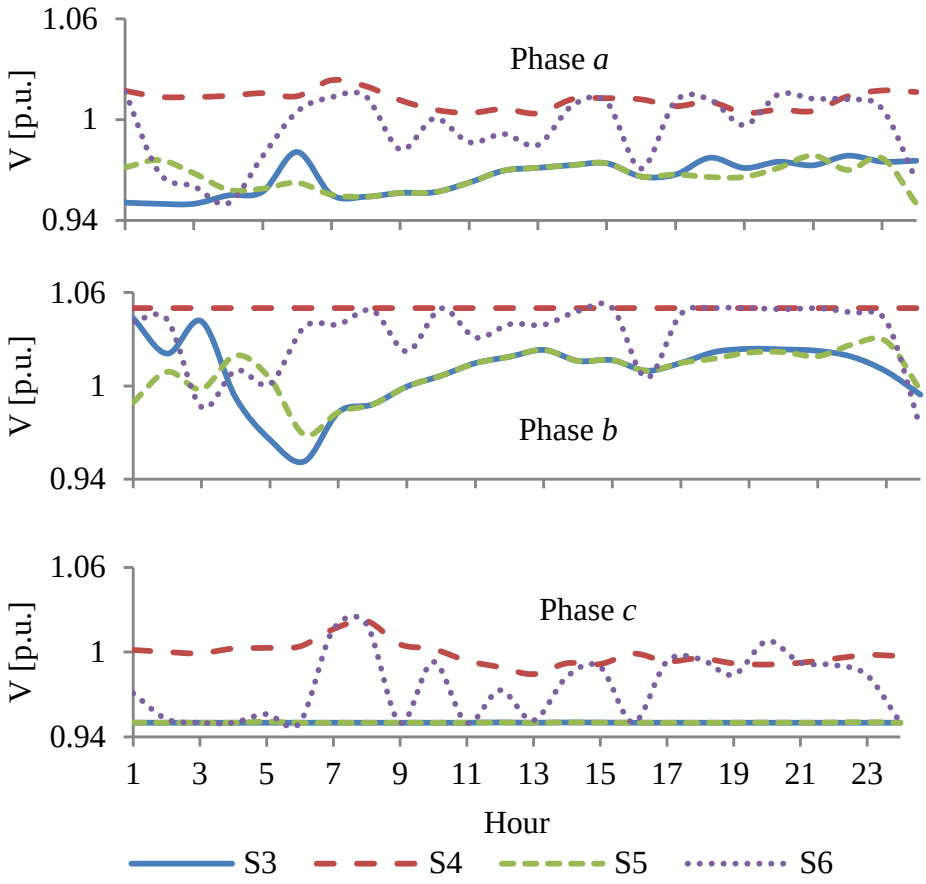

Figure 3.17: Phase voltages at Node 675 for ZIP loads for S_3-S_6.

Table 3.8: Probabilistic studies for uncontrolled charging scenario S_1.

Expected energy drawn by LDC [kWh]	71,356
Expected feeder losses [kWh]	2,022
Expected PEV charging cost of customers [$/day]	174
Expected cost of energy drawn by LDC [$/day]	3,047

3.5.5 Probabilistic Analysis

Uncontrolled Charging Scenario (S_1)

As discussed in Section 3.6.1, S_1 assumes that all the PEVs start charging simultaneously at 8 PM and have a charging time of 2 hours, which leads to a concentrated charging load during 8-10 PM; also, as per Section 3.6.1, SOC^i is assumed to be 20%. These assumptions represent the worst case scenario for the feeder, since full battery charging takes place early, quickly, and simultaneously, coinciding with the system peak demand. However, in practice, the starting time of PEV charging and SOC^i depend on the customers' driving pattern, i.e., miles traveled by the PEV. To model these uncertainties, the starting time of charging and SOC^i are modeled here as lognormal probability distribution function (p.d.f.s), as suggested in [97] and shown in Figure 3.18, for each load node separately. The above distributions are chosen such that the mean values of the starting charging time and SOC^i are 8 PM and 0.35, respectively, since these can be reasonably considered to be the likely plug-in time and battery levels for residential customers.

The resulting plots of probability distributions of the energy drawn by the LDC and the cost of PEV charging obtained from the model are shown in Figure 3.19. The expected values of various decision variables are given in Table 3.8, where it can be observed that these are somewhat lower than those obtained in the deterministic case presented in Section 3.6.1., as expected. These results were obtained using a Monte Carlo Simulation (MCS) approach [98].

Smart Charging Scenarios (S_3-S_6)

As discussed in Section 3.6.1, smart charging scenarios assume an initial SOC of 20%, and a charging window from 7 PM to 7 AM within which the optimal schedules are determined. Unlike S_1, in these scenarios, there is no specified fixed starting time for charging. Modeling the SOC^i using a lognormal p.d.f. as before, Table 3.9 presents the expected values of various decision variables obtained using an MCS approach, i.e., energy drawn by the

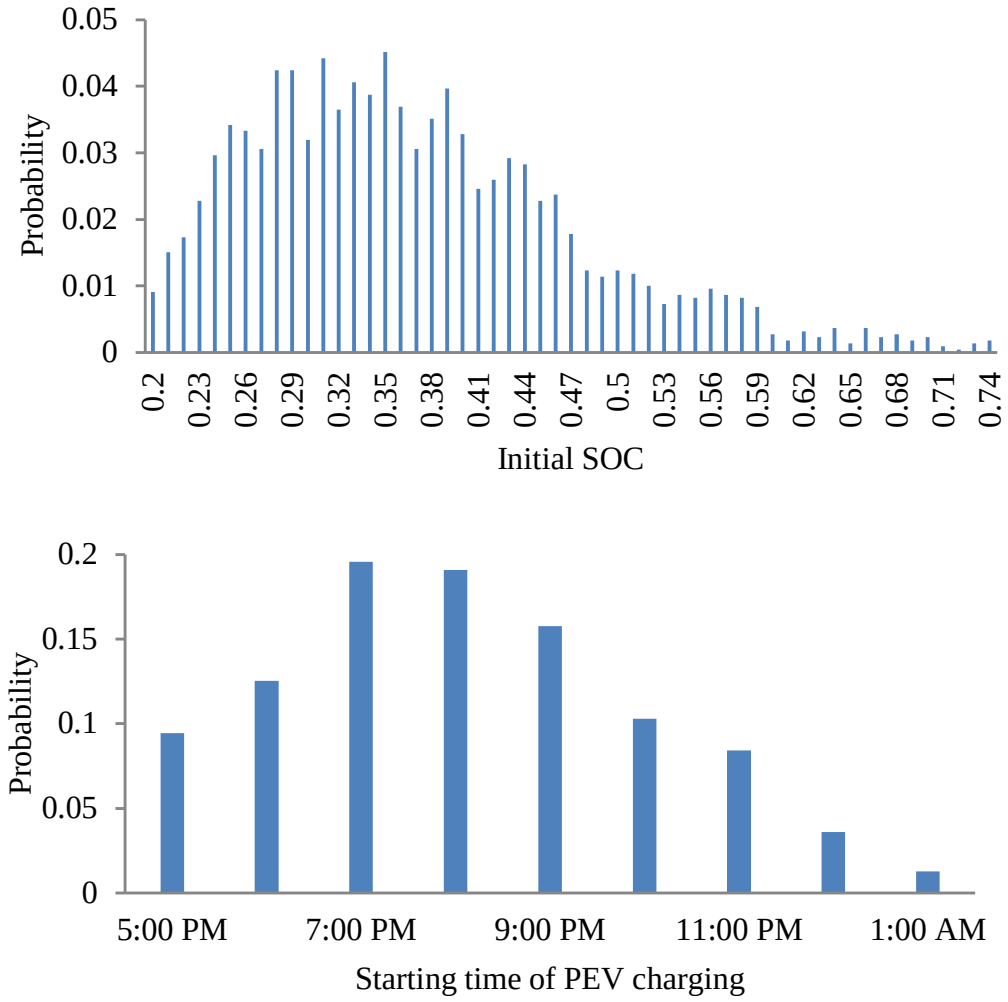

Figure 3.18: Lognormally distributed customers' travel patterns for Node 634.

LDC, feeder losses, PEV charging cost, and cost of energy drawn by the LDC. The expected values obtained are lower than those obtained in the deterministic case (Table 3.5).

Figure 3.20 shows four different plots of p.d.f.s of the decision variables, corresponding to the scenarios in which these variables are being optimized. For example, Figure 3.20(a) shows the probability distribution of the energy drawn by the LDC for scenario S_3, which has the objective of minimizing the energy drawn; similarly, Figure 3.20(b) shows the probability distribution of system losses when the LDC's objective is loss minimization

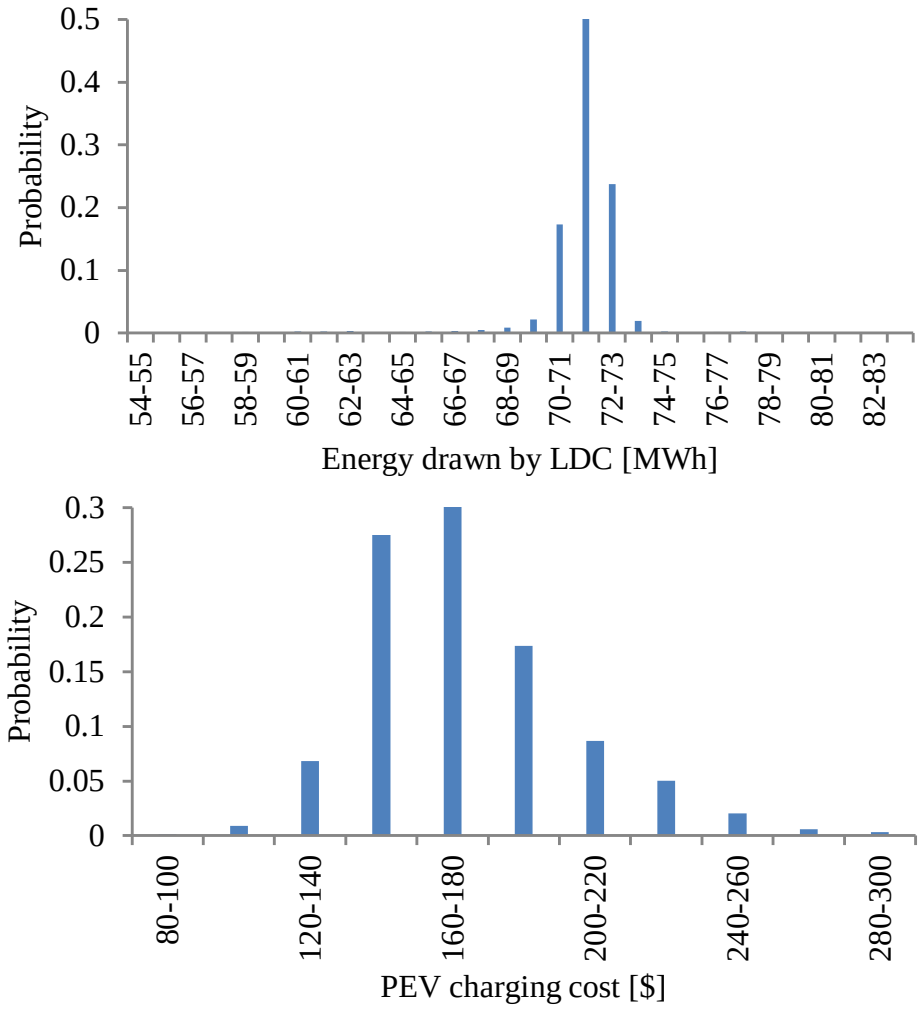

Figure 3.19: Decision variable values for probabilistic uncontrolled charging.

(S_4). These probability distributions depict the range of the values over which the system variables are expected to vary, for the assumed initial SOC lognormal p.d.f.

The probabilistic analyses presented here show that the deterministic studies discussed earlier are reasonable, and correspond to results close to the expected trends for the various relevant variables under study.

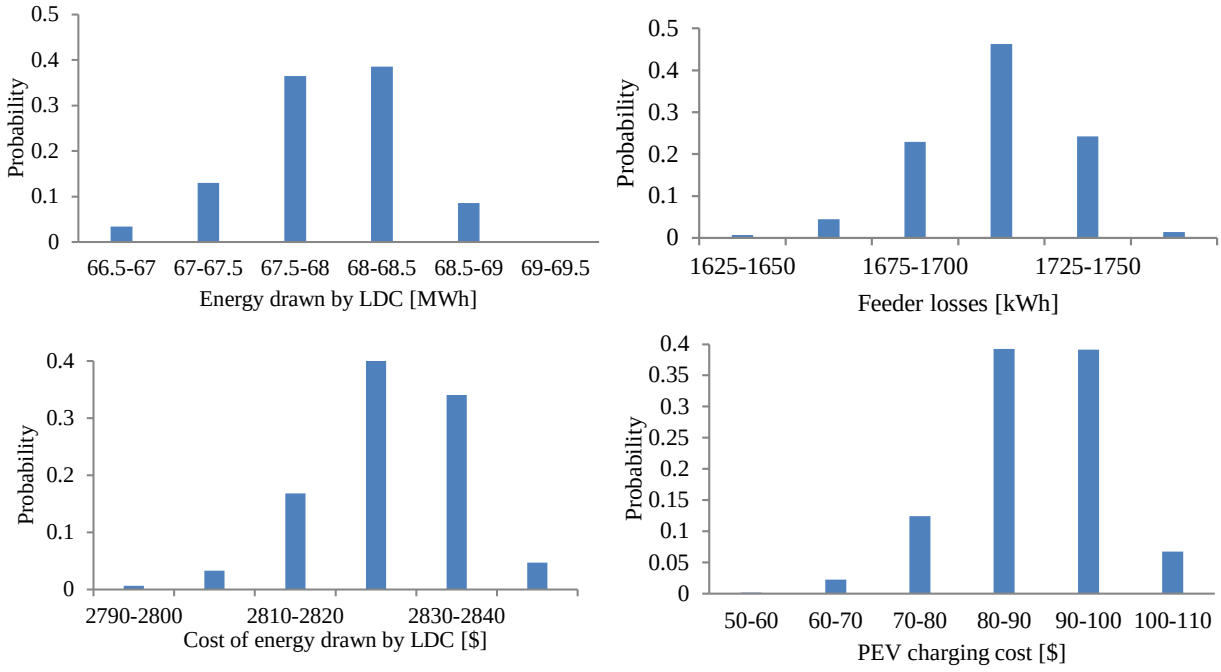

Figure 3.20: Decision variable values for probabilistic smart charging scenarios.

Table 3.9: Probabilistic studies for smart charging scenarios.

	S_3	S_4	S_5	S_6
Expected energy drawn by LDC [kWh]	67,930	68,029	68,067	72,525
Expected feeder losses [kWh]	1,743	1,710	1,779	2,078
Expected PEV charging cost of customers [$/day]	120	108	90	89
Expected cost of energy drawn by LDC [$/day]	2,853	2,846	2,827	3,016

Table 3.10: Number of PEVs at each node and phase for the real distribution feeder.

Node	a	b	c	Node	a	b	c
4	500	502	536	25	-	69	-
6	72	72	72	27	36	-	-
8	250	215	298	30	-	-	46
10	46	46	46	31	41	36	46
13	1	1	1	34	-	-	49
14	50	17	15	36		19	-
22	-	11	-	37	13		11
23	2	-	-	41	170	161	187

3.6 Real Distribution Feeder Results

Simulations are also carried out considering the real unbalanced distribution feeder presented in [21], and depicted in Figure 3.21. This feeder has three 3-phase transformers equipped with LTCs and a single phase transformer. There are 16 load nodes, with all loads being modeled as constant impedances. The feeder current limit information is not available in this case; hence, constraint (3.20) is not included in the DOPF model. Table 3.10 presents the distribution of PEVs at all load nodes and each phase for a 50% PEV penetration, as per (3.25).

Uncontrolled PEV charging (S_1 and S_2) and smart charging scenarios (S_3, S_4, S_5 and S_6) are also studied for this feeder. Table 3.11 presents the summary results for the uncontrolled charging scenarios. The improvements in various parameters, such as energy drawn by the LDC, PEV charging costs, etc., in S_2 as compared to S_1 are very similar to those of the IEEE 13-node test feeder.

Table 3.12 presents the summary results for the smart charging scenarios. Observe that scenarios S_5 and S_6 result in the same PEV charging cost, since both the LDC and the

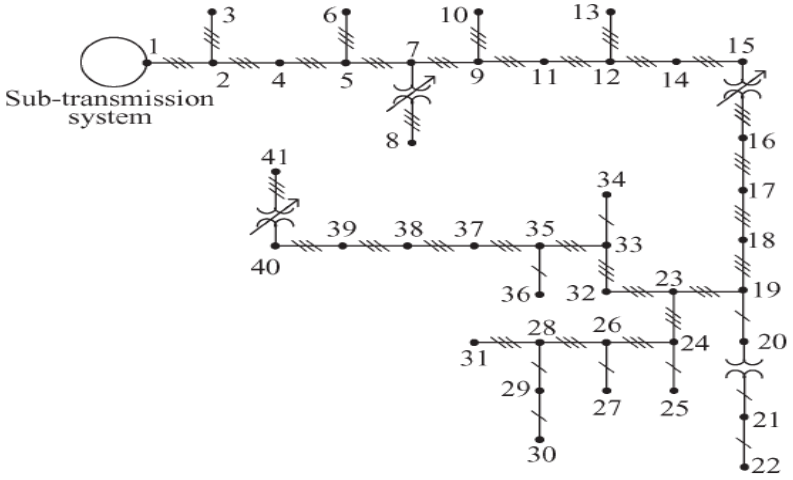

Figure 3.21: Real distribution feeder.

customers are trying to minimize their respective costs.

It should be mentioned that in the uncontrolled scenario S_2 (Table 3.1), node voltage limits are not considered, and hence the resultant node voltage profiles tend to be lower than the nominal limits. Furthermore, since loads are modeled as voltage dependent, they draw less energy from the grid, and consequently incur lower feeder losses as compared to S_3 and S_4, respectively. This also applies to the IEEE 13 node test feeder, as can be observed in Tables 3.4 and 3.5.

It should be noted from the analysis of the results for the two feeders that S_5 is an optimal scenario for both the LDC and the customers. Scenario S_4 results in a fairly uniform load profile, and hence does not require the peak-demand constraint (3.23) in the DOPF model. Scenarios S_3 and S_6 are extreme scenarios, with S_3 representing the perspective of the LDC only, while S_6 represents the customer interests while taking into account grid constraints; therefore, scenario S_3 results in minimum energy drawn by the LDC, but at maximum charging cost for the customers, and vice versa for S_6.

3.7 Computational Details

The proposed DOPF model was programmed and executed in the GAMS environment [80], on a Dell PowerEdge R810 server, Windows 64-bit operating system, with 4 Intel

Table 3.11: Summary results of uncontrolled PEV charging scenarios for the real feeder.

	S_1	S_2	S_2 vs S_1 change [%]
Energy drawn by LDC [kWh]	276,958	262,858	-5.1
Feeder losses [kWh]	5,045	4,413	-12.5
PEV charging cost of customers [$/day]	867	517	-40.4
Cost of energy drawn by LDC [$/day]	11,580	10,645	-8.1

Table 3.12: Summary results of smart PEV charging scenarios for the real feeder.

	S_3	S_4	S_5	S_6
Energy drawn by LDC [kWh]	272,282	272,568	272,397	279,590
Feeder losses [kWh]	4,759	4,612	4,711	5,049
PEV charging cost of customers [$/day]	671	652	617	617
Cost of energy drawn by LDC [$/day]	11,216	11,329	11,165	11,491

Table 3.13: Model and computational statistics.

	IEEE 13-node test feeder		Real distribution feeder
	Z loads	ZIP loads	Z loads
Number of Equations	27,014	31,791	66,279
Number of Variables	25,802	30,615	63,507
Model generation time [s]	0.141	0.156	0.483
Execution time [s]	0.172	1.388	2.527

Xeon 1.87 GHz processors, and 64 GB of RAM. The proposed NLP DOPF model is solved using the SNOPT solver [81]. The model and solver statistics for the IEEE 13-node test feeder and the real distribution feeder are summarized in Table 3.13, which demonstrate the practical feasibility of the proposed approach for PEV smart charging in distribution feeders.

3.8 Summary

This chapter presented a DOPF model which incorporates detailed representation of PEVs within a three-phase unbalanced distribution system. The proposed DOPF model was

applied to study the effects on distribution feeders of uncontrolled PEV charging vis-à-vis smart charging schedules. These smart charging schedules were obtained from the LDC operator's point of view based on various criteria, and considering system operational constraints, and customer's rational behavior.

Studies on realistic test feeders were carried out considering uncontrolled and controlled (smart) charging. The effect of the LDC imposing a cap on system peak-demand was also studied for the smart charging scenarios. Probabilistic studies, to account for different and uncertain customers' travel patterns, were carried out for uncontrolled and smart charging scenarios to determine the expected values and p.d.f.s of the various decision variables. It was observed from these studies that uncontrolled PEV charging can result in violation of grid constraints such as feeder current limits, bus voltages, and may also result in demand spikes. On the other hand, smart charging was found to be effective in scheduling the PEV charging loads at appropriate hours, while meeting feeder constraints for the various objectives considered. Therefore, controlled charging through smart charging schedules is demonstrated to be a necessary approach for PEV charging in the context of smart grids.

Chapter 4

Smart Distribution System Operations with Price-Responsive and Controllable Loads

4.1 Introduction

This chapter presents a new modeling framework for analysis of impact and scheduling of price-responsive and controllable loads in a three-phase unbalanced distribution system. The price-responsive loads are assumed to be linearly or exponentially dependent on price, i.e., demand reduces as price increases and vice versa. Also, a novel constant energy load model, which is controllable by the LDC, is proposed in the chapter. Such controllable loads are assumed here to be scheduled by the LDC through remote signals, DR programs, or through customer-end HEMS.

The effect of uncontrolled price-responsive loads on the distribution feeder is studied as customers seek to reduce their energy cost. On the other hand, minimization of cost of energy drawn by LDC, feeder losses, and customers cost for controllable loads are considered as objectives from the LDC's and customers' perspective. The effect of a peak demand constraint on the controllability of the load is also examined. The proposed models are tested on two feeders: the IEEE 13-node test feeder and a practical LDC feeder system. The presented studies examine the operational aspects of price-responsive and controllable loads on the overall system.

4.2 Nomenclature

Indices

C_n	Controllable capacitor banks at node n.
k	Hours, k=1,2,...,24.
l	Series elements.
L	Loads.
L_n	Loads at node n.
n	Nodes.
p	Phases, p=a, b, c.
r_n	Receiving-ends connected at node n.
s_n	Sending-ends connected at node n.
SS	Substation node.

Parameters

α	Share of price-responsive load [p.u.].
α_1	Share of controllable/dispatchable loads [p.u.].
β_1, β_2	Customer defined constants [p.u.].
φ	LDC defined peak demand cap [p.u.].
γ	Decay rate of demand with price [kWh/$].
θ	Load power factor angle [rad].
ρ	Electricity price [$/kWh].
ρ_1	Retail electricity price [$/kWh].
ρ_{max}, ρ_{min}	Maximum and minimum energy price [$/kWh].
Io	Load phase current at nominal values [A].
m	Slope of a linear price-responsive demand function.
P^{max}	Maximum demand [W].
PD	Total load profile [W].
PD^o, PD^{Cr}	Given and critical real power load [W].
PD^{Exp}	Exponential price-responsive real power load [W].
PD^{Lin}	Linear price-responsive real power load [W].
$\overline{PD}, \underline{PD}$	Maximum and minimum real power demand [W].
QD^o, QD^{Cr}	Given and critical reactive power load [VAr].

Variables

I'	Current supplying the variable demand [A].
I	Current phasor [A].

J_1, J_2, J_3	Objective functions.
P'	Real power of controllable loads [W].
Q'	Reactive power of controllable loads [VAr].
tap	Tap position.
V	Voltage phasor [V].

4.3 Mathematical Modeling Framework

The distribution system is modeled here as discussed in Section 3.3, but without considering PEVs. Parts of the loads, on the other hand, are modeled as uncontrolled price-responsive or as constant energy controlled loads, as discussed next.

4.3.1 Uncontrolled Price-Responsive Loads

An overview of the proposed smart distribution system operational framework with uncontrolled price-responsive loads is presented in Figure 4.1. It is assumed that customers would be equipped with HEMS [11], based on which they respond to price ρ_k by adjusting their consumption $PD_k(\rho_k)$. Two different price-demand relationships namely, linear and exponential, are considered for the studies. The reason for choosing the linear model is its simplicity in representing the price-demand relationship, while the exponential model is chosen since it represents a typical nonlinear price-demand relationship [28]-[30]. The price-responsiveness of customers can effectively be determined in real-life through historical data of price and load demand, or using a thorough customer survey; thus, parameters of the proposed models can be estimated using historical data sets.

In Figure 4.1, it is also assumed that the LDC would be equipped with a Smart Load Estimator (SLE), which receives real-time load consumption data from customers' smart meters to develop price-responsive models for the loads. These price-responsive load models, estimated by the SLE, would be used as input by the LDC for real-time smart distribution system operation through the proposed DOPF to optimally control the distribution feeder using an MPC approach [27]. Thus, the proposed model would be executed based on the frequency of the incoming real-time data, which could be every 5, 10, or 15 minutes to take care of changes in the system parameters, particularly load demand, which can change dynamically. Furthermore, it is assumed here that some fraction of the loads would respond to electricity prices by increasing or decreasing their consumption as per their

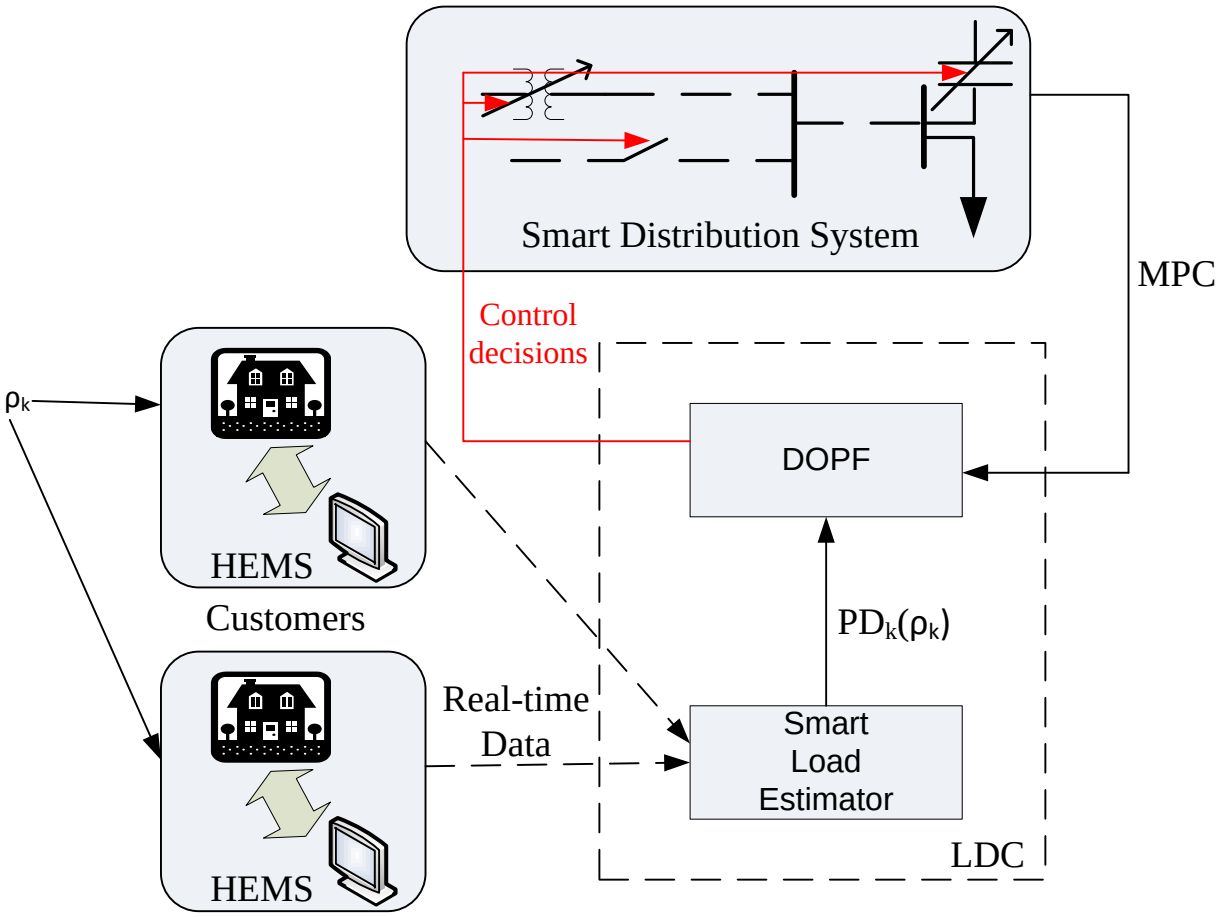

Figure 4.1: Smart distribution system with uncontrollable price-responsive loads.

convenience, or behaving as deferrable loads, while the rest would continue to be fixed or critical loads.

Linear Price-Responsive Load Model

In this case, the customers respond to electricity price increases by reducing the consumption linearly as RTP increases, and vice versa. Figure 4.2 shows the demand variation of the price-responsive component. The 24-hour load profile considering fixed (critical) and linear price-responsive components is given by:

$$PD_{L,p,k} = PD^{Cr}_{L,p,k} + PD^{Lin}_{L,p,k} \quad \forall L, \forall p, \forall k \tag{4.1}$$

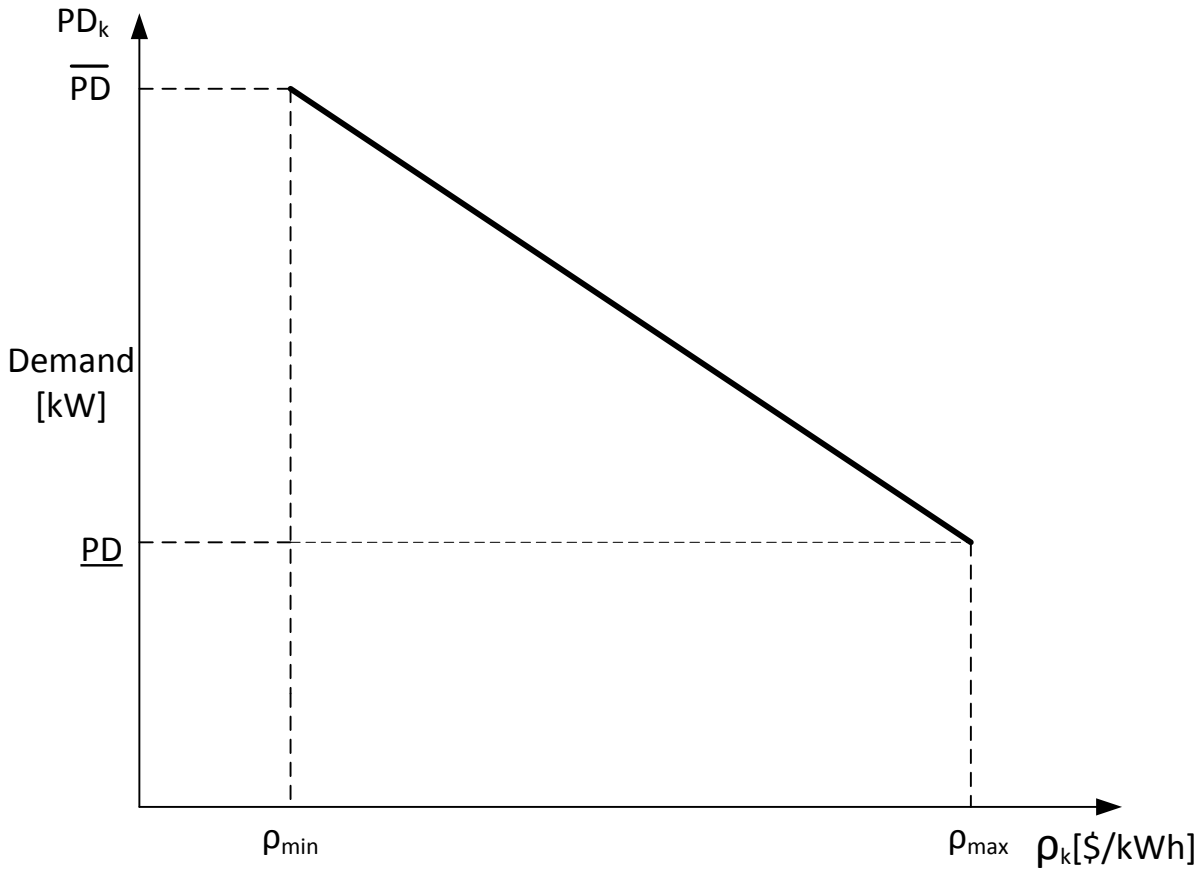

Figure 4.2: Linear relation between demand and electricity price.

$$QD_{L,p,k} = QD^{Cr}_{L,p,k} + QD^{Lin}_{L,p,k} \quad \forall L, \forall p, \forall k \tag{4.2}$$

The 24-hour load profile for the real and reactive components for the fixed component of the load is given by:

$$\begin{cases} PD^{Cr}_{L,p,k} = (1-\alpha) PD^{o}_{L,p,k} & \forall L, \forall p, \forall k \\ QD^{Cr}_{L,p,k} = (1-\alpha) QD^{o}_{L,p,k} & \forall L, \forall p, \forall k \end{cases} \tag{4.3}$$

where α is the fraction of load that can be deferred or interrupted. Similarly, the 24-hour load profile for the price-responsive component of load (Figure 4.2) can be represented as:

$$PD^{Lin}_{L,p,k} = \begin{cases} m_{L,p,k}(\rho_k - \rho_{min}) + \overline{PD}_{L,p,k} & \rho_{min} < \rho_k < \rho_{max} \\ \overline{PD}_{L,p,k} & \rho_k \leq \rho_{min} \\ \underline{PD}_{L,p,k} & \rho_k \geq \rho_{max} \end{cases} \tag{4.4}$$

where

$$\begin{aligned} m_{L,p,k} =& \frac{\underline{PD}_{L,p,k} - \overline{PD}_{L,p,k}}{\rho_{max} - \rho_{min}} && \forall L, \forall p, \forall k \\ \overline{PD}_{L,p,k} =& \beta_1 \alpha PD^{o}_{L,p,k} && \forall L, \forall p, \forall k \\ \underline{PD}_{L,p,k} =& \beta_2 \alpha PD^{o}_{L,p,k} && \forall L, \forall p, \forall k \end{aligned} \tag{4.5}$$

where m represents the slope of the line, and is always negative. As per (4.4), when the price lies in the range $\rho_{min} < \rho_k < \rho_{max}$, there is a reduction in demand; when $\rho_k \leq \rho_{min}$, the price-responsive demand component is capped at $\overline{PD}$; while for $\rho_k \geq \rho_{max}$, this component is fixed at $\underline{PD}$. The parameters ρ_{max}, ρ_{min}, β_1, and β_2 represent the customers' characteristics and reflect the impact of the energy prices on the demand. It should be noted that the reactive power consumption of the linear price-responsive component of the loads QD^{Lin} is obtained from (4.4) considering a fixed power factor.

Exponential Price-Responsive Load Model

In this case, the customers respond to electricity price increase by reducing the consumption exponentially as RTP increases, and vice versa. Figure 4.3 shows the demand variation with respect to the RTP for the exponentially price-responsive and the fixed component of the loads, which yield the following 24-hour load profile:

$$PD_{L,p,k} = PD^{Cr}_{L,p,k} + PD^{Exp}_{L,p,k} \quad \forall L, \forall p, \forall k \tag{4.6}$$

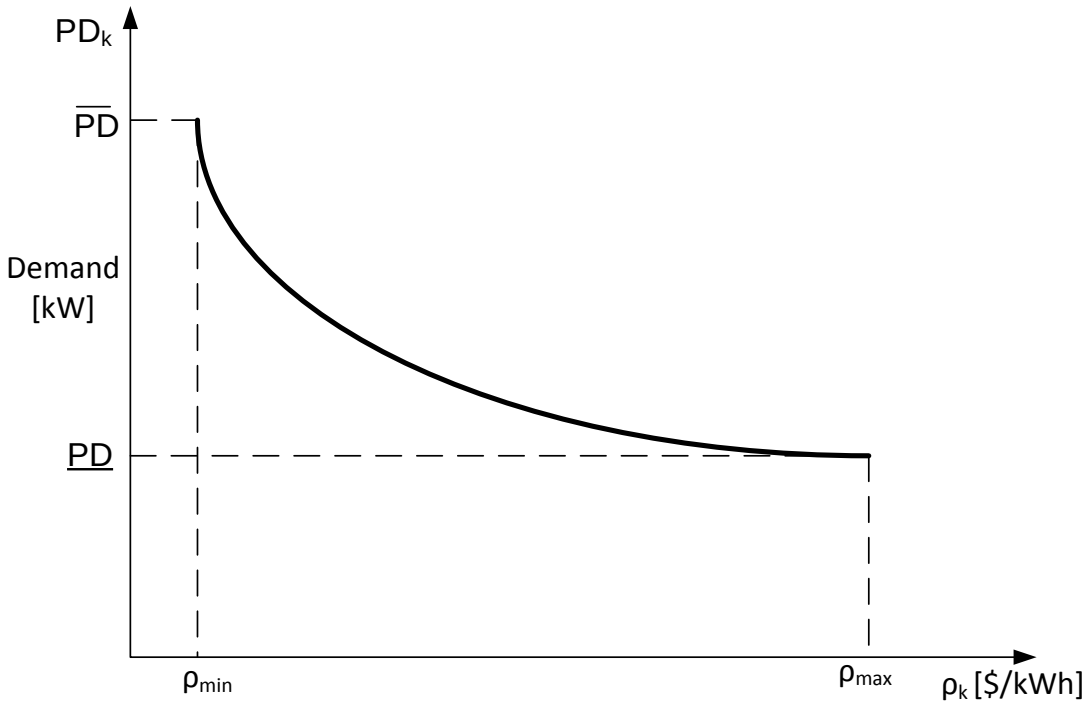

Figure 4.3: Exponential relation between demand and electricity price.

The fixed component of the load profile is similar to that discussed in (4.3) while the exponential component is given by:

$$PD^{Exp}_{L,p,k} = \begin{cases} \overline{PD} e^{-\gamma(\rho_k - \rho_{min})} & \rho_{min} < \rho_k < \rho_{max} \\ \overline{PD}_{L,p,k} & \rho_k \leq \rho_{min} \\ \underline{PD}_{L,p,k} & \rho_k \geq \rho_{max} \end{cases} \tag{4.7}$$

where γ represents the customers' sensitivity to energy prices, i.e., the decay rate of the demand with respect to price. As per (4.7), when the price lies in the range $\rho_{min} < \rho_k < \rho_{max}$, there is a reduction in demand; when $\rho_k \leq \rho_{min}$, the price-responsive demand component is capped at $\overline{PD}$; while for $\rho_k \geq \rho_{max}$, this component is fixed at $\underline{PD}$. As in the previous model, the load power factor is assumed constant in both components of the load.

4.3.2 LDC Controlled Loads

Figure 4.4 presents the operational framework for the LDC with controllable loads. With the introduction of RTP or TOU tariffs, there is a possibility that customers would tend to shift their demand by scheduling their appliance usage, as much as possible, to times when electricity prices are low. However, such demand shifts may create unwarranted new peaks in the distribution feeder. In order to alleviate this problem in the proposed framework, it is envisaged that the LDC will send control/dispatch signals to individual appliances at the house level, while also determining optimal decisions on its feeder operating variables such as taps and switch capacitors. The loads which respond to the LDC's operating objective and can be shifted across intervals, while keeping the energy consumption of the customer constant over a day, play an important role in smoothening the system load profile. In this case, there is a need to ensure that no new peaks are created while shifting the controllable loads across intervals. Hence, the LDC defines a peak demand cap $\overline{PD}_k$ for the system, considering grid constraints and operating limits at any interval, and schedules the controllable loads accordingly. The proposed DOPF, considering objective functions from the perspective of the LDC and customers, would provide the required smart operating decisions. This category of load models considers deferrable loads which cannot be interrupted but can be shifted to other hours, thus ensuring the same energy consumption from the customer over the day.

Here, the fixed or critical component of the load is modeled as in (3.5), while the controllable component of the load is modeled as:

$$|I'_{L,p,k}|(\angle V_{L,p,k} - \angle I'_{L,p,k}) = |Io_{L,p,k}|\angle\theta_{L,p,k} \quad \forall L, \forall p, \forall k \tag{4.8}$$

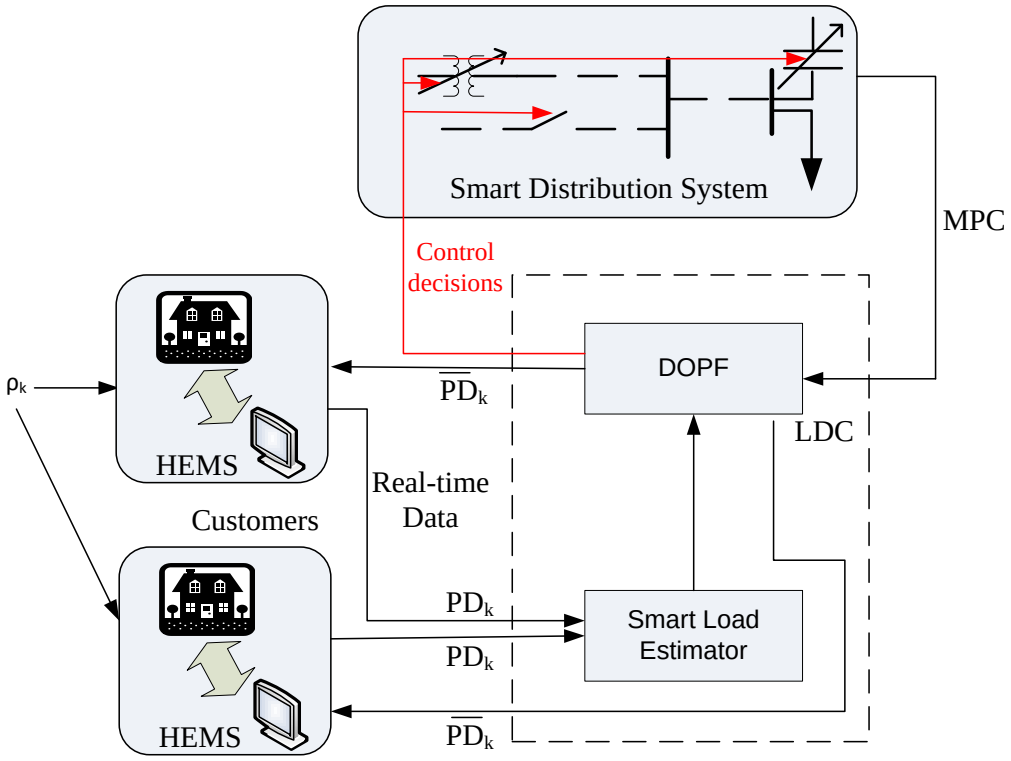

Figure 4.4: Smart distribution system with controllable loads.

$$V_{L,p,k} I^{'*}_{L,p,k} = P^{'}_{L,p,k} + jQ^{'}_{L,p,k} \qquad \forall L, \forall p, \forall k \tag{4.9}$$

In order to ensure that there is no change in the total daily energy consumption, so that the load is only shifted over the day, the following constraint is included:

$$\sum_{k} P^{'}_{L,p,k} + (1-\alpha_1) \sum_{k} PD^{o}_{L,p,k} = \sum_{k} PD^{o}_{L,p,k} \; \forall L, \forall p \tag{4.10}$$

With this constraint, there is a possibility that significant amounts of load are shifted to certain specific hours, resulting in a new peak in the system. In order to ensure that no such new peak is created, an additional constraint is added:

$$P^{'}_{L,p,k} + (1-\alpha_1) PD^{o}_{L,p,k} \leq \varphi P^{max}_{L,p,k} \quad \forall L, \forall p, \forall k \tag{4.11}$$

where φ determines the peak demand cap enforced by the LDC to maintain system conditions within acceptable operating limits. This load model is included in the DOPF, by

modifying (3.13) including the load current of the constant energy model as follows:

$$\sum_{l} I_{l,p,k}(\forall r_n) = \sum_{l} I_{l,p,k}(\forall s_n) + \sum_{L} I_{L_n,p,k} + \sum_{C} I_{C_n,p,k} + \sum_{L} I'_{L_n,p,k} \quad \forall n, \forall p, \forall k \quad (4.12)$$

4.4 Smart Distribution System Operations

The three-phase DOPF model determines feeder operating decisions for various objective functions considering grid operational constraints for both price-responsive and LDC controlled loads. The objective functions are formulated either from the perspective of the LDC or customers, as follows:

- Minimize the total cost of energy drawn by the LDC from the external grid over a day:

$$J_1 = \sum_{k} \left(\sum_{n} \sum_{p} Re\left(V_{SS_{k,n,p}} I^*_{SS_{k,n,p}} \right) * \rho(k) \right) \quad (4.13)$$

  This objective assumes that the LDC purchases energy from the external electricity market at the prevailing hourly prices. Observe that the LDC's profit maximization objective would ideally be considered as the criteria to represent its interest; however, the retail price of energy ρ_1 at which LDC sells electricity to customers is not known, and consequently its revenue earnings are unknown. In the absence of such information, the maximization of LDC's profit is not possible in the present framework; hence, the cost of energy drawn J_1 is minimized instead.

- Minimize total feeder loss over a day:

$$J_2 = \sum_{k} \sum_{n} \sum_{p} Re\left(V_{k,n,p} I^*_{s_{k,n,p}} - V_{k,n,p} I^*_{r_{k,n,p}} \right) \quad (4.14)$$

  Since loads are considered to be voltage dependent, this objective seeks to improve the voltage profile across distribution nodes.

- Minimize the energy cost of customers with controllable loads:

$$J_3 = \sum_{k} \left(\sum_{n} \sum_{p} P'_{k,n,p} \right) \rho_1(k) \quad (4.15)$$

This objective is formulated from the perspective of the customer, and can be used by the LDC to study the system impact of controllable smart loads, which typically seek to minimize their energy costs. It is assumed that all customer homes are equipped with smart meters and are subject to an RTP or TOU tariff $\rho_1(k)$, and that customers have sufficient information or smart load controls to schedule their appliances accordingly. In real life, the retail price $\rho_1(k)$ is not the same as $\rho(k)$, because $\rho_1(k)$ should include the LDC network costs, global adjustments, etc. In the absence of knowledge on retail electricity prices, and since retail pricing is beyond the scope of this research, for minimization of J_3, a simplifying assumption is made that $\rho_1(k) = \rho(k)$.

It should be mentioned that in traditional interruptible load management problems, a cost of load curtailment is usually considered in the objective function [28]. However, in this work such a cost has not been considered for the following reasons:

- Price-responsive Loads: In this case, the entire demand is considered to be parametric, and thus the change in demand to price variations is calculated exogenously, based on the pre-defined linear or exponential functions, which are then input to the proposed DOPF. Thus, the DR is not a variable but known a priori to the LDC (as given), and hence there is no need to consider the cost of load shifting in the objective function J_1.
- Controllable Loads: In this case, the controllable component is modeled as a variable in the proposed DOPF, with (4.10) ensuring that the total energy consumption remains constant over the day. Since the cost of load shifting is not being considered, it may happen that the entire controllable component of load could be shifted out from an hour to another hour, which is acceptable since the customer has already declared to the LDC the amount of load that is shiftable and thus controllable. Another possibility is that the variable component of the load at any given time may be zero, if no cost is attached to it. This behavior is expected in DR programs that have one-time incentives as opposed to incentives based on operations. For example, some programs have in-kind incentives such as a free installation of thermostats or vouchers, in which one cannot consider a cost of load curtailment, as is the case of the peaksaver PLUS® Program in Ontario [99], implemented by LDCs in the province, in which there is no direct payment to customers for controlling their loads. Since, from the distribution feeder operational point of view, this model represents the extremes of load shifting, no costs are assumed here. However, the cost of load curtailment could be included in the proposed DOPF by adding a cost term associated with load shifting to J_1 in (4.13).

It should be mentioned that the proposed DOPF is somewhat similar to reliability-based DR programs; however, the present study applies to the distribution feeder level, and hence the model formulated is not the traditional security constrained power flow or OPF, but a DOPF. In this context, using the proposed DOPF with controllable loads can bring about significant modifications to the LDC's load curve and thus affect system reliability, especially considering peak demand constraints, that directly affect the overall reliability of the system, at all voltage levels.

Observe that the DOPF considers each component of the distribution feeder such as the transformers, cables, switches, and loads at each node and phase, representing loads in a variety of ways. This results in a rather complex, and challenging optimization problem, as compared to the traditional reliability-based DR programs. In this case, the objective function (minimize costs and losses) represent the LDC's "normal" operational perspective, and thus the model seeks to examine how DR programs will affect the distribution feeder (not the transmission system) operation. Thus, the proposed approach is different from the traditional, transmission system view and analysis of DR programs, rather concentrating on the impact and applications of these programs to distribution feeders and LDC operations.

Finally, since the main purpose of this research is to study the impact of price-responsive and controllable loads on the feeder, and not their optimal voltage control; taps and capacitors are modeled as continuous variables to avoid introducing integer variables, thus resulting in an NLP DOPF model, which is computationally manageable. A case study is presented in Section 4.5.1 that examines the small difference in results when continuous variables are considered, compared to sets of integer solutions. Hence, although MINLP problems can be solved using various heuristic methods, the difference might not be very significant, as suggested, for example, in [100], wherein an OPF for various load conditions with discrete and continuous taps of LTCs is shown to produce similar results.

4.4.1 Scenario 1: Uncontrolled Price-Responsive Loads

In this scenario, it is assumed that the customers respond to electricity prices, as per the price-responsive load models introduced in Section 4.3.2, and seek to reduce their energy cost as much as possible over the day, with all customers being equipped with HEMS that has access to a 24-hour price forecast. Based on this information, customers respond to electricity prices by deferring or interrupting some of their loads, without regard for system conditions. The LDC thus receives a revised load profile for which it optimally determines the tap and capacitor operation schedule to maintain voltages and currents within prescribed limits.

Two different objective functions are considered within this scenario, minimization of J_1 and J_2 given by (4.13) and (4.14), respectively. For the linear price-responsive load model, the demand can be calculated using (4.1) to (4.5), and for the exponential price-responsive load, the demand is calculated using (4.3), (4.6), and (4.7). The 3-phase distribution feeder and its components, modeled by (3.1) to (3.8), and appropriately modified network equations (3.13) and (3.14), are the constraints of the controlled system operational model, with variable taps and capacitors. The operating limits for this scenario are given by (3.19) to (3.22).

4.4.2 Scenario 2: LDC Controlled Loads

In this mode of operation, it is assumed that the LDC incorporates a peak demand constraint within its DOPF program, and the controllable/dispatchable component of the load (α_1) is a variable which is optimally scheduled by the DOPF for customers. The objective functions considered here are the minimization of J_1 and J_2, from the LDC's perspective, and the minimization of J_3 from the customers' perspective, as discussed earlier. The 3-phase distribution feeder and its components (3.1) to (3.8), network equations (4.12) and an appropriately modified (3.14), and the constant energy model given by (4.8) to (4.11) are the constraints of the DOPF in this scenario. Additional operating constraints include limits on tap operation, capacitor switching, voltage and feeder current limits as discussed in (3.19) to (3.22). Note that no direct interruptible component is assumed in these controllable loads, and hence the issue of cold load pick-up or load recovery characteristics is not considered here.

It should be noted that price elasticity matrices can also be used to determine the lateral movement of loads across time in response to prices; however, these models are not implemented in this research, since a constant energy model is proposed instead to determine optimal load shifting. In this context, the controllable loads become variables to optimally compute their lateral shifting subject to grid constraints; hence, price elasticity matrix models would effectively be variables which would be determined simultaneously (and optimally) from the model, based on the energy price and grid conditions.

4.5 Results and Analysis

The proposed new DOPF models are validated on the IEEE 13-node test feeder (Figure 3.3), and a realistic distribution feeder (Figure 3.21). For the 13-node feeder, the capacitors

are modeled as multiple capacitor banks with switching options. For example, the capacitor at Bus 675 (Figure 3.3) is assumed to comprise 5 blocks of 100 kVAr capacitors in each phase, and Bus 611 to have 5 blocks of 50 kVAr capacitors in phase c.

The practical LDC feeder system has three three-phase transformers equipped with LTCs and a single phase transformer. There are 16 load nodes, with all loads modeled as constant impedances. The feeder current limit information is not available in this case; hence, constraint (3.20) is not included in the DOPF models. A 24 hour base load profile is generated using the procedure discussed in [21].

In Ontario, the HOEP is calculated every hour and can be considered an RTP, that applies to customers participating in the wholesale electricity market [92]. The HOEP is therefore used for the analysis reported in this research for a specific weekday of June 30, 2011.

The Scenario 1 case studies are carried out assuming $\alpha = 0.20$ (20% of the load is price-responsive), while Scenario 2 assumes that the share of controllable/dispatchable loads is $\alpha_1 = 0.20$. Customer defined constants for the linear load model are assumed to be: $\beta_1 = 0.5$, and $\beta_2 = 1.5$. For the exponential price-responsive model, the decay constant is assumed to be $\gamma = 0.8$. Voltages are maintained within $\pm 5\%$ for both Scenarios 1 and 2.

4.5.1 IEEE 13-node Feeder

Scenario 1

Figure 4.5 shows the system load profile for linear and exponential price-responsive load models, compared with the base load. Observe that the load decreases when the price is high, from 1-5 PM and also at 10 PM, as compared to the base load profile. Increase in the demand is observed when prices are low in the early morning and late evening hours. Note that the linear model is more sensitive to price signals as compared to the exponential model, and the increase or decrease in demand is more, for the same prices.

Table 4.1 presents the summary results of LDC operation with base load (100% load is fixed), and for linear and exponential price-responsive load models considering minimization of J_1 and J_2. For the base load operation of LDC, the demand is considered to be non-responsive to prices, and taps and capacitors are considered variables. Note that there is an overall reduction in the cost of energy drawn by the LDC and the customers' energy cost when the loads are price-responsive, be it linear or exponential. This indicates that the deployment of smart energy management devices in the distribution feeders could be advantageous for both parties. The energy drawn and feeder losses increase when loads

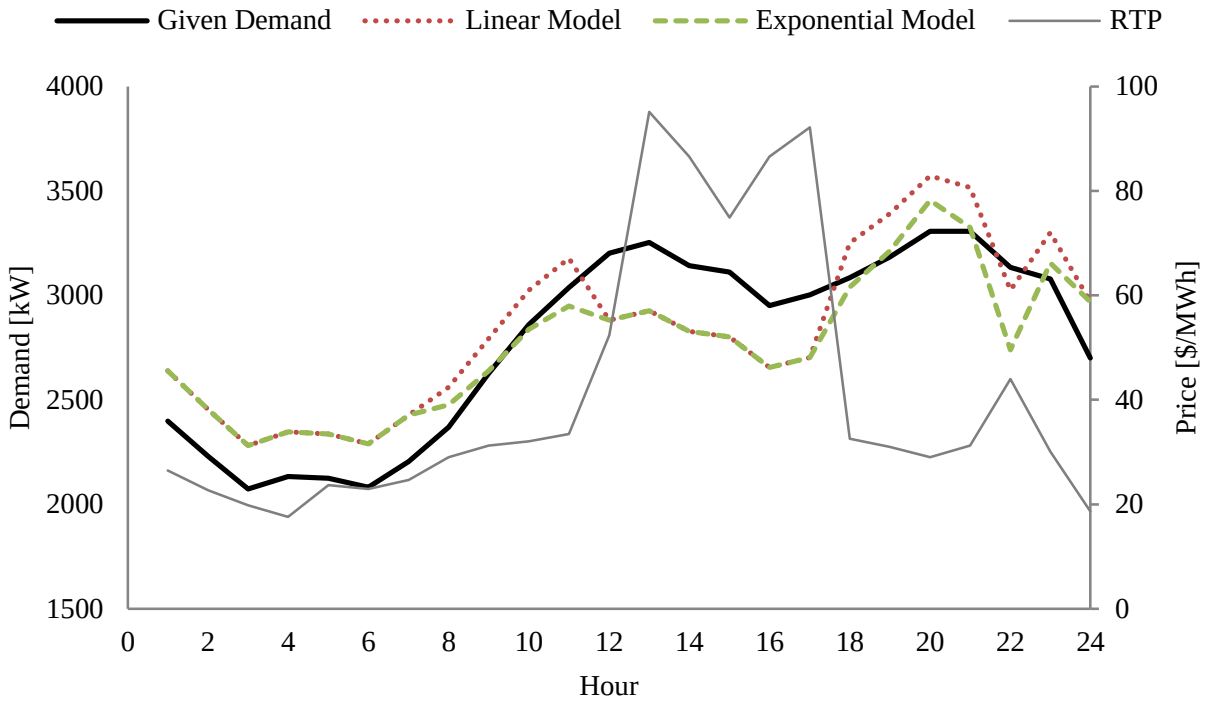

Figure 4.5: System load profiles for uncontrolled price-responsive loads.

are linearly price-responsive, and decrease when loads are exponentially price-responsive, which can be attributed to the price-demand relationships in each case and the associated parameters of the price-responsive models.

Since demand increases at low price hours in the late evening and early morning for price-responsive loads, the voltage profiles obtained from a DLF with fixed taps and capacitor banks, are lower than that for base load (α=0). On the other hand, when the price-responsive demand falls during peak-price hours, the corresponding voltage profile from a DLF is better than that for the base-load case. A comparison of the voltage profile at Node 675 in phase c with and without tap and capacitor control (Figure 4.6), shows that, a proper voltage profile within stipulated limits can be attained through controlled tap and capacitor switching operations.

Table 4.1: Results for Scenario 1.

		Total energy drawn by LDC [kWh]	Total feeder loss [kWh]	Total cost of energy drawn by LDC [$]	Total energy cost to customers [$]
Base Load	J_1	62,967	1,524	2,733	2,665
	J_2	63,060	1,512	2,736	2,668
Linear Load	J_1	64,487	1,583	2,667	2,602
	J_2	64,577	1,573	2,670	2,605
Exponential Load	J_1	62,667	1,493	2,607	2,544
	J_2	62,763	1484	2,610	2,548

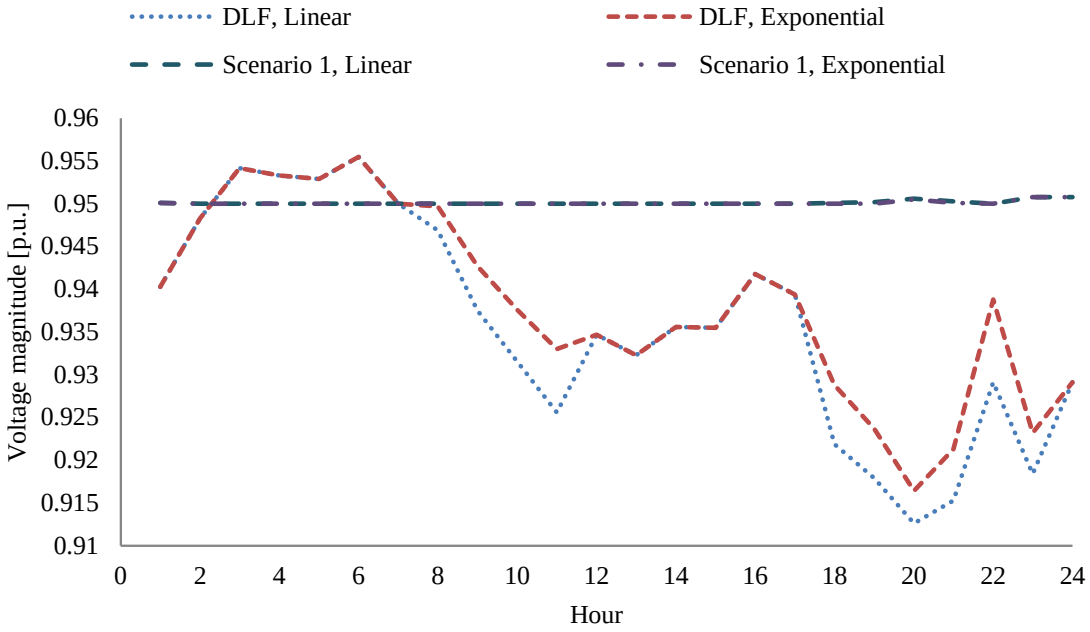

Figure 4.6: Voltage magnitude at Node 675 in phase c for Scenario 1.

Scenario 2

Figure 4.7 presents the resulting system load profile when the LDC schedules the controllable/dispatchable portion of the loads, considering minimization of J_1, J_2, and J_3.

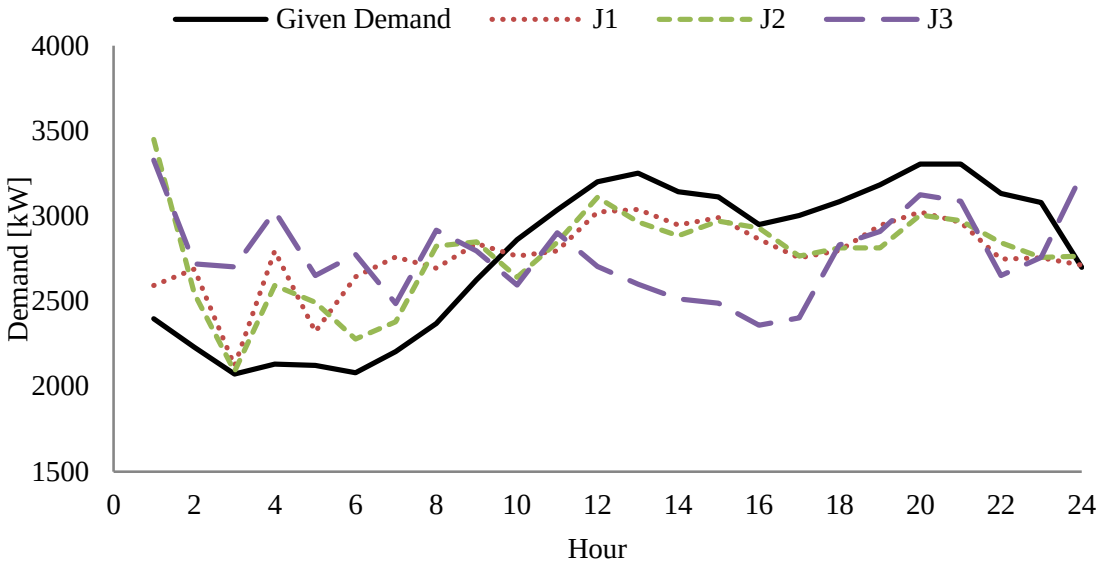

Figure 4.7: System load profiles for LDC controlled loads.

Observe that in this scenario the LDC imposes the peak demand constraint (4.11) to ensure that no new peaks are created when there is load shifting across hours. The system load profiles are observed to be very similar for J_1 and J_2, and the demand decreases as compared to the base case between 1 PM to midnight, and increases during the early morning hours, illustrating a shift of the loads within the 24 hour period, with the same energy consumption over the day. Although a new peak is created at 1 AM with J_2, this is still within the LDC's prescribed peak demand constraint. Minimization of J_3 results in significant shifting of demand from afternoon and evening hours to early morning hours, since electricity prices are cheaper at these hours; this results in almost a flat load profile, which is desirable for the LDC. Thus, the use of J_3 by the LDC as an objective function for dispatching controllable loads benefits both the LDC and customers.

The effect of varying the peak demand constraint is examined next, together with the minimum level of the peak demand constraint that the system can handle. This case study is carried out considering J_1 only. Figure 4.8 presents the effect of variation of the peak demand constraint (φ is reduced from 1.0 to 0.83) on the energy drawn by the LDC and feeder losses. Note that as φ decreases, i.e., the peak demand is reduced, the LDC draws less energy, feeder losses reduce, and consequently, its cost of energy drawn (Figure 4.9) as

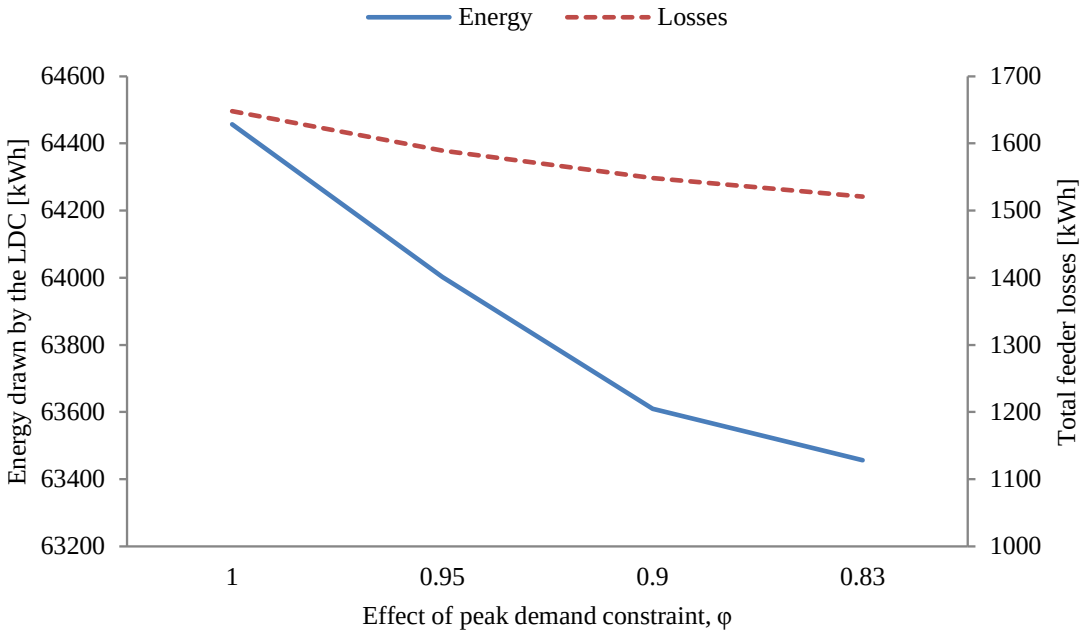

Figure 4.8: Effect of peak demand constraint on LDC energy drawn and feeder losses.

well as the customers' cost of energy decrease.

The minimum peak demand constraint that the system can sustain without requiring any load curtailment is $\varphi = 0.83$; the system load profile for this case is presented in Figure 4.10. Observe that the system load profile is evenly distributed over 24 hours.

Uncertainty Analysis

The analysis presented for Scenario 1 models the price-responsive loads with a selected set of parameters (m and γ), which are highly unpredictable and difficult to estimate. Hence MCS are carried out in this section considering uncontrolled price-responsive loads (Scenario 1) and minimization of J_1, with electricity price and parameters of the price-responsive load models considered uncertain.

Figure 4.11 presents the MCS results for the linear and exponential price-responsive load models. In the linear price-responsive load model, the slope $m_{L,p,k}$ given by (4.4)-(4.5) is varied considering the price to be uniformly distributed in the range of ± 15 \$/MWh with respect to its nominal value. For the exponential price-responsive load model, the decay

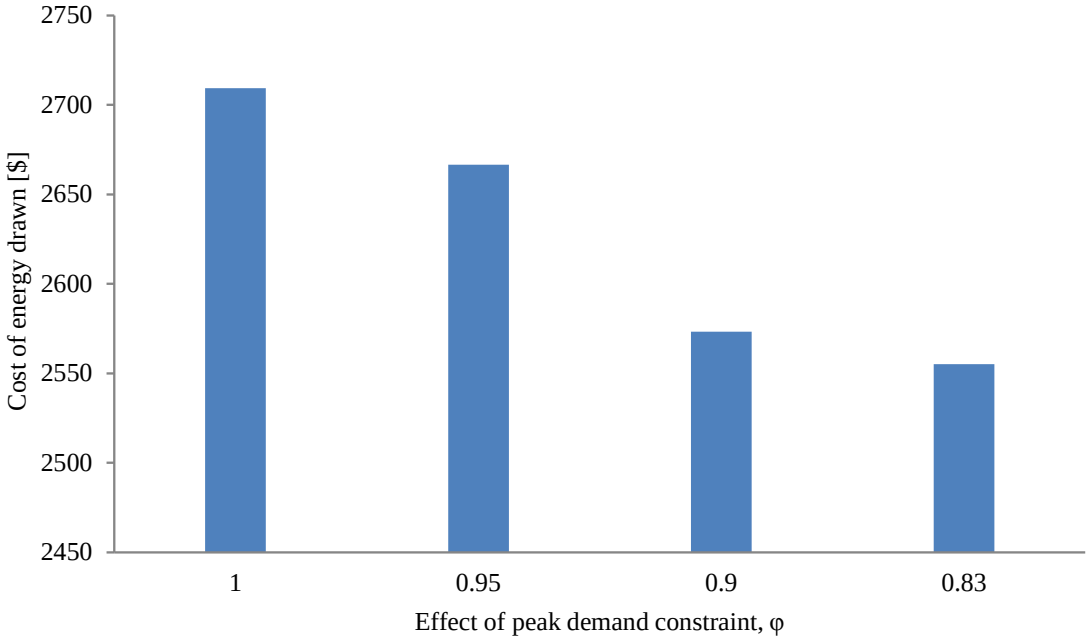

Figure 4.9: Effect of peak demand constraint on cost of LDC energy drawn.

parameter γ, representing the sensitivity of customers to prices, is varied using a uniform distribution in a range of 0.05 to 0.12. The simulations are performed for 2000 samples, since the expected energy cost converges after about 1000 sample runs. The resulting expected energy cost is \$2,595 and \$2,542 for the linear and exponential price-responsive load models, respectively. These expected values are very close to those obtained for a specific set of chosen parameters (Table 4.1).

Variability of Model Parameters Across Time

The analysis presented so far assumes that m and γ remain unchanged for the entire 24 hour operation. However, this may not be the case in real-life, since, for example, a customer may reduce its load more at 10 AM to the same price increase than it would do at 7 PM. Thus, to represent the variability of the elasticity parameters across time, MCS are carried out considering uncontrolled price-responsive loads and minimization of J_1; in this case, random sample sets are generated simultaneously for 24-hourly m or γ. For the linear price-responsive load model, the slope $m_{L,p,k}$ given by (4.4)-(4.5) is varied

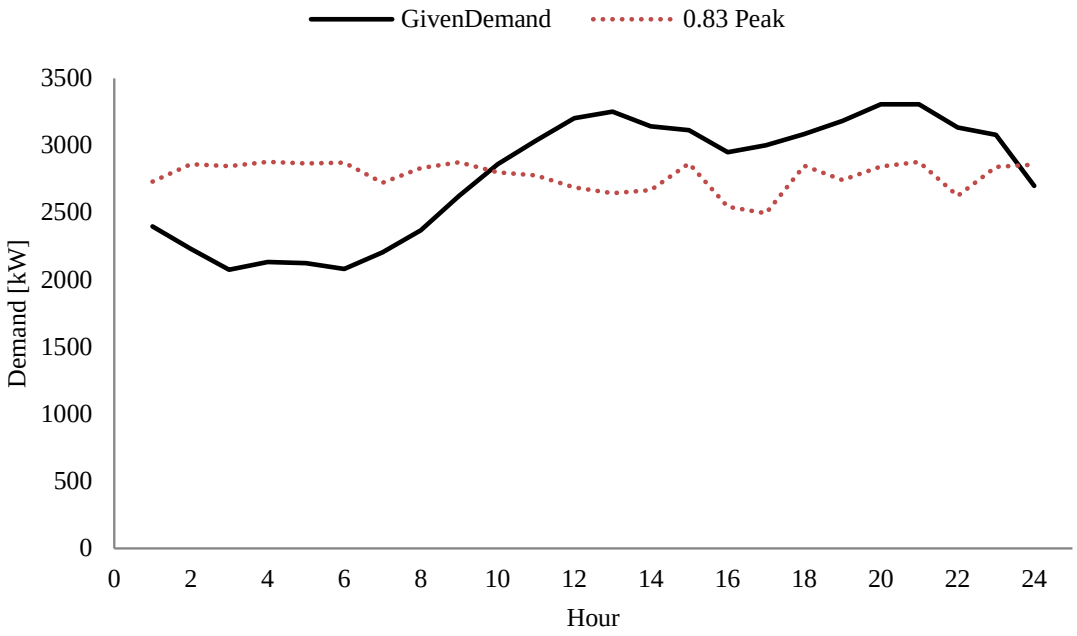

Figure 4.10: System load profile for $\varphi = 0.83$, J_1.

Table 4.2: Model parameter hourly uncertainties in Scenario 1.

Case Studies	Linear Model	Exponential Model
Expected total Energy drawn by LDC [kWh]	64,494	62,570
Expected total feeder losses [kWh]	1,584	1,491
Expected total LDC cost [$]	2,668	2,603
Expected total energy cost to customers [$]	2,602	2,541

hourly considering a uniform distribution in the range of $0.7m_{L,p,k}$ to $1.3m_{L,p,k}$. For the exponential price-responsive load model, γ is varied hourly using a uniform distribution in the range of 0.05 to 0.12. The simulations are performed for 2000 samples.

Table 4.2 presents the expected values of solution outputs, i.e., LDC energy drawn, feeder losses, cost of LDC energy drawn, and energy cost to customers. Observe that the expected values are very close to those obtained in the deterministic case (Table 4.1).

Figures 4.12 and 4.13 show four different plots of p.d.f.s of the solution outputs for linear and exponential price-responsive load models, respectively. These p.d.f.s depict the range

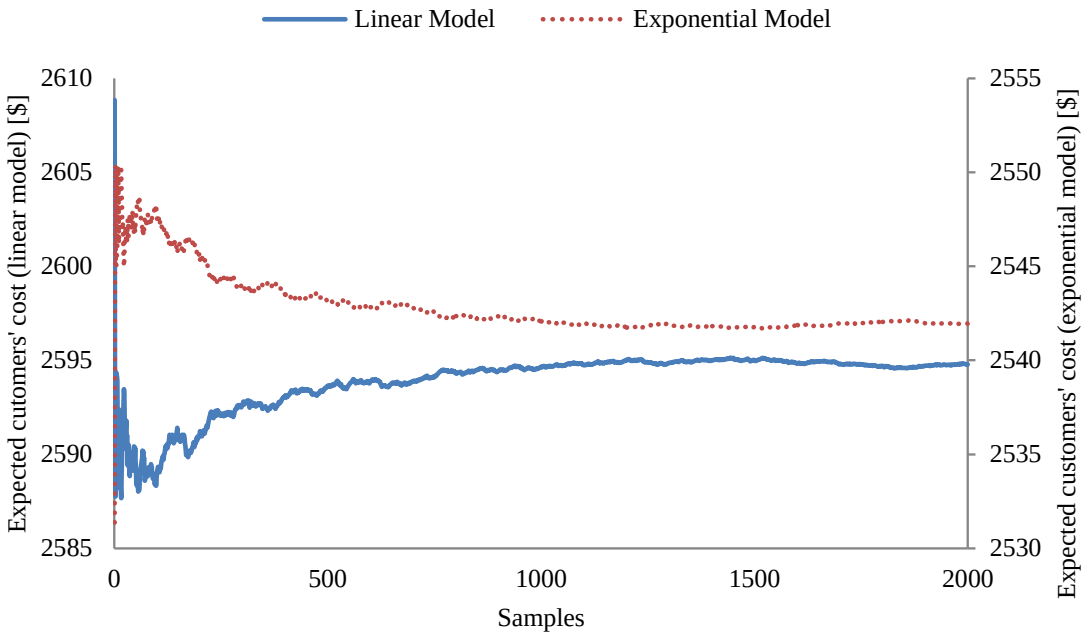

Figure 4.11: Monte Carlo simulation of price-responsive loads.

of values over which the system variables are expected to vary hourly, for the assumed uniformly distributed parameters m and γ. The plots depict narrow variations around the mean, thus showing that the deterministic studies discussed earlier are reasonable, since the results are close to the expected trends for the assumed model parameters.

Differences in Continuous Versus Discrete Modeling

The analyses reported thus far, consider the taps and capacitors to be continuous variables. Therefore, in this section, the following simple approach is used to examine the difference in the results when these are modeled as discrete variables:

1. The modified DOPF is executed with taps and capacitors as continuous variables.
2. The optimal solutions of the continuous variables $T_{t,p,k}$ and $cap_{C,p,k}$ from Step 1 are rounded-up (RUp) and rounded-down (RDn) to the nearest discrete values.
3. The proposed DOPF is then run for all possible combinations of RUp and RDn

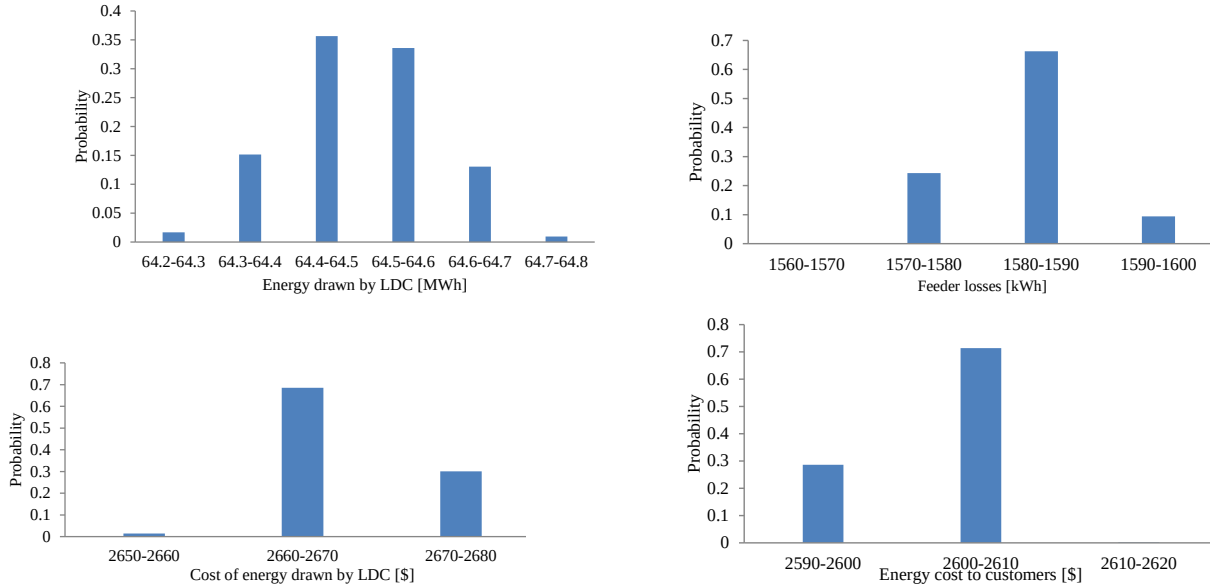

Figure 4.12: Probability distribution of solution outputs for linear price-responsive loads.

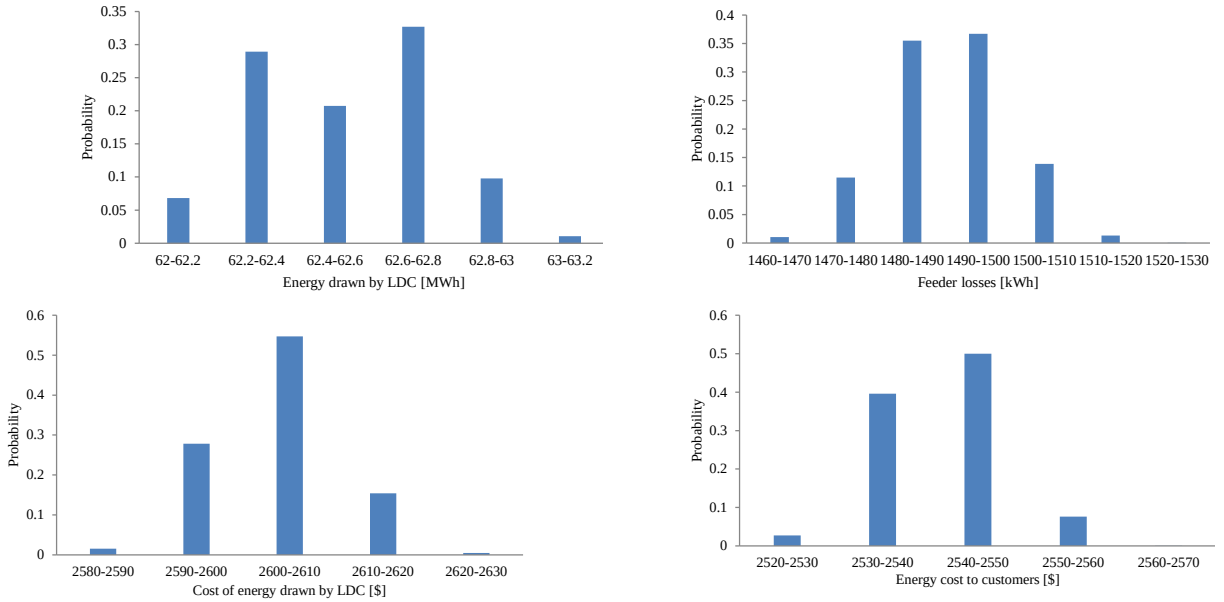

Figure 4.13: Probability distribution of solution outputs for exponential price-responsive loads.

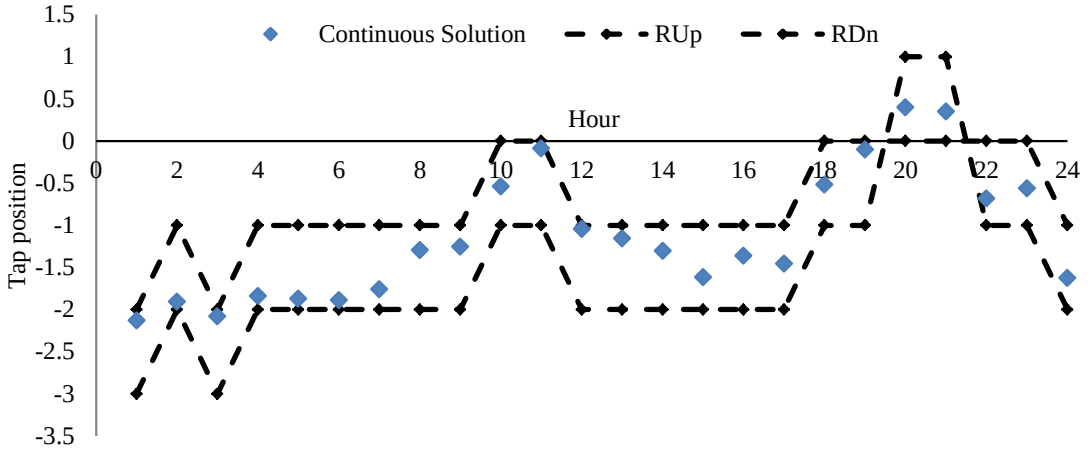

Figure 4.14: Continuous optimal tap_{650} and its corresponding RUp and RDn values.

values of taps and capacitors to obtain the “outlier" solutions associated with the corresponding discrete values.

The aforementioned approach is applied to the uncontrolled price-responsive loads for the minimization of J_1. Figure 4.14 illustrates the continuous solution and the RUp and RDn integer values for $T_{t,p,k}$ only, for the linear price-responsive load model. All the possible combinations obtained from the RUp and RDn values are shown in Table 4.3, and all the possible outlier DOPF solutions for the linear price-responsive load model are presented in Table 4.4. Notice that the solution differences are minimal for the continuous versus the discrete values. Similar results were obtained for the exponential price-responsive load model.

4.5.2 Realistic LDC Feeder

Scenario 1

Studies are carried out considering a practical LDC feeder with linear and exponential price-responsive load models. The resulting system load profiles with these models, as presented in Figure 4.15, are very similar to those obtained for the IEEE 13-node test feeder, with the linear model being more sensitive to price signals as compared to the

Table 4.3: Possible discrete combinations of tap and capacitor values.

	tap_{650}	cap_{675}	cap_{611}
Outlier 1	RUp	RUp	RUp
Outlier 2	RUp	RUp	RDn
Outlier 3	RUp	RDn	RUp
Outlier 4	RUp	RDn	RDn
Outlier 5	RDn	RUp	RUp
Outlier 6	RDn	RUp	RDn
Outlier 7	RDn	RDn	RUp
Outlier 8	RDn	RDn	RDn

Table 4.4: Continuous and discrete DOPF solution for linear price-responsive model.

	Total Energy drawn by LDC[kWh]	Total feeder losses [kWh]	Total LDC cost [$]	Total energy cost to customers [$]
Continuous	64,487	1,583	2,667	2,602
Outlier 1	64,517	1,586	2,667	2,601
(Diff. %)	(0.046)	(0.186)	(-0.031)	(-0.036)
Outlier 2	64,495	1,585	2,666	2,601
(Diff. %)	(0.012)	(0.153)	(-0.049)	(-0.055)
Outlier 3	63,769	1,577	2,635	2,570
(Diff. %)	(-1.114)	(-0.349)	(-1.232)	(-1.249)
Outlier 4	63,749	1,577	2,634	2,569
(Diff. %)	(-1.145)	(-0.342)	(-1.25)	(-1.267)
Outlier 5	65,162	1,601	2,695	2,629
(Diff. %)	(1.047)	(1.132)	(1.042)	(1.038)
Outlier 6	65,141	1,600	2,695	2,629
(Diff. %)	(1.013)	(1.1)	(1.024)	(1.019)
Outlier 7	64,406	1,592	2,663	2,597
(Diff. %)	(-0.126)	(0.594)	(-0.173)	(-0.189)
Outlier 8	64,386	1,592	2,662	2,597
(Diff. %)	(-0.157)	(0.601)	(-0.191)	(-0.207)

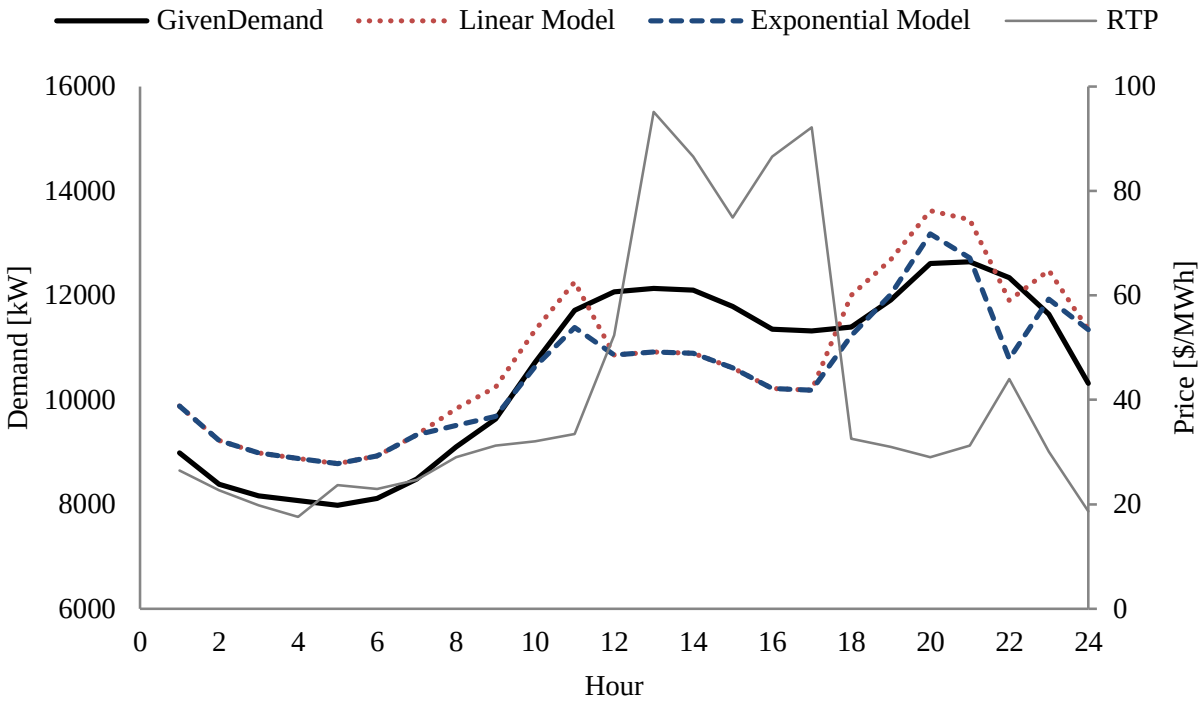

Figure 4.15: System load profile for uncontrolled mode for a realistic LDC feeder.

exponential. The demand decreases when the price is high (between 1 to 5 PM) and increases when low (early morning and late evenings).

Table 4.5 presents the main results of LDC's operation for the base load case, and with the linear and exponential price-responsive load models considering minimization of J_1 and J_2. Observe that the price-responsive load models result in reduced cost of energy drawn by the LDC and energy cost to customers as compared to the base load case, a desirable result for both the LDC and customers.

Scenario 2

Figure 4.16 presents a comparison of the system load profiles obtained considering minimization of J_1, J_2, and J_3, for the controlled load profiles vis-à-vis the base load profile. Note that the controlled load profiles using J_1 and J_2 are very similar, i.e., the load decreases from afternoon onwards to midnight, shifting it to early morning hours and resulting in a

Table 4.5: Results for Scenario 1 for a realistic LDC feeder.

		Total energy drawn by LDC [kWh]	Total feeder loss [kWh]	Total cost of energy drawn by LDC [$]	Total energy cost to customers [$]
Base Load	J_1	244	3.835	10,552	10,379
	J_2	246	3.825	10,670	10,497
Linear Load	J_1	250	3.997	10,317	10,153
	J_2	252	3.987	10,427	10,263
Exponential Load	J_1	243	3.753	10,096	9,940
	J_2	246	3.744	10,206	10,050

Table 4.6: Results for controlled loads for Scenario 2 for a realistic LDC feeder.

Case Studies	J_1	J_2	J_3
Total Energy drawn by LDC [MWh]	245	248	251
Total feeder losses [MWh]	3.792	3.773	4.114
Total LDC cost [$]	10,091	10,267	10163
Controllable customers' cost [$]	1,669	1,711	1,450

more uniform profile. Minimization of J_3 and peak demand constraint results in a fairly flat but elevated load profile at early morning hours.

Table 4.6 presents a comparison of the LDC controlled cases considering minimization of J_1, J_2, and J_3. Observe that minimization of J_1 results in the lowest energy drawn by the LDC, while the customers' cost pertaining to the variable component of the load is lowest when J_3 is minimized, although feeder losses increase when compared to minimization of J_1 and J_2. Finally, note that the overall operational trends for a realistic LDC feeder are similar to those obtained for the IEEE 13-node test feeder.

4.5.3 Modeling, Algorithm, and Computational Challenges

The proposed DOPF model has been programmed and executed on a Dell PowerEdge R810 server, in the GAMS environment [81], Windows 64-bit operating system, with 4 Intel Xeon 1.87 GHz processors and 64 GB of RAM. The mathematical model is an NLP

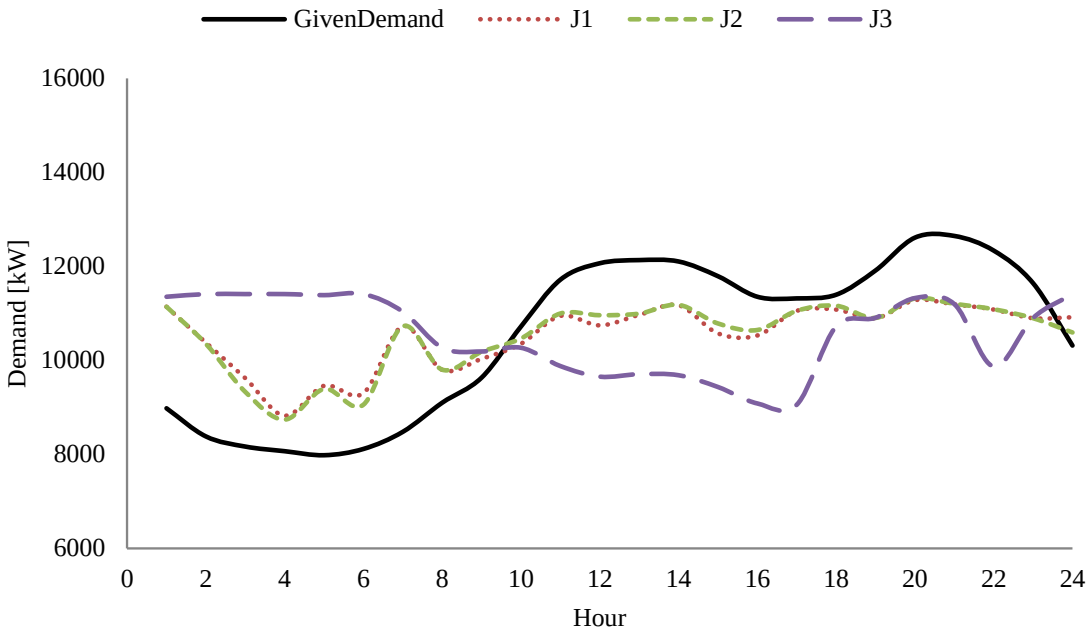

Figure 4.16: System load profile considering J_1, J_2 and J_3 for a realistic LDC feeder.

Table 4.7: Computational statistics.

	IEEE 13-node test feeder		Real distribution feeder	
	Price-responsive	Controllable load	Price-responsive	Controllable load
No. of Equations	21,914	26,155	56,199	65,459
No. of Variables	21,026	25,250	54,003	63,194
Execution time [s]	0.141	3.089	2.452	1.046

problem which is solved using the SNOPT solver [81]. The model and solver statistics for the IEEE 13-node test feeder and the real distribution feeder are summarized in Table 4.7.

Some of the modeling, algorithmic, and computational challenges of the proposed approach are the following:

- There is a need for real-time data from customer loads, measured through smart meters, to accurately estimate the parameters using the proposed SLE for the price-responsive load models.

- Modeling of controllable loads introduces sine and cosine functions in the load representation, which increase the model complexity.
- With the introduction of controllable loads, the number of equations and variables increase as compared to price-responsive loads, and introduces inter-temporal constraints in the NLP optimization problem, which make it more challenging to solve.
- As shown in Table 4.7, the size and complexity of the proposed DOPF problem is quite significant, but the execution times are quite reasonable and appropriate for the proposed real-time applications.

4.6 Summary

This chapter proposed two representations of customer load models in the context of smart grids, integrating them within an unbalanced distribution system operational framework. In the first model, uncontrolled price-responsive load models were formulated, considering that these respond to price signals either linearly or in an exponential manner. The resulting load profile can be used by the LDC to determine the impact on feeder operations. The second model assumes LDC controlled, constant energy loads, which could be shifted across intervals.

A novel operational framework from the LDC's perspective was developed, ensuring that no new peak is created in the system, while smart loads are optimally shifted. Various case studies were considered from the perspective of both the LDC and customers and tested on realistic feeders, considering uncertainty on the price-responsive load parameters. The controlled load model resulted in a more uniform system load profile with respect to uncontrolled loads, and a peak demand cap led to decrease in energy drawn as the cap was reduced, consequently reducing feeder losses and LDC's and customers' costs.

Chapter 5

Residential Micro-hub Load Model using Neural Networks

5.1 Introduction

This chapter presents the load modeling of a residential micro-hub based on real measurements, as well as simulation data obtained using the EHMS model of residential hub proposed in [50]. An NN is used for the load model as a function of time, temperature, peak demand, and energy price (TOU). Different functions are used and their performances are compared to determine the best function that can be used, based on the available data. Furthermore, the number of hidden layer neurons are varied to obtain the best fit for the NN model.

The remainder of this chapter is structured as follows: Section 5.2 presents the nomenclature of all parameters and variables of the NN model. A brief description of the EHMS residential micro-hub model is presented in Section 5.3. Section 5.4 presents the inputs and outputs used in the NN model. A detailed analysis of the training process and the resulting NN model is presented in Section 5.5. Finally, Section 5.6 summarizes the main contribution of the chapter.

5.2 Nomenclature

Indices

a	Index of appliances in a house, $a \in A$.
i	Index for hidden layer nodes.
j	Index for input layer nodes.
k	Index for time interval.
l	Index for output layer nodes.

Parameters

$\beta_1 ... \beta_{N_H}$	Bias of a hidden layer neuron.
Em	Measured energy consumed by the load [MWh].
Es	Simulated energy consumed by the load [MWh].
Γ_{N_O}	Bias associated with output layer neuron.
$H^1 ... H^{N_H}$	Output of a hidden layer neuron.
J	Objective function.
N_H	Number of neurons in the hidden layer.
N_I	Number of neurons in the input layer.
N_O	Number of neurons in the output layer.
$\overline{P}$	LDC imposed load cap on the micro-hub [kW].
P_a	Rated power of a given appliance a [kW].
Pm	Measured load profile [kW].
Ps	Simulated load profile [kW].
ρ	TOU tariff [$/MWh].
S_a	State of appliance at a time k; $S_a = 1$ denotes ON, and $S_a = 0$ otherwise.
θ	External temperature [Celsius].
$w_{i,j}$	Weight of the connection between input layer neuron and hidden layer neurons.
$W_{i,l}$	Weight of the connection between hidden layer and output layer neurons.

5.3 EHMS Residential Micro-hub Model [50]

The EHMS residential micro-hub model comprises an objective function, an LDC imposed constraint on the peak demand, and other operational constraints pertaining to the hub components. Thus, the general form of the optimization model for the residential energy hub is as follows [50]:

$$\begin{aligned} \min \quad & J = \text{Objective Function} \\ \text{s. t.} \quad & \sum_{a} P_a S_a(k) \leq \overline{P} \qquad (5.1) \\ & \text{Device } a \text{ operational constraints} \quad \forall a \in A \qquad (5.2) \end{aligned}$$

Different objective functions can be adopted to solve the optimization problem. In this work, minimization of the customer's total energy costs is used as the optimization objective. Constraint (5.1) sets a cap on the demand of the residential micro-hub, ensuring that the power consumption at any given time does not exceed a specified value. Equations (5.2) represent the operational constraints of the appliances. In this work, four appliances are considered, namely, air-conditioning, dishwasher, washer, and dryer; the models for these appliances can be found in [50]. A 24-hour scheduling horizon with time intervals of 5 minutes is used in this work.

5.4 Residential NN Load Model

5.4.1 Inputs

External weather conditions have a significant impact on the energy consumption of heating and cooling systems in a household. Heat transfer through walls and solar radiation are examples of how outdoor conditions can affect indoor temperature. Nowadays, accurate weather forecasts are available for every hour, which are used in this work to generate the EHMS optimal schedules for a day.

Electricity prices will also impact the scheduling of appliances, especially when the objective is to minimize the customer's cost of energy consumption. For example, customers would like to schedule some of the appliances when electricity prices are low. Summer TOU tariff rates applicable in Ontario are used in this work to determine the EHMS optimal schedules.

Another input used to determine the micro-hub optimal schedules is the peak demand constraint ($\overline{P}$) imposed by the LDC. The LDC may impose such a cap at the micro-hub level to guarantee proper grid conditions, as discussed in the previous two chapters, and customers can accordingly schedule their appliance usage with the help of EHMS. This demand cap is set as an external input to the EHMS, in such a way that the LDC can take advantage of load reduction from each micro-hub during peak hours. Thus, for a given

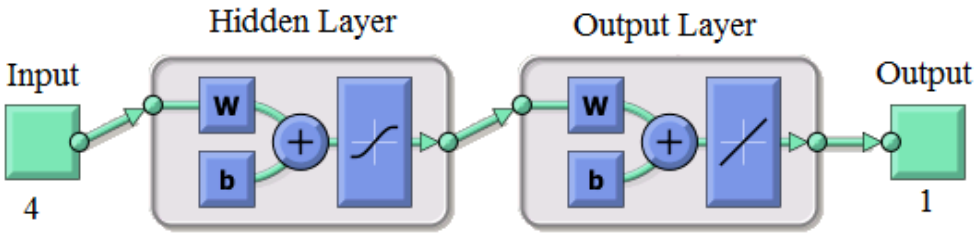

Figure 5.1: NN EHMS residential micro-hub model structure.

day, the value of $\overline{P}$ may vary, as per the macro-hub optimal decisions (see Chapter 4), to obtain corresponding optimal schedules for the micro-hub.

Here, the estimated residential load profile using NNs (Ps_k) is expressed as a function of time (k), outside temperature (θ_k), TOU tariff (ρ_k), and peak demand ($\overline{P}_k$), as follows:

$$Ps_k = f(k, \theta_k, \rho_k, \overline{P}_k) \tag{5.3}$$

This EHMS residential micro-hub NN model is developed based on data for the months of May, June, and July of 2012 for weekdays, considering the actual temperature profiles and TOU prices of those dates, to obtain smart-load profiles for a residential customer for different $\overline{P}_k$ values imposed by the LDC. The model is developed considering 5 minute time intervals. The NN is trained considering simulated and actual measured data to capture the load behavior of a real residential micro-hub. An input matrix is created with simulated and measured data having a dimension of 84,960 x 4, with the dimension of the output vector being 84,960.

5.4.2 NN Structure

The structure of the feedforward NN used in this work is presented in Figure 5.1. Observe that there are four sets of input data: k, θ_k, ρ_k, and $\overline{P}_k$; and one output data set Ps_k. Accordingly, there are four input layer neurons and one output layer neuron. Furthermore, the considered NN has one hidden layer with N_H number of neurons in the hidden layer. During the training process N_H is varied to arrive at the best fit for the load model. The NN is trained in MATLAB^{TM} using the Levenberg-Marquardt algorithm for back propagation [101].

While training the NN, the entire dataset is divided into three subsets [102]. The first subset is the training set, used for computing the gradient and updating the network weights and biases. The second subset is the validation set, which is used to monitor the error during the training process, that normally decreases during the initial phase of training, as does the training set error. However, when the network begins to over-fit the data, the error on the validation set typically begins to rise. The third subset or test set is used to compare different models, using the test set error during the training process to evaluate the accuracy of the NN model.

There are four functions available in MATLAB^{TM} for dividing the data set into training, validation and test sets, namely, *dividerand*, *divideblock*, *divideint*, and *divideind*, which have the following characteristics [102]:

- *dividerand*: This function divides the data set into three subsets using random indices.
- *divideblock*: This function divides the data set into three subsets using blocks of indices.
- *divideint*: This function divides the data set into three subsets using interleaved indices.
- *divideind*: This function divides the data set into three subsets using specified indices.

5.5 Results and Analysis

5.5.1 Choice of Data Division Function

In order to identify the best function to divide the data sets into training, validation and testing subsets, the four aforementioned functions are used to train the NN. For this study, ratios of training, validation, and test sets are assumed to be 0.7, 0.15, and 0.15, respectively. The number of neurons in the hidden layer is fixed at $N_H = 5$. After training the NN using the four functions, the corresponding values of R-squared[1] are compared. The estimated total energy consumed by the load (Es) using the simulated load profile

[1]In statistics, the coefficient of determination, denoted by R-squared, indicates how well the data points fit a statistical model; the value of R-squared close to unity is a desired fit [103].

Ps_k, for each function, is then compared with the energy consumed by the load (Em) obtained from the measured load profile Pm_k. These energy values are given by:

$$Es = \sum_k Ps_k \tag{5.4}$$

$$Em = \sum_k Pm_k \tag{5.5}$$

Figures 5.2-5.5 present a comparison between Ps_k and Pm_k for 600 samples at 5-minute time intervals. Note that the functions *dividerand*, *divideblock*, and *divideint* can closely capture the behavior of the micro-hub load model, where the output obtained using the *divideind* function is clearly not a good fit for the dataset used in this study. It is to be noted that the latter function relies on the specifications of the training data subset in order for the NN to attain acceptable performance, which is highly dependent on the modelers knowledge of the dataset; therefore, this restricts this function's wider application in training models. Observe as well that none of the methods are able to capture the spikes in the load profile, which is a difficult issue for all forecasting systems, and illustrates the limitations of the proposed NN mdoel.

Table 5.1 compares the four data division functions and their respective network performances. Observe that for the given input dataset, the *dividerand* function is found to be the best fit to estimate the load model based on the R-squared values. The value of R-squared for *divideblock* and *divideint* functions are very close to each other but somewhat lower than that with *dividerand*, while the *divideind* function has a very low value. The measured energy E_m is 84.454 MW and its difference with respect to Es is minimal in the case of the *dividerand* function, but also reasonably low with *divideblock* and *divideint* functions; however, there is a large error in Es obtained using the *divideind* function. Therefore, it can be concluded that the *dividerand* function performs best for the dataset used to estimate the residential micro-hub load, and hence this function has been considered for all the subsequent analysis reported here.

5.5.2 Effect of Varying N_H

In this section, the number of neurons in the hidden layer N_H are varied, and using the *dividerand* function, to determine the suitable value for which the best fit for the residential load model can be obtained. The ratios of training, validation, and test sets are assumed to be same as before, i.e., 0.7, 0.15, and 0.15, respectively. Table 5.2 summarizes the effect

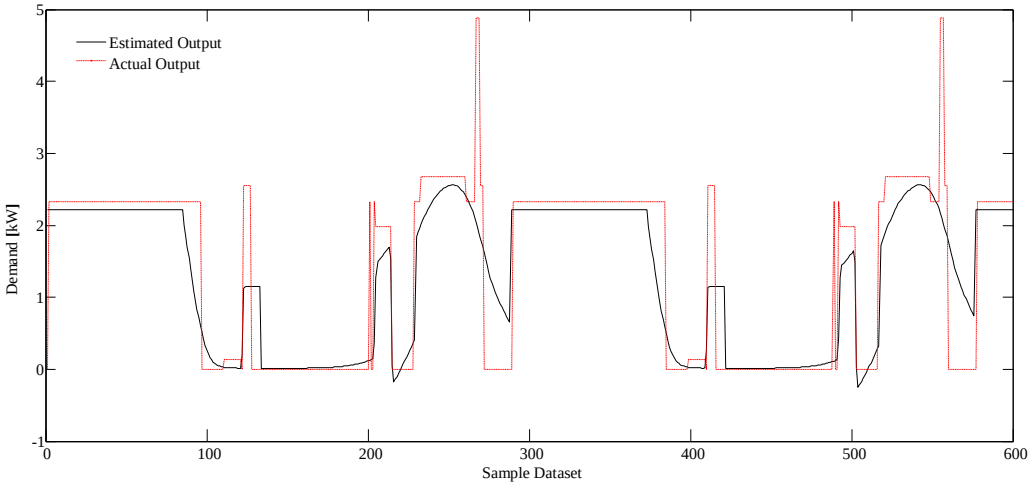

Figure 5.2: Estimated output using the *dividerand* function.

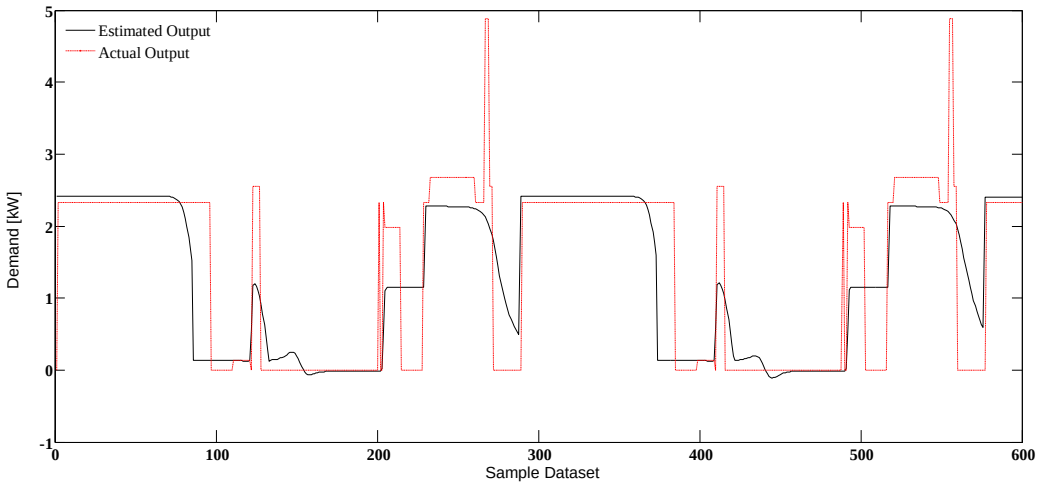

Figure 5.3: Estimated output using the *divideblock* function.

of varying N_H on the NN performance. Note from the R-squared value and the percentage error that the best fit is obtained for $N_H = 7$, with the corresponding value of R-squared being higher high as compared to those obtained with other values of N_H. Furthermore, the simulated value of total energy Es obtained is also very close to the measured energy Em with a difference of 0.01%. Figure 5.6 presents a comparison between Ps_k and Pm_k for 600 samples at 5-minute time intervals for $N_H = 7$ hidden-layer neurons; observe that

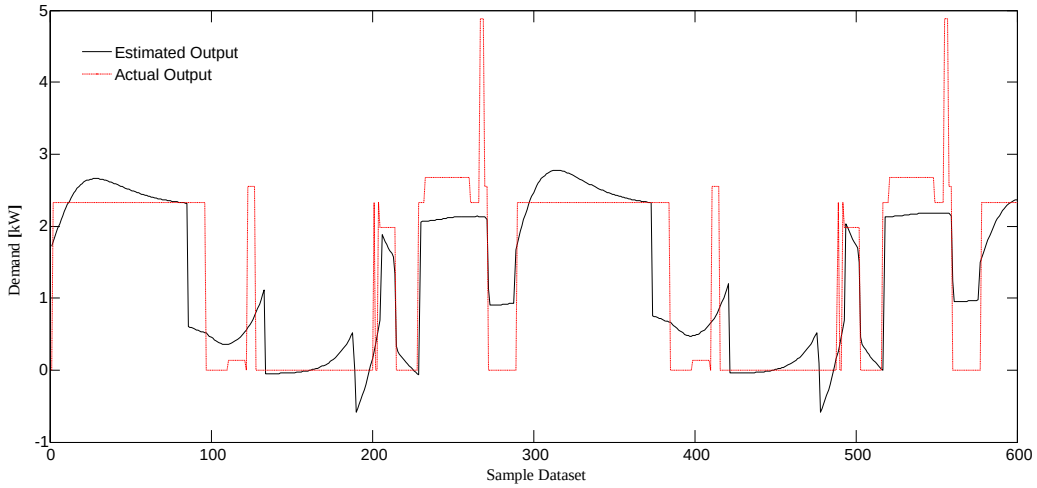

Figure 5.4: Estimated output using the *divideint* function.

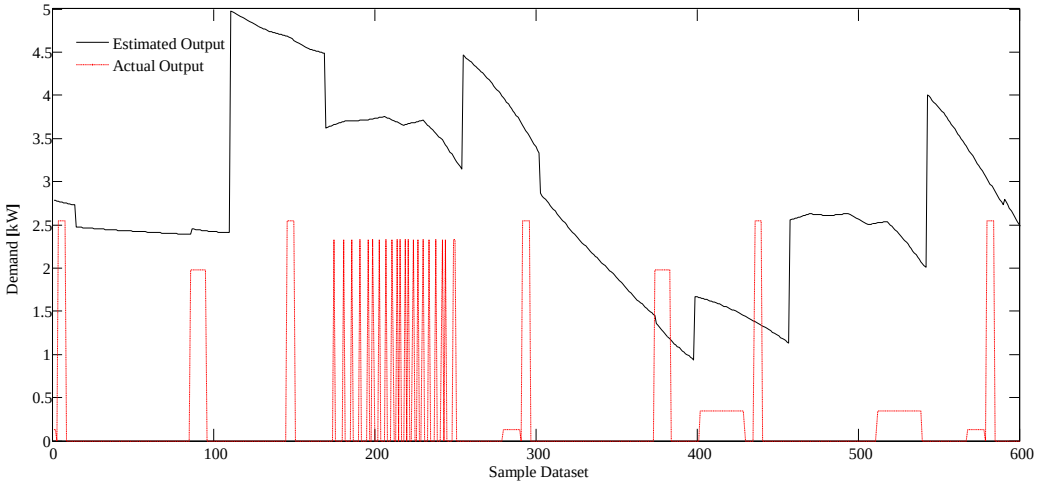

Figure 5.5: Estimated output using the *divideind* function.

the NN is able to capture the demand spikes and is a good fit for Pm_k.

Table 5.1: Comparison of data division functions and NN performance.

Function	R-squared	Em [MWh]	Es [MWh]	Error
dividerand	0.7326	84.454	84.5	-0.06%
divideblock	0.6779	84.454	84.96	-0.6%
divideint	0.6806	84.454	84.33	0.15%
divideind	0.0614	84.454	239.2	-183.23%

Table 5.2: Effect of varying N_H on NN performance.

N_H	R-squared	Em [MWh]	Es [MWh]	Error
2	0.59256	84.454	84.529	-0.09%
3	0.665513	84.454	84.309	0.17%
4	0.689149	84.454	84.497	-0.05%
5	0.7326	84.454	84.5	-0.05%
6	0.734655	84.454	84.324	0.15%
7	0.806925	84.454	84.446	0.01%
8	0.739445	84.454	84.372	0.1%
9	0.713315	84.454	84.68	-0.27%
10	0.734586	84.454	84.524	-0.08%

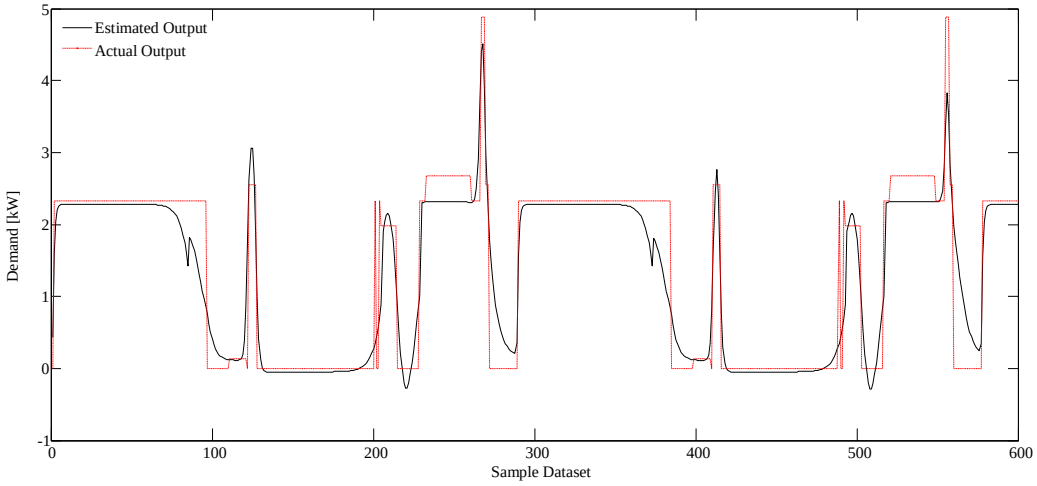

Figure 5.6: Estimated output using the *divideind* function with N_H=7.

5.5.3 Mathematical Functions of NN Model

In order to obtain a mathematical function of Ps from the trained NN, the output from each hidden layer neuron H_k^1 to H_k^7, is determined first. The incoming inputs with appropriate weights $w_{i,j}\ \ \forall i \in 1, ..., N_H, j \in 1, ..., N_I$, are summed up at each hidden layer neuron. Also, each hidden layer neuron has an additional input, the bias (β_1 to β_7), which is used in the network to generalize the solution and to avoid a zero value of the output, even when an input is zero. This summed signal is passed through an activation function ($tansig$) associated with each hidden layer neuron, which transforms the net weighted sum of all incoming signals into an output signal from the hidden layer neuron. Accordingly, H_k^1 to H_k^7 are given by:

$$H_k^1 = tansig(w_{1,1}\theta_k + w_{1,2}\overline{P}_k + w_{1,3}\rho_k + w_{1,4}k + \beta_1) \tag{5.6}$$

$$H_k^2 = tansig(w_{2,1}\theta_k + w_{2,2}\overline{P}_k + w_{2,3}\rho_k + w_{2,4}k + \beta_2) \tag{5.7}$$

$$H_k^3 = tansig(w_{3,1}\theta_k + w_{3,2}\overline{P}_k + w_{3,3}\rho_k + w_{3,4}k + \beta_3) \tag{5.8}$$

$$H_k^4 = tansig(w_{4,1}\theta_k + w_{4,2}\overline{P}_k + w_{4,3}\rho_k + w_{4,4}k + \beta_4) \tag{5.9}$$

$$H_k^5 = tansig(w_{5,1}\theta_k + w_{5,2}\overline{P}_k + w_{5,3}\rho_k + w_{5,4}k + \beta_5) \tag{5.10}$$

$$H_k^6 = tansig(w_{6,1}\theta_k + w_{6,2}\overline{P}_k + w_{6,3}\rho_k + w_{6,4}k + \beta_6) \tag{5.11}$$

$$H_k^7 = tansig(w_{7,1}\theta_k + w_{7,2}\overline{P}_k + w_{7,3}\rho_k + w_{7,4}k + \beta_7) \tag{5.12}$$

The weight matrix connecting the input layer neurons to the hidden layer neurons, i.e., $w_{i,j}\ \ \forall i \in 1, ..., N_H, j \in 1, ..., N_I$ is given by:

$$w_{i,j} = \begin{bmatrix} 0.0121 & -0.0046 & 0.1115 & 0.7641 \\ 0.0057 & -0.0003 & 0.1008 & 0.5240 \\ -8.6261 & -0.0623 & -29.3987 & -30.26196 \\ 0.2576 & 0.0871 & -139.8230 & 181.7761 \\ 0.2651 & 0.1480 & 58.4377 & 203.0100 \\ -26.2529 & -35.3216 & -14.6354 & 1.5813 \\ -0.1842 & -112.1618 & -109.1634 & 14.3121 \end{bmatrix} \tag{5.13}$$

The bias $\beta_i \ \ \forall i \in 1, ..., N_H$ associated with each hidden layer neuron is given by:

$$\beta_i = \begin{bmatrix} 0.9145 & 1.13509 & -7.3000 & 82.8379 & -121.7264 & 21.7426 & -8.9571 \end{bmatrix}^T \quad (5.14)$$

Finally, Ps_k can be obtained from the output neuron of the trained NN as follows:

$$Ps_k = purelin(H_k^1 W_{1,1} + H_k^2 W_{1,2} + H_k^3 W_{1,3} + H_k^4 W_{1,4} + H_k^5 W_{1,5} + H_k^6 W_{1,6} + H_k^7 W_{1,7} + \Gamma) \quad (5.15)$$

where *purelin* is a linear transfer function available in MATLAB^{TM} [104]. The weight matrix connecting the hidden layer neurons with the single output layer neuron $W_{i,l} \quad \forall i \in 1, ..., N_H, l \in 1, ..., N_O$ is given by:

$$W_{i,l} = \begin{bmatrix} -34.4710 & 69.4583 & 0.3763 & 0.2950 & -0.3221 & 0.0155 & 0.0838 \end{bmatrix} \quad (5.16)$$

and the bias associated with the output layer neuron is given by:

$$\Gamma = -32.5756 \quad (5.17)$$

5.6 Summary

This chapter presented a novel technique for estimating the load of a residential micro-hub using NNs. The NN was trained using actual household data from a residential in Ontario over a period of 3 months. Various NN training models and configurations of hidden layer neurons were tested to arrive at the best data division function and NN structure for demand estimation. The proposed demand model can be used in the previously described micro-hub models and thus help in the realization of smart girds.

Chapter 6

Conclusions

6.1 Summary

The research presented in this thesis concentrates on the optimal operation of distribution feeder operation in the context of smart grids. The motivation for this research was presented in Chapter 1, and the main research objectives were laid out based on a critical review of the existing literature.

In Chapter 2, the background topics relevant to the research on optimal operation of distribution feeders with smart loads were reviewed. Distribution system components such as switches, LTCs, capacitors, and loads were discussed briefly. DSM and DR programs, and their objectives, strategies, and approaches were presented. An overview of PEV loads, and some silent features of the communication and control infrastructure in smart distribution system was presented. An overview of mathematical programming models, their solution methods, and optimization solvers used here were discussed as well. Finally, a brief overview of NNs and EHMS concepts used here to develop residential micro-hub load models was also presented.

Chapter 3 presented a smart distribution system operation framework including PEV smart charging. Through a three-phase DOPF, the PEV smart charging schedules and operating decisions for LTCs, capacitors and switches for the next day were determined. Uncontrolled versus smart charging schemes were compared for various scenarios from both the customer's and LDC's perspective; considering both constant impedance and ZIP load models. The impact of variable initial SOC and charging start time, to take into account the uncertainty in customers' driving patterns, were studied based on an MCS approach.

The effect of peak demand constraints imposed by the LDC was also studied within the framework of smart charging. The studies were carried out on two distribution systems: the IEEE 13-node test feeder and a real distribution feeder.

In Chapter 4, two categories of elastic loads were considered: price-responsive and controlled loads, to study the smart operation of unbalanced distribution systems, based on the DOPF model developed in Chapter 3. Price-responsive loads were modeled using a parametric linear and exponential representation of the load as a function of the RTP, assuming rational behavior of customers. Furthermore, a novel and controllable constant energy load model was proposed to represent critical and deferrable loads. MCS was used to study uncertainty in the price-responsive load models. Finally, the impact of continuous and discrete modeling of LTCs and capacitors was studied. The proposed load models and their impact on optimal distribution system operation were studied on the IEEE 13-node test feeder and a real distribution feeder.

Chapter 5 presented an NN model of an EHMS residential micro-hub, based on measured and simulated data obtained from an actual implementation of the EHMS micro-hub model. The proposed model is based on external inputs: temperature, time, peak demand, and TOU tariff. The developed function can be readily applied to the proposed DOPF for real-time optimal operation and control of LDC distribution feeders.

6.2 Contributions

The main contributions of the research presented in this thesis are as follows:

- For the first time, a comprehensive representation of the LDC's operating criteria in smart grids in a three-phase DOPF model for smart charging of PEVs was proposed. Furthermore, a thorough examination of uncontrolled versus smart PEV charging and their impact on LDC operation is carried out.
- While several authors have incorporated price-responsive loads in power system operations, the impact of such loads are studied in an unbalanced distribution system at the retail customer level, for the purpose of optimal feeder operation, based on DOPF approach. In this context, a new mathematical model is proposed to represent controllable or dispatchable loads in an unbalanced distribution feeder, thus allowing LDCs to study the impact of indirect load control in the context of DR programs.
- For the first time, real measurement data from residential micro-hubs is used to develop accurate EHMS load models using NNs. The proposed NN model is developed

into a nonlinear function of time, external temperature, peak demand, and TOU prices for direct use in DOPF-based applications.

The main contents and contributions of Chapter 3 have been published in IEEE Transactions on Smart Grid [105]. The main contents of Chapter 4 have been submitted to IEEE Transactions on Smart Grid and is currently under review [106].

6.3 Future Work

Based on the research presented in this thesis, the following are some ideas and directions for further research:

- In this work, LTC taps and capacitors are modeled as continuous variables. However, in practice, these are discrete transforming the proposed DOPF into an MINLP problem, which is very challenging problem to solve. Hence, adequate and fast solution methods for such DOPF problem could be explored.
- Using real data, the price-responsive load parameters could be properly estimated to use them to study the optimal operation of distribution feeders. Hence, the price-responsiveness of customers could be studied in practice through historical data of price and load demand.
- The proposed DOPF is based on a deterministic framework. Thus, this model could be modified to directly consider stochastic parameters like initial SOC, arrival time of customers, number of PEVs at a node and phase, etc.
- Based on the proposed NN load model, the next step should be to integrate it into the proposed DOPF model to study optimal LDC operational decisions, and hence representing DR of EHMS residential micro-hubs in this framework.

References

[1] "International Energy Agency: World Energy Outlook 2013." [Online]. Available: http://www.worldenergyoutlook.org

[2] "Ontario Power Authority: Long Term Energy Plan 2013." [Online]. Available: http://www.powerauthority.on.ca/power-planning/long-term-energy-plan-2013

[3] "Ontaro Power Authority." [Online]. Available: http://www.powerauthority.on.ca/about-us/directives-opa-minister-energy-and-infrastructure

[4] "Ontario Power Authority." [Online]. Available: http://powerauthority.on.ca/news/opas-demand-response-3-program-activated-yesterday

[5] "Ontario Power Authority: saveONenergy." [Online]. Available: https://www.saveonenergy.ca/Business/Program-Overviews/Retrofit-for-Commercial.aspx

[6] "Ontario Power Authority: saveONenergy." [Online]. Available: https://saveonenergy.ca/Consumer/Programs/PeaksaverPlus/Energy-Display.aspx

[7] "Minitry of Transportation - Ontario." [Online]. Available: http://www.mto.gov.on.ca/english/dandv/vehicle/electric/electric-vehicles.shtml

[8] E. Ungar and K. Fell, "Plug in, turn on, and load up," *IEEE Power and Energy Magazine*, vol. 8, no. 3, pp. 30–35, May-June 2010.

[9] CanmetENERGY Report, "Electric Vehicle Technology Road Map for Canada," 2009. [Online]. Available: http://canmetenergy.nrcan.gc.ca/sites/canmetenergy.nrcan.gc.ca/files/pdf/fichier/81890/ElectricVehicleTechnologyRoadmap_e.pdf

[10] Waterloo Institure for Sustainable Energy, "Towards an Ontario Action Plan for Plug-in Electric Vehicles (PEVs)," in *Univeristy of Waterloo*, May 2010. [Online].

Available: http://www.plugndriveontario.ca/pdf/Waterloo%20PHEV%20Report%20June%%202010%20FINAL.pdf

[11] M. Bozchalui, S. Hashmi, H. Hassen, C. Cañizares, and K. Bhattacharya, "Optimal operation of residential energy hubs in smart grids," *IEEE Transactions on Smart Grid*, vol. 3, no. 4, pp. 1755–1766, 2012.

[12] G. Heydt, "The next generation of power distribution systems," *IEEE Transactions on Smart Grid*, vol. 1, no. 3, pp. 225–235, 2010.

[13] R. Baldick and F. Wu, "Efficient integer optimization algorithms for optimal coordination of capacitors and regulators," *IEEE Transactions on Power Systems*, vol. 5, no. 3, pp. 805–812, 1990.

[14] Y.-Y. Hsu and F.-C. Lu, "A combined artificial neural network-fuzzy dynamic programming approach to reactive power/voltage control in a distribution substation," *IEEE Transactions on Power Systems*, vol. 13, no. 4, pp. 1265–1271, 1998.

[15] J. Kearly, A. Chikhani, R. Hackam, M. Salama, and V. Quintana, "Microprocessor controlled reactive power compensator for loss reduction in radial distribution feeders," *IEEE Transactions on Power Delivery*, vol. 6, no. 4, pp. 1848–1855, 1991.

[16] M. Salama, N. Manojlovic, V. Quintana, and A. Chikhani, "Real-time optimal reactive power control for distribution networks," *International Journal of Electrical Power & Energy Systems*, vol. 18, no. 3, pp. 185 – 193, 1996.

[17] I. Roytelman, B. K. Wee, and R. L. Lugtu, "Volt/var control algorithm for modern distribution management system," *IEEE Transactions on Power Systems*, vol. 10, no. 3, pp. 1454–1460, 1995.

[18] M. Salama and A. Chikhani, "A simplified network approach to the var control problem for radial distribution systems," *IEEE Transactions on Power Delivery*, vol. 8, no. 3, pp. 1529–1535, 1993.

[19] M. Elkhatib, R. El-Shatshat, and M. Salama, "Novel coordinated voltage control for smart distribution networks with DG," *IEEE Transactions on Smart Grid*, vol. 2, no. 4, pp. 598–605, 2011.

[20] S. Bruno, S. Lamonaca, G. Rotondo, U. Stecchi, and M. La Scala, "Unbalanced three-phase optimal power flow for smart grids," *IEEE Transactions on Industrial Electronics*, vol. 58, no. 10, pp. 4504 –4513, Oct. 2011.

[21] S. Paudyal, C. Cañizares, and K. Bhattacharya, "Optimal operation of distribution feeders in smart grids," *IEEE Transactions on Industrial Electronics*, vol. 58, no. 10, pp. 4495 –4503, Oct. 2011.

[22] M. Liu, C. Cañizares, and W. Huang, "Reactive power and voltage control in distribution systems with limited switching operations," *IEEE Transactions on Power Systems*, vol. 24, no. 2, pp. 889 –899, May 2009.

[23] A. Bose, "Smart transmission grid applications and their supporting infrastructure," *IEEE Transactions on Smart Grid*, vol. 1, no. 1, pp. 11–19, 2010.

[24] A. Bouhouras, G. Andreou, D. Labridis, and A. Bakirtzis, "Selective automation upgrade in distribution networks towards a smarter grid," *IEEE Transactions on Smart Grid*, vol. 1, no. 3, pp. 278–285, 2010.

[25] A. P. S. Meliopoulos, G. Cokkinides, R. Huang, E. Farantatos, S. Choi, Y. Lee, and X. Yu, "Smart grid technologies for autonomous operation and control," *IEEE Transactions on Smart Grid*, vol. 2, no. 1, pp. 1–10, 2011.

[26] E. Santacana, G. Rackliffe, L. Tang, and X. Feng, "Getting smart," *IEEE Power and Energy Magazine*, vol. 8, no. 2, pp. 41–48, 2010.

[27] C. Chen, J. Wang, Y. Heo, and S. Kishore, "MPC-based appliance scheduling for residential building energy management controller," *IEEE Transactions on Smart Grid*, vol. 4, no. 3, pp. 1401–1410, 2013.

[28] K. Bhattacharya, M. Bollen, and J. Daalder, "Real time optimal interruptible tariff mechanism incorporating utility-customer interactions," *IEEE Transactions on Power Systems*, vol. 15, no. 2, pp. 700–706, 2000.

[29] D. Kirschen, G. Strbac, P. Cumperayot, and D. de Paiva Mendes, "Factoring the elasticity of demand in electricity prices," *IEEE Transactions on Power Systems*, vol. 15, no. 2, pp. 612–617, 2000.

[30] E. Bompard, Y. Ma, R. Napoli, and G. Abrate, "The demand elasticity impacts on the strategic bidding behavior of the electricity producers," *IEEE Transactions on Power Systems*, vol. 22, no. 1, pp. 188–197, 2007.

[31] H. Aalami, M. Parsa Moghaddam, and G. R. Yousefi, "Demand response modeling considering interruptible/curtailable loads and capacity market programs," *Applied Energy*, vol. 87, no. 1, pp. 243 – 250, 2010.

[32] A. Khodaei, M. Shahidehpour, and S. Bahramirad, "SCUC with hourly demand response considering intertemporal load characteristics," *IEEE Transactions on Smart Grid*, vol. 2, no. 3, pp. 564–571, Sept 2011.

[33] A. Abdollahi, M. Moghaddam, M. Rashidinejad, and M. Sheikh-El-Eslami, "Investigation of economic and environmental-driven demand response measures incorporating uc," *IEEE Transactions on Smart Grid*, vol. 3, no. 1, pp. 12–25, 2012.

[34] K. Dietrich, J. Latorre, L. Olmos, and A. Ramos, "Demand response in an isolated system with high wind integration," *IEEE Transactions on Power Systems*, vol. 27, no. 1, pp. 20–29, 2012.

[35] J. Aghaei and M.-I. Alizadeh, "Critical peak pricing with load control demand response program in unit commitment problem," *IET Generation, Transmission Distribution*, vol. 7, no. 7, pp. 681–690, 2013.

[36] C. De Jonghe, B. Hobbs, and R. Belmans, "Optimal generation mix with short-term demand response and wind penetration," *IEEE Transactions on Power Systems*, vol. 27, no. 2, pp. 830–839, 2012.

[37] H. Jorge, C. Antunes, and A. Martins, "A multiple objective decision support model for the selection of remote load control strategies," *IEEE Transactions on Power Systems*, vol. 15, no. 2, pp. 865–872, May 2000.

[38] J. Medina, N. Muller, and I. Roytelman, "Demand response and distribution grid operations: opportunities and challenges," *IEEE Transactions on Smart Grid*, vol. 1, no. 2, pp. 193–198, Sept. 2010.

[39] S. Shao, M. Pipattanasomporn, and S. Rahman, "Demand response as a load shaping tool in an intelligent grid with electric vehicles," *IEEE Transactions on Smart Grid*, vol. 2, no. 4, pp. 624–631, Dec. 2011.

[40] ——, "Grid integration of electric vehicles and demand response with customer choice," *IEEE Transactions on Smart Grid*, vol. 3, no. 1, pp. 543–550, March 2012.

[41] A. Masoum, S. Deilami, P. Moses, M. Masoum, and A. Abu-Siada, "Smart load management of plug-in electric vehicles in distribution and residential networks with charging stations for peak shaving and loss minimisation considering voltage regulation," *IET Generation, Transmission Distribution*, vol. 5, no. 8, pp. 877–888, August 2011.

[42] D. Steen, L. A. Tuan, O. Carlson, and L. Bertling, "Assessment of electric vehicle charging scenarios based on demographical data," *IEEE Transactions on Smart Grid*, vol. 3, no. 3, pp. 1457–1468, Sept. 2012.

[43] K. Qian, C. Zhou, M. Allan, and Y. Yuan, "Modeling of load demand due to EV battery charging in distribution systems," *IEEE Transactions on Power Systems*, vol. 26, no. 2, pp. 802–810, May 2011.

[44] S. Deilami, A. Masoum, P. Moses, and M. Masoum, "Real-time coordination of plug-in electric vehicle charging in smart grids to minimize power losses and improve voltage profile," *IEEE Transactions on Smart Grid*, vol. 2, no. 3, pp. 456–467, Sept. 2011.

[45] K. Clement-Nyns, E. Haesen, and J. Driesen, "The impact of charging plug-in hybrid electric vehicles on a residential distribution grid," *IEEE Transactions on Power Systems*, vol. 25, no. 1, pp. 371–380, Feb 2010.

[46] E. Sortomme, M. Hindi, S. MacPherson, and S. Venkata, "Coordinated charging of plug-in hybrid electric vehicles to minimize distribution system losses," *IEEE Transactions on Smart Grid*, vol. 2, no. 1, pp. 198–205, March 2011.

[47] P. Richardson, D. Flynn, and A. Keane, "Local versus centralized charging strategies for electric vehicles in low voltage distribution systems," *IEEE Transactions on Smart Grid*, vol. 3, no. 2, pp. 1020–1028, 2012.

[48] ——, "Optimal charging of electric vehicles in low-voltage distribution systems," *IEEE Transactions on Power Systems*, vol. 27, no. 1, pp. 268–279, 2012.

[49] M. Geidl and G. Andersson, "Optimal power flow of multiple energy carriers," *IEEE Transactions on Power Systems*, vol. 22, no. 1, pp. 145–155, 2007.

[50] M. C. Bozchalui, "Optimal Operation of Energy Hubs in the Context of Smart Grids," PhD Thesis, University of Waterloo, Department of Electrical and Computer Engineering, 2011.

[51] "Energy Hub Management System ." [Online]. Available: http://www.energyhub.uwaterloo.ca/

[52] J. Mathieu, P. Price, S. Kiliccote, and M. Piette, "Quantifying changes in building electricity use, with application to demand response," *IEEE Transactions on Smart Grid*, vol. 2, no. 3, pp. 507–518, Sept. 2011.

[53] O. Corradi, H. Ochsenfeld, H. Madsen, and P. Pinson, "Controlling electricity consumption by forecasting its response to varying prices," *IEEE Transactions on Power Systems*, vol. 28, no. 1, pp. 421–429, 2013.

[54] "The smart grid: an introduction." [Online]. Available: http://energy.gov/sites/prod/files/oeprod/DocumentsandMedia/DOE_SG_Book_Single_Pages.pdf

[55] "U.S. Department of Energy." [Online]. Available: http://www.smartgrid.gov/

[56] "Hydro One." [Online]. Available: http://www.hydroone.com/MyHome/MyAccount/MyMeter/Pages/SmartMeters.aspx

[57] IESO, "Modernizing Ontario's Electricity System: Next Steps," in *Report of the Ontario Smart Grid Forum*, May 2011. [Online]. Available: http://www.ieso.ca/imoweb/pubs/smart_grid/Smart_Grid_Forum-Report-May_2011.pdf

[58] W. H. Kersting, *Distribution System Modeling and Analysis*, 2nd ed. CRC Press, 2006.

[59] P. A. Gnadt and J. S. Lawler, *Automating Electric Utility Distribution Systems*. Prentice Hall, 1990.

[60] M. Baran and M.-Y. Hsu, "Volt/VAr control at distribution substations," *IEEE Transactions on Power Systems*, vol. 14, no. 1, pp. 312 –318, Feb 1999.

[61] A. Sanghvi, "Flexible strategies for load/demand management using dynamic pricing," *IEEE Transactions on Power Systems*, vol. 4, no. 1, pp. 83–93, 1989.

[62] C.-S. Chen and J. T. Leu, "Interruptible load control for Taiwan power company," *IEEE Transactions on Power Systems*, vol. 5, no. 2, pp. 460–465, May 1990.

[63] F. Schweppe, R. Tabors, J. Kirtley, H. Outhred, F. Pickel, and A. Cox, "Homeostatic utility control," *IEEE Transactions on Power Apparatus and Systems*, vol. PAS-99, no. 3, pp. 1151–1163, May 1980.

[64] T. Logenthiran, D. Srinivasan, and T. Z. Shun, "Demand side management in smart grid using heuristic optimization," *IEEE Transactions on Smart Grid*, vol. 3, no. 3, pp. 1244–1252, 2012.

[65] P. Jazayeri, A. Schellenberg, W. D. Rosehart, J. Doudna, S. Widergren, D. Lawrence, J. Mickey, and S. Jones, "A survey of load control programs for price and system stability," *IEEE Transactions on Power Systems*, vol. 20, no. 3, pp. 1504–1509, 2005.

[66] "FERC Staff Report: Assesment of Demand Response and Advanced Metering," Dec. 2012. [Online]. Available: http://www.ferc.gov/legal/staff-reports/12-20-12-demand-response.pdf

[67] S. Rahman and Rinaldy, "An efficient load model for analyzing demand side management impacts," *IEEE Transactions on Power Systems*, vol. 8, no. 3, pp. 1219–1226, Aug 1993.

[68] C. W. Gellings and H. L. Forgey, "Integrating load management into utility planning," *IEEE Transactions on Power Apparatus and Systems*, vol. PAS-104, no. 8, pp. 2079–2085, Aug 1985.

[69] EPRI, "EPRI Innovative Rate Design Study," Jan. 1985.

[70] D. Tuttle and R. Baldick, "The evolution of plug-in electric vehicle-grid interactions," *IEEE Transactions on Smart Grid*, vol. 3, no. 1, pp. 500 –505, March 2012.

[71] Z. Darabi and M. Ferdowsi, "Aggregated impact of plug-in hybrid electric vehicles on electricity demand profile," *IEEE Transactions on Sustainable Energy*, vol. 2, no. 4, pp. 501–508, Oct. 2011.

[72] P. Denholm and W. Short, "An evaluation of utility system impacts and benefits of optimally dispatched plug-in hybrid electric vehicles," in *National Renewable Energy Laboratory*, 2006.

[73] W. L. Winston and M. Venkataramanan, *Introduction to Mathematical Programming*, 4th ed. Curt Hinrichs, 2003.

[74] E. Castillo, A. J. Conejo, P. Pedregal, R. Garcia, and N. Alguacil, *Buildiing and Solving Mathematical Programming Models in Engineering and Science*. Wiley, 2002.

[75] A. J. Conejo, E. Castillo, R. Minquez, and R. Garcia-Bertrand, *Decomposition Techniques in Mathematical Programming*. Springer, 2006.

[76] D. E. Goldberg, *Genetic Algorithms in Search Optimization, and Machine Learning*. Addison-Wesley Publishing Company Inc., 1953.

[77] A. H. Mantawy, Y. Abdel-Magid, and S. Selim, "Integrating genetic algorithms, tabu search, and simulated annealing for the unit commitment problem," *IEEE Transactions on Power Systems*, vol. 14, no. 3, pp. 829–836, Aug 1999.

[78] "BARON: Branch and Reduce optimization navigator," University of Illinois at Urbana-Champaign. [Online]. Available: :http://archimedes.scs.uiuc.edu/

[79] "DICOPT," GAMS Development Corporation. [Online]. Available: http://archimedes.scs.uiuc.edu/

[80] "GAMS Release 2.25," A Users Guide, GAMS Development Corporation, 1998. [Online]. Available: http://www.gams.com/

[81] "GAMS Solver Description." [Online]. Available: http://www.gams.com/solvers/solvers.htm

[82] K. Gurney, *An Introduction to Neural Networks*, 1st ed. UCL Press Limited, 1997.

[83] J. C. Principe, N. R. Euliano, and W. C. Lefebvre, *Neural and Adaptive Systems: Fundamentals through Simulations*, 1st ed. John Wiley & Sons, Inc., 2000.

[84] D. Park, M. El-Sharkawi, I. Marks, R.J., L. Atlas, and M. Damborg, "Electric load forecasting using an artificial neural network," *IEEE Transactions on Power Systems*, vol. 6, no. 2, pp. 442–449, May 1991.

[85] H. Sasaki, M. Watanabe, J. Kubokawa, N. Yorino, and R. Yokoyama, "A solution method of unit commitment by artificial neural networks," *IEEE Transactions on Power Systems*, vol. 7, no. 3, pp. 974–981, Aug 1992.

[86] D. Chen and R. Mohler, "Neural-network-based load modeling and its use in voltage stability analysis," *IEEE Transactions on Control Systems Technology*, vol. 11, no. 4, pp. 460–470, July 2003.

[87] M. Geidl, G. Koeppel, P. Favre-Perrod, B. Klockl, G. Andersson, and K. Frohlich, "Energy hubs for the future," *IEEE Power and Energy Magazine*, vol. 5, no. 1, pp. 24–30, 2007.

[88] R. Cespedes, "New method for the analysis of distribution networks," *IEEE Transactions on Power Delievery*, vol. 5, no. 1, pp. 391–396, 1990.

[89] C. Roe, A. Meliopoulos, J. Meisel, and T. Overbye, "Power system level impacts of plug-in hybrid electric vehicles using simulation data," in *2008. ENERGY 2008. IEEE Energy 2030 Conference*, Nov. 2008, pp. 1 –6.

[90] A. Hajimiragha, C. Cañizares, M. Fowler, and A. Elkamel, "Optimal transition to plug-in hybrid electric vehicles in ontario, canada, considering the electricity-grid limitations," *IEEE Transactions on Industrial Electronics*, vol. 57, no. 2, pp. 690 –701, Feb. 2010.

[91] M. Yilmaz and P. Krein, "Review of battery charger topologies, charging power levels, and infrastructure for plug-in electric and hybrid vehicles," *IEEE Transactions on Power Electronics*, vol. 28, no. 5, pp. 2151–2169, 2013.

[92] "IESO." [Online]. Available: http://www.ieso.ca/imoweb/marketdata/hoep.asp

[93] H. Zareipour, C. Cañizares, and K. Bhattacharya, "The operation of ontario's competitive electricity market: Overview, experiences, and lessons," *Power Systems, IEEE Transactions on*, vol. 22, no. 4, pp. 1782–1793, 2007.

[94] "IESO." [Online]. Available: http://www.ieso.ca/imoweb/siteshared/tou_rates.asp

[95] W. H. Kersting, "Radial distribution test feeders," in *2001 IEEE Power Engineering Society Winter Meeting*, vol. 2, 2001, pp. 908 –912.

[96] I. Sharma, C. A. Cañizares, and K. Bhattacharya, "Modeling and impacts of smart charging pevs in residential distribution systems," in *Proc. IEEE Power and Energy Society General Meeting*, July 2012, pp. 1 –8.

[97] M. Shaaban, Y. Atwa, and E. El-Saadany, "PEVs modeling and impacts mitigation in distribution networks," *IEEE Transactions on Power Systems*, vol. 28, no. 2, pp. 1122–1131, 2013.

[98] S. M. Ross, *Introduction to Probability Models*, 10th ed. Elsevier Publisher, 2010.

[99] "Peaksaver Plus Program." [Online]. Available: http://www.hydroone.com/MyHome/SaveEnergy/Pages/Peaksaver.aspx

[100] A. Papalexopoulos, C. F. Imparato, and F. Wu, "Large-scale optimal power flow: effects of initialization, decoupling and discretization," *IEEE Transactions on Power Systems*, vol. 4, no. 2, pp. 748–759, 1989.

[101] "Mathworks: Levenberg-Marquardt." [Online]. Available: http://www.mathworks.com/help/nnet/ref/trainlm.html

[102] "MATLAB." [Online]. Available: http://www.mathworks.com/help/nnet/ug/divide-data-for-optimal-neural-network-training.html

[103] E. Kreyszig, *Advanced Engineering Mathematics*, 10th ed. Wiley, 2011.

[104] "MathWorks: Linear Transfer Function." [Online]. Available: http://www.mathworks.com/help/nnet/ref/purelin.html

[105] I. Sharma, C. Cañizares, and K. Bhattacharya, "Smart charging of PEVs penetrating into residential distribution systems," *IEEE Transactions on Smart Grid*, vol. 5, no. 3, pp. 1196–1209, May 2014.

[106] I. Sharma, K. Bhattacharya, and C. Cañizares, "Smart distribution system operations with price-responsive and controllable loads," *IEEE Transactions on Smart Grid*, under revision.